Defense Threat Reduction Agency
8725 John J. Kingman Road, MS-6201
Fort Belvoir, VA 22060-6201

DTRA-TR-23-048

TECHNICAL REPORT

Parameterization of a Time-Dependent Physiological Model of Combined Injury for a Locally Irradiated Superficial Thermal Burn

December 2023

HDTRA1-14-D-0003

Prepared by:
Applied Research Associates, Inc.
801 N. Quincy Street
Suite 700
Arlington, VA 22203

UNIT CONVERSION TABLE

U.S. customary units to and from international units of measurement*

U.S. Customary Units	Multiply by → / ← Divide by†		International Units
Length/Area/Volume			
inch (in)	2.54	$\times 10^{-2}$	meter (m)
foot (ft)	3.048	$\times 10^{-1}$	meter (m)
yard (yd)	9.144	$\times 10^{-1}$	meter (m)
mile (mi, international)	1.609 344	$\times 10^{3}$	meter (m)
mile (nmi, nautical, U.S.)	1.852	$\times 10^{3}$	meter (m)
barn (b)	1	$\times 10^{-28}$	square meter (m^2)
gallon (gal, U.S. liquid)	3.785 412	$\times 10^{-3}$	cubic meter (m^3)
cubic foot (ft^3)	2.831 685	$\times 10^{-2}$	cubic meter (m^3)
Mass/Density			
pound (lb)	4.535 924	$\times 10^{-1}$	kilogram (kg)
atomic mass unit (AMU)	1.660 539	$\times 10^{-27}$	kilogram (kg)
pound-mass per cubic foot ($lb\ ft^{-3}$)	1.601 846	$\times 10^{1}$	kilogram per cubic meter ($kg\ m^{-3}$)
Pound-force (lbf avoirdupois)	4.448 222		Newton (N)
Energy/Work/Power			
electron volt (eV)	1.602 177	$\times 10^{-19}$	joule (J)
erg	1	$\times 10^{-7}$	joule (J)
kiloton (kT) (TNT equivalent)	4.184	$\times 10^{12}$	joule (J)
British thermal unit (Btu) (thermochemical)	1.054 350	$\times 10^{3}$	joule (J)
foot-pound-force (ft lbf)	1.355 818		joule (J)
calorie (cal) (thermochemical)	4.184		joule (J)
Pressure			
atmosphere (atm)	1.013 250	$\times 10^{5}$	pascal (Pa)
pound force per square inch (psi)	6.984 757	$\times 10^{3}$	pascal (Pa)
Temperature			
degree Fahrenheit (°F)	[T(°F) − 32]/1.8		degree Celsius (°C)
degree Fahrenheit (°F)	[T(°F) + 459.67]/1.8		kelvin (K)
Radiation			
activity of radionuclides [curie (Ci)]	3.7	$\times 10^{10}$	per second (s^{-1}‡)
air exposure [roentgen (R)]	2.579 760	$\times 10^{-4}$	coulomb per kilogram ($C\ kg^{-1}$)
absorbed dose (rad)	1	$\times 10^{-2}$	joule per kilogram ($J\ kg^{-1}$§)
equivalent and effective dose (rem)	1	$\times 10^{-2}$	joule per kilogram ($J\ kg^{-1}$**)

*Specific details regarding the implementation of SI units may be viewed at http://www.bipm.org/en/si/.

†Multiply the U.S. customary unit by the factor to get the international unit. Divide the international unit by the factor to get the U.S. customary unit.

‡The special name for the SI unit of the activity of a radionuclide is the becquerel (Bq). ($1\ Bq = 1\ s^{-1}$).

§The special name for the SI unit of absorbed dose is the gray (Gy). ($1\ Gy = 1\ J\ kg^{-1}$).

**The special name for the SI unit of equivalent and effective dose is the sievert (Sv). ($1\ Sv = 1\ J\ kg^{-1}$).

REPORT DOCUMENTATION PAGE

PLEASE DO NOT RETURN YOUR FORM TO THE ABOVE ORGANIZATION.

1. REPORT DATE	2. REPORT TYPE	3. DATES COVERED	
		START DATE	END DATE
12-01-2023	Technical Report		

4. TITLE AND SUBTITLE

Parameterization of a Time-Dependent Physiological Model of Combined Injury for a Locally Irradiated Superficial Thermal Burn

5a. CONTRACT NUMBER	5b. GRANT NUMBER	5c. PROGRAM ELEMENT NUMBER
HDTRA1-14-D-0003		
5d. PROJECT NUMBER	**5e. TASK NUMBER**	**5f. WORK UNIT NUMBER**

6. AUTHOR(S)

Quintessa Hay, Amy Creel, Kyle Gaffney, PhD

7. PERFORMING ORGANIZATION NAME(S) AND ADDRESS(ES)	8. PERFORMING ORGANIZATION REPORT NUMBER
Applied Research Associates, Inc. 801 N. Quincy Street, Suite 700 Arlington, VA 22203	

9. SPONSORING/MONITORING AGENCY NAME(S) AND ADDRESS(ES)	10. SPONSOR/MONITOR'S ACRONYM(S)	11. SPONSOR/MONITOR'S REPORT NUMBER(S)
Defense Threat Reduction Agency - Nuclear Technologies Department 8725 John J. Kingman Road, Mail Stop 6201 Fort Belvoir, VA 22060-6201	DTRA-RD-NTS	DTRA-TR-23-048

12. DISTRIBUTION/AVAILABILITY STATEMENT

DISTRIBUTION A. Approved for public release: distribution is unlimited.

13. SUPPLEMENTARY NOTES

14. ABSTRACT

Multi-test extended Fourier Amplitude Sensitivity Test (MeFAST), a global sensitivity analysis method, was applied to a time-dependent physiological model describing the local inflammatory response and early fibroblast activity triggered by a superficial thermal burn and immune cell delays and dysfunction triggered by localized radiation exposure. A reduced parameter space was then sampled and results generated reasonable parameter estimates for implementation of the model in relevant software.

15. SUBJECT TERMS

Locally irradiated thermal burn, combined injury, modeling, global sensitivity analysis, MeFAST, parameter sampling

16. SECURITY CLASSIFICATION OF:			17. LIMITATION OF ABSTRACT	18. NUMBER OF PAGES
a. REPORT	b. ABSTRACT	C. THIS PAGE		
U	U	U	U	78

19a. NAME OF RESPONSIBLE PERSON	19b. PHONE NUMBER *(Include area code)*
Lee Alleman; Maj Joseph Curro	+1 (571) 616-2599; +1 (571) 616-4220

PREVIOUS EDITION IS OBSOLETE.

STANDARD FORM 298 (REV. 5/2020)

Prescribed by ANSI Std. Z39.18

This page intentionally left blank.

Table of Contents

List of Figures

List of Tables

Acknowledgements

We gratefully acknowledge Mr. Lee Alleman, Dr. Lawrence Herskowitz, and DTRA's Nuclear Technologies Survivability Division for programmatic support. This work was performed under DTRA contract HDTRA1-14-D-0003.

Executive Summary

In a nuclear detonation, ionizing radiation exposure will accompany tissue injuries from thermal and blast sources, affecting survival and recovery. Quantifying this effect of radiation on local inflammatory responses is a key factor in understanding how combined injury impacts outcomes for medical planning and performance assessment. The Defense Threat Reduction Agency (DTRA) developed Health Effects from Nuclear and Radiological Environments (HENRE) software to provide analysts with insight into these questions. To continue evolving the capabilities of this tool, modelers at Applied Research Associates (ARA) have developed a mechanistic mathematical modeling framework of combined injury, anchored in wound healing. These models can predict outcomes of interest, such as quantification of delay in predicted wound healing times and insight into pathophysiological responses that affect clinical outcomes. Proving the efficacy of this approach, ARA first developed a model of superficial thermal burn, for which wound healing time is known. Successful implementation was followed by expansion into incorporating local radiation effects. To utilize this locally irradiated thermal burn model to support combined injury analyses though pathophysiological mechanisms, parameterization was then required. Following established methods, ARA performed global sensitivity analysis to identify influential model parameters and Latin-hypercube parameter sampling to estimate unknown values. Sensitivity analysis results identified 26 of the 73 total model parameters as influential in model output, thus reducing the parameter space prior to sampling methods. As previously described, parameter sampling methods are employed to exhaustively examine the parameter space and identify plausible parameter sets based on qualitative features of the model output. The only modification in methodology was made to ensure accuracy in the more complex model; therefore MeFAST – with its additional statistical tests – was used for sensitivity analysis instead of the eFAST methodology used for the non-irradiated model. The newly parameterized model includes immunological interactions within the thermal burn perimeter as well as resident tissue populations of radiosensitive cells subject to radiation injury. Radiation effects include known immunological delays in cell infiltration, cellular dysfunction, and the introduction of potential pathogen exposure. This parameterized time-dependent physiological model of locally irradiated thermal burn represents the first combined injury within the wound healing framework and is a crucial step towards a systems-level model of combined injury effects that will inform measures of clinical outcomes and performance decrement for combined injury in the event of a nuclear detonation.

Section 1. Introduction

Developed by Applied Research Associates, Inc. (ARA) for the Defense Threat Reduction Agency (DTRA), the Health Effects from Nuclear and Radiological Environments (HENRE) engine predicts casualties and performance decrement for the given environmental conditions following a nuclear detonation (NUDET) event. Following a NUDET event, potential injuries and casualties occur from air blast related injuries, thermal burns, ionizing radiation, and a combination of these effects (Reeves, 2018). Recent efforts from ARA have focused on developing time-dependent physiological models (TDPMs) to deal with injuries that do not immediately result in casualties but where some performance issues are expected. Most recent TDPMs have included a superficial and superficial partial-thickness thermal burn, referred to herein as the superficial thermal burn model (STBM) (Jennings et al., 2022a, 2022b) and the expansion of this model for a combined injury of a thermal burn and localized ionizing radiation exposure, referred to herein as the locally irradiated thermal burn model (LITBM) (Hay et al., 2022). These models serve as the initial steps for developing TDPMs that will support dynamic estimates of performance decrement and other outcomes.

Combined injuries are a crucial component of assessing nuclear survivability and performance outcomes due to their prevalence in NUDET events. Historical evidence shows that the majority of casualties are expected to be caused by more than one insult, particularly radiation exposure and thermal injury (DiCarlo et al., 2008; Iijima, 1982; Kishi, 2000; Palmer et al., 2011; Pellmar & Ledney, 2005). The increased severity of combined injury and lack of mathematical models in this area have prompted this need for further development for HENRE. The most recent advancement, a LITBM, is the first model developed for a combined injury, focusing on a thermal burn injury with local irradiation. This addition of localized radiation exposure to an existing TDPM serves as a necessary steppingstone to developing more complex models involving whole-body irradiation combined with other injuries. However, in the initial model formulation (Hay et al., 2022), manually calibrated parameter estimates were used to demonstrate model behavior and radiation effects.

While early parameter estimates reproduced biologically observed trends, a formal parameterization process must be performed to optimize predictive accuracy. The limited data for this type of injury and model complexity necessitates the use of a sensitivity analysis (SA) to identify influential parameters for a parameter estimation procedure. SA methods provide quantitative measures of the impact of each parameter on the model output and allow for a reduction of the estimated parameter space, ensuring computational resources are efficiently allocated.

For combined injury model development for HENRE, we have established a procedure demonstrated in technical reports (TRs) DTRA-TR-21-063 R1 and DTRA-TR-22-026 R1 (Creel, Jennings, et al., 2022; Jennings et al., 2022b). To summarize, a global SA method was paired with brute-force Latin hypercube sampling to identify and estimate influential model parameters. Resulting parameter sets were then assessed based on whether the resulting model outputs satisfied required qualitative features. A representative parameter set for the accepted parameters was chosen by comparing the accepted parameter sets to the average model output obtained from these sets. Parameterization of the LITBM model presented herein employed this method for sensitivity analysis and parameter sampling but relied on the slightly improved MeFAST sensitivity method for parameter selection.

Section 2. Model Background

The irradiated thermal burn model, previously formulated in DTRA-TR-22-067 (Hay et al., 2022), consists of 16 ordinary differential equations and 73 total parameters. The model variables are split into two compartments: the burn injury compartment encompassing the infiltration of immune cells and interactions within the injury site and the surrounding tissue compartment which includes radiation effects of delayed infiltration of necessary cells and damaged cell populations as a proxy for cellular dysfunction. The inclusion of radiation injury also prompted the introduction of a pathogen variable. Superficial thermal burns alone have little to no risk of complications from infection (Abazari et al., 2020; Jeschke et al., 2020; Wang, 2014), however, radiation injury is associated with a risk of infection even at the localized level (Hill et al., 2004) and is elevated for irradiated burns (Ledney et al., 1991). The presence of pathogen presents an additional barrier to healing and increased burden on the immune system. In the absence of radiation, the model reduces to the STBM formulated in DTRA-TR-22-032 (Jennings et al., 2022a) with dynamic populations of leukocytes in the surrounding tissue.

Model equations are available in Appendix A contained in equations (A.1) - (A.16) with auxiliary equations (A.17) - (A.28). Table 1 includes descriptions of the model variables with corresponding initial conditions used in simulations. Various levels of a prompt radiation dose (in Gray (Gy)) were explored corresponding to low (1 Gy), medium (7 Gy), and high (14 Gy) levels of radiation.

Table 2 contains the parameters, their descriptions, their baseline values used in numerical simulations of the model in the initial formulation (Hay et al., 2022), the minimum and maximum values calculated for the sensitivity analysis and sampling methods, and the estimated values calculated later in this report. The method from which parameter bounds were calculated can be found in DTRA-TR-22-063 (Creel, Jennings, et al., 2022, Appendix B).

Table 1. TDPM state variable symbols, definitions, and initial conditions by compartment. Initial conditions refer to varying levels of a prompt radiation dose at a low level (1 Gy), medium level (7 Gy), or high level (14 Gy). Current model inputs for radiation dose are assumed to be doses of radiation with a relative biological effectiveness of 1.

SYMBOL	DESCRIPTION	INITIAL CONDITIONS		
		IC1 (low)	IC2 (med)	IC3 (high)
$\boldsymbol{t}$	Time (in hours)	-	-	-
$\boldsymbol{Dose_{rad}}$	Radiation dose (in Gy)	1 Gy	7 Gy	14 Gy
Local Irradiated Tissue				
$\boldsymbol{\bar{N}_{st}^{ud}}$	Resting neutrophils from the blood vessels in the surrounding tissue	0	0	0
$\boldsymbol{\bar{M}_{st}^{ud}}$	Undamaged resting tissue-resident monocytes/macrophages and their influx from the blood vessels in the surrounding tissue	$0.95 \times \bar{M}_{st,0}$	$0.95 \times \bar{M}_{st,0}$	$0.95 \times \bar{M}_{st,0}$
$\boldsymbol{\bar{M}_{st}^{d}}$	Damaged resting resident monocytes/macrophages in the surrounding tissue	$(1-0.95) \times \bar{M}_{st,0}$	$(1-0.95) \times \bar{M}_{st,0}$	$(1-0.95) \times \bar{M}_{st,0}$
$\boldsymbol{F_{st}^{ud}}$	Undamaged resident fibroblasts and influx from the connective tissue in the surrounding tissue	$0.3 \times F_{st,0}$	$0.01 \times F_{st,0}$	$0.001 \times F_{st,0}$
$\boldsymbol{F_{st}^{d}}$	Damaged resident fibroblasts in the surrounding tissue	$(1-0.3) \times F_{st,0}$	$(1-0.01) \times F_{st,0}$	$(1-0.001) \times F_{st,0}$
$\boldsymbol{L_{st}^{ud}}$	Undamaged resident lymphocytes and influx from the blood vessels in the surrounding tissue	$0.8 \times L_{st,0}$	$0.3 \times L_{st,0}$	$0.3 \times L_{st,0}$
$\boldsymbol{L_{st}^{d}}$	Damaged resident T lymphocytes in the surrounding tissue	$(1-0.8) \times L_{st,0}$	$(1-0.3) \times L_{st,0}$	$(1-0.3) \times L_{st,0}$
Local Thermal Burn				
$\boldsymbol{Dam_{tb}}$	Damaged tissue (unitless)	0.9	0.9	0.9
$\boldsymbol{Deb_{tb}}$	Debris (unitless)	0.9	0.9	0.9
$\boldsymbol{N_{tb}}$	Activated neutrophils at the wound site	0	0	0
$\boldsymbol{M1_{tb}}$	Classically activated macrophages (M1) at the wound site	0	0	0
$\boldsymbol{M2_{tb}}$	Alternatively activated macrophages (M2) at the wound site	0	0	0
$\boldsymbol{F_{tb}}$	Fibroblasts at the wound site	0	0	0
$\boldsymbol{L1_{tb}}$	Pro-inflammatory T lymphocytes at the wound site, which includes γδ-T cells, TH1 cells, and TH17 cells	0	0	0
$\boldsymbol{L2_{tb}}$	Anti-inflammatory T lymphocytes at the wound site, which includes TH2 cells and regulatory T cells	0	0	0
$\boldsymbol{P_{tb}}$	Pathogen levels at the wound site	0.8	0.8	0.8

Note:
*State variables that are assumed to be at steady state prior to and following irradiated thermal injury.
*Steady state values for macrophages ($\bar{M}_{st,0}$), lymphocytes ($L_{st,0}$), and fibroblasts ($F_{st,0}$) are strictly positive constants such that each is less than or equal to its corresponding healed steady-state value, i.e.,

$$0 < \bar{M}_{st,0} \leq \frac{s_{mr}}{d_{mr}}, \qquad 0 < L_{st,0} \leq \frac{s_{lr}}{d_{lr}}, \quad \text{and} \quad 0 < F_{st,0} \leq \frac{s_f}{d_{fr} - k_{ftb}^{ud}}$$

Table 2. Parameter descriptions, units, baseline values, estimated values, and ranges. Baseline values were obtained from the initial formulation of this model in DTRA-TR-22-067 (Hay et al., 2022, Appendix B). Estimated minimums and maximums were calculated using the process and acceptability criteria described for the superficial thermal burn model (STBM) in DTRA-TR-21-063 (Creel, Jennings, et al., 2022, Appendix B). Estimated values were obtained through the parameterization process described in this report. Parameters indicated as "FIXED" were not estimated and were fixed at their baseline values. The parameter marked with "-" does not included estimated values since its value is defined by a combination of other parameters.

PARAMETER		DESCRIPTION	UNITS	BASELINE VALUE	ESTIMATED VALUE	ESTIMATED MINIMUM	ESTIMATED MAXIMUM
Inhibition (non-radiation related)	Deb_{dam}^{∞}	Constant controlling the effectiveness of Deb_{tb} at inhibiting damage repair	D-units	0.0100	FIXED	3.9804×10^{-5}	0.0302
	Deb_H	Constant controlling the effectiveness of Deb_{tb} at inhibiting phagocytic removal of debris by $N_{tb}, M1_{tb}$ and $M2_{tb}$	D-units	0.0610	FIXED	4.7343×10^{-5}	0.1695
	N_1^{∞}	Constant controlling the effectiveness of N_{tb} at inhibiting the activity on other immune cells	N-units	0.1417	0.1978	0.0136	0.3574
	N_2^{∞}	Constant controlling the effectiveness of N_{tb} at inhibiting proliferation and activation of F_{tb}	N-units	0.1000	FIXED	1.5803×10^{-4}	0.2966
	$M1_1^{\infty}$	Constant controlling the effectiveness of $M1_{tb}$ at inhibiting activation of $M2_{tb}$	M-units	0.1457	0.0760	0.0031	0.3738

PARAMETER		DESCRIPTION	UNITS	BASELINE VALUE	ESTIMATED VALUE	ESTIMATED MINIMUM	ESTIMATED MAXIMUM
	$M1_2^{\infty}$	Constant controlling the effectiveness of $M1_{tb}$ at inhibiting proliferation and activation of F_{tb}	M-units	0.0843	FIXED	5.8151×10^{-4}	0.2369
	$M2^{\infty}$	Constant controlling the effectiveness of $M2_{tb}$ at inhibiting activation of N_{tb} and $M1_{tb}$	M-units	0.4734	1.3842	0.0068	1.4075
	F^{∞}	Constant controlling the effectiveness of F_{tb} at inhibiting the activation of $M2_{tb}$ and $L2_{tb}$	F-units	0.5314	FIXED	0.0135	1.3639
	$L2_1^{\infty}$	Constant controlling the effectiveness of $L2_{tb}$ at inhibiting the activation of N_{tb}, $M1_{tb}$ and $L1_{tb}$	L-units	0.4738	FIXED	0.0041	1.3233
	$L2_2^{\infty}$	Constant controlling the effectiveness of $L2_{tb}$ at inhibiting collateral damage associated with N_{tb} and $M1_{tb}$	L-units	0.4738	FIXED	0.0023	1.2374
Inhibition (radiation	ω_{dam}	Constant controlling the effectiveness of F_{st}^{d} at inhibiting removal of Dam_{tb} by F_{tb}	F-units	0.0200	FIXED	3.4661×10^{-4}	0.0545

PARAMETER		DESCRIPTION	UNITS	BASELINE VALUE	ESTIMATED VALUE	ESTIMATED MINIMUM	ESTIMATED MAXIMUM
	ω_{m2}	Constant controlling the effectiveness of $\bar{M}_{st}^{d}$ at inhibiting activation of $\bar{M}_{st}^{ud}$ and $\bar{M}_{st}^{d}$ to $M2_{tb}$	M-units	10	FIXED	0.0068	28.0525
	ω_f	Constant controlling the effectiveness of F_{st}^{d} at inhibiting proliferation of F_{tb}	F-units	0.0200	0.0052	1.5042×10^{-4}	0.0539
	γ_n	Constant controlling the effectiveness of $Dose_{rad}$ at inhibiting $\bar{N}_{bv}$ infiltration to the surrounding tissue	Gy/h	0.1667	0.0498	0.0011	0.4529
	γ_m	Constant controlling the effectiveness of $Dose_{rad}$ at inhibiting $\bar{M}_{bv}$ infiltration to the surrounding tissue	Gy/h	0.1000	0.2553	0.0017	0.2777
	γ_l	Constant controlling the effectiveness of $Dose_{rad}$ at inhibiting L_{bv} infiltration to the surrounding tissue	Gy/h	0.1667	FIXED	4.7178×10^{-4}	0.4336
	γ_f	Constant controlling the effectiveness of $Dose_{rad}$ at inhibiting F_{ct} infiltration to the surrounding tissue	Gy/h	0.0500	FIXED	7.8996×10^{-5}	0.1347

PARAMETER		DESCRIPTION	UNITS	BASELINE VALUE	ESTIMATED VALUE	ESTIMATED MINIMUM	ESTIMATED MAXIMUM
Damage/Debris	k_{dn}	Maximum collateral tissue damage rate caused by N_{tb} at the local wound site	D-units/h	1.7500×10^{-4}	FIXED	3.3324×10^{-6}	4.7174×10^{-4}
	k_{dm1}	Maximum collateral tissue damage rate caused by $M1_{tb}$ at the local wound site	D-units/h	$\sigma_{dm1} \cdot k_{dn}$	-	-	-
	σ_{dm1}	Tissue damage scaling coefficient for $M1_{tb}$	Unitless	0.5000	FIXED	6.8467×10^{-4}	1.3854
	N_H	Hill constant for tissue damage associated with N_{tb}	N-units	0.0600	FIXED	4.6798×10^{-4}	0.1526
	$M1_H$	Hill constant for tissue damage associated with $M1_{tb}$	M-units	0.0600	FIXED	1.7054×10^{-4}	0.1705
	ρ_{dam}	Baseline tissue damage repair rate via a combination of repair, resolution, and regeneration	1/h	0.0040	FIXED	1.0340×10^{-5}	0.0103
	k_{df}	Repair rate on Dam_{tb} by F_{tb}	1/(F-units·h)	0.0200	FIXED	2.2186×10^{-4}	0.0550
	k_{dnp}	Phagocytosis rate of Deb_{tb} by N_{tb}	D-units/(N-units·h)	0.0130	0.0199	1.8480×10^{-5}	0.0356

PARAMETER		DESCRIPTION	UNITS	BASELINE VALUE	ESTIMATED VALUE	ESTIMATED MINIMUM	ESTIMATED MAXIMUM
	k_{dm1p}	Phagocytosis rate of Deb_{tb} by $M1_{tb}$	D-units/(M-units·h)	0.0176	0.0148	9.9108×10^{-5}	0.0459
	k_{dm2p}	Phagocytosis rate of Deb_{tb} by $M2_{tb}$	D-units/(M-units·h)	0.0101	FIXED	7.4963×10^{-5}	0.0286
	d_{deb}	Decay rate of Deb_{tb}	1/h	0.0001	FIXED	7.5224×10^{-7}	2.7590×10^{-4}
Neutrophils	s_{nr}	Recruitment rate of circulating neutrophils $\bar{N}_{bv}$ to the local wound site	N-units/h	0.0137	0.0370	1.1795×10^{-4}	0.0419
	d_{nr}	Decay rate of $\bar{N}_{st}^{ud}$	1/h	0.0190	FIXED	1.0989×10^{-5}	0.0571
	d_n	Decay rate of N_{tb}	1/h	0.0206	0.0509	3.6046×10^{-5}	0.0520
	k_{nd}	Activation rate of resting neutrophils $\bar{N}_{st}^{ud}$ to N_{tb} by Deb_{tb}	1/(D-units·h)	0.2432	0.4247	5.4412×10^{-4}	0.6557
	k_{np}	Activation rate of resting neutrophils $\bar{N}_{st}^{ud}$ to N_{tb} by P_{tb}	1/(P-units·h)	7.325	FIXED	0.0430	19.4112

PARAMETER		DESCRIPTION	UNITS	BASELINE VALUE	ESTIMATED VALUE	ESTIMATED MINIMUM	ESTIMATED MAXIMUM
	k_{nn}	Activation rate of resting neutrophils $\bar{N}_{st}^{ud}$ to N_{tb} by N_{tb} and its byproducts	1/(N-units·h)	0.0169	FIXED	5.1827×10^{-5}	0.0464
	k_{nm1p}	Phagocytosis rate of N_{tb} by $M1_{tb}$	1/(M-units·h)	0.1208	0.1034	5.9308×10^{-4}	0.3455
	k_{nm2p}	Phagocytosis rate of N_{tb} by $M2_{tb}$	1/(M-units·h)	0.3628	FIXED	0.0019	1.0187
Macrophages	s_{mr}	Recruitment rate of fixed tissue and circulating monocytes to the local wound site	M-units/h	1.7575	1.3192	0.0798	5.0321
	d_{mr}	Decay rate of $\bar{M}_{st}^{ud}$	1/h	0.0221	0.0265	9.4221×10^{-5}	0.0571
	d_{mr}^{d}	Decay rate of $\bar{M}_{st}^{d}$	1/h	0.0331	FIXED	9.4221×10^{-5}	0.5710
	d_{m1}	Decay rate of $M1_{tb}$	1/h	0.0497	0.1020	0.0015	0.1337
	d_{m2}	Decay rate of $M2_{tb}$	1/h	0.1236	FIXED	0.1653	0.3021
	k_{m1d}	Activation rate of resting monocytes $\bar{M}_{st}^{ud}$ and $\bar{M}_{st}^{d}$ to $M1_{tb}$ by Deb_{tb}	1/(D-units·h)	0.0035	0.0040	2.3602×10^{-6}	0.0106

PARAMETER		DESCRIPTION	UNITS	BASELINE VALUE	ESTIMATED VALUE	ESTIMATED MINIMUM	ESTIMATED MAXIMUM
	k_{m1p}	Activation rate of resting monocytes $\bar{M}_{st}^{ud}$ and $\bar{M}_{st}^{d}$ to $M1_{tb}$ by P_{tb}	1/(P-units·h)	1.5433×10^{-4}	1.7066×10^{-5}	5.5214×10^{-9}	4.2329×10^{-4}
	k_{m1n}	Activation rate of resting monocytes $\bar{M}_{st}^{ud}$ and $\bar{M}_{st}^{d}$ to $M1_{tb}$ by N_{tb} and its byproducts	1/(N-units·h)	0.0346	0.0688	3.9191×10^{-5}	0.0999
	k_{m1m1}	Activation rate of resting monocytes $\bar{M}_{st}^{ud}$ and $\bar{M}_{st}^{d}$ to $M1_{tb}$ by $M1_{tb}$ and its byproducts	1/(M-units·h)	3.7879×10^{-5}	FIXED	7.5871×10^{-8}	1.0781×10^{-4}
	k_{m1l1}	Activation rate of resting monocytes $\bar{M}_{st}^{ud}$ and $\bar{M}_{st}^{d}$ to $M1_{tb}$ by $L1_{tb}$ and its byproducts	1/(L-units·h)	1.5542×10^{-4}	FIXED	3.5963×10^{-7}	4.3360×10^{-6}
	k_{m2m1}	Activation rate of resting monocytes $\bar{M}_{st}^{ud}$ and $\bar{M}_{st}^{d}$ to $M2_{tb}$ by $M1_{tb}$ and its byproducts	1/(M-units·h)	0.0219	0.0504	5.0616×10^{-5}	0.0678
	k_{m2m2}	Activation rate of resting monocytes $\bar{M}_{st}^{ud}$ and $\bar{M}_{st}^{d}$ to $M2_{tb}$ by $M2_{tb}$ and its byproducts	1/(M-units·h)	6.7667×10^{-4}	FIXED	2.1256×10^{-6}	0.0019

PARAMETER		DESCRIPTION	UNITS	BASELINE VALUE	ESTIMATED VALUE	ESTIMATED MINIMUM	ESTIMATED MAXIMUM
	k_{m2l2}	Activation rate of resting monocytes $\bar{M}_{st}^{ud}$ and $\bar{M}_{st}^{d}$ to $M2_{tb}$ by $L2_{tb}$ and its byproducts	1/(L-units·h)	0.0049	FIXED	1.4035×10^{-5}	0.0132
	θ_{m1m2}	Transition rate of $M1_{tb}$ to $M2_{tb}$	M-units/N-units	0.6901	FIXED	0.0029	1.8611
Fibroblasts	s_f	Non-injury recruitment rate of fibroblasts to the local wound site	F-units/h	0.0014	FIXED	2.6508×10^{-6}	0.0043
	k_{ftb}^{ud}	Rate of transition of undamaged fibroblasts $\left(F_{st}^{ud}\right)$ from the surrounding tissue to the thermal burn	1/h	0.0042	FIXED	1.0665×10^{-5}	0.0111
	k_{ftb}^{d}	Rate of transition of damaged fibroblasts $\left(F_{st}^{ud}\right)$ from the surrounding tissue to the thermal burn	1/h	0.0013	FIXED	3.0379×10^{-6}	0.0035
	d_{fr}^{ud}	Decay rate of F_{st}^{ud}	1/h	0.0091	FIXED	2.5070×10^{-5}	0.0248
	d_{fr}^{d}	Decay rate of F_{st}^{d}	1/h	0.0136	FIXED	1.3188×10^{-6}	0.2479
	d_f	Decay rate of F_{tb}	1/h	0.0091	FIXED	2.4534×10^{-5}	0.0252

PARAMETER		DESCRIPTION	UNITS	BASELINE VALUE	ESTIMATED VALUE	ESTIMATED MINIMUM	ESTIMATED MAXIMUM
	k_f	Baseline proliferation and activation rate of F_{tb}	1/h	0.0053	FIXED	4.7467×10^{-5}	0.0141
	α_{m2}	Constant controlling the up-regulation of F_{tb} proliferation and activation by $M2_{tb}$	1/(M-units·h)	0.0455	FIXED	1.3038×10^{-4}	0.1305
	α_{dam}	Constant controlling the up-regulation of F_{tb} proliferation and activation by Dam_{tb}	1/(D-units·h)	0.0667	FIXED	1.7910×10^{-4}	0.1829
T Lymphocytes	$s_{\ell r}$	Recruitment rate of circulating T lymphocytes to the local wound site	L-units/h	0.0283	FIXED	8.7940×10^{-5}	0.0718
	$d_{\ell r}^{ud}$	Decay rate of L_{st}^{ud}	1/h	0.0565	FIXED	2.8508×10^{-4}	0.1631
	$d_{\ell r}^{d}$	Decay rate of L_{st}^{d}	1/h	0.0848	FIXED	2.8508×10^{-4}	1.6311
	k_{l1}	Induction rate of L_{st}^{ud} and L_{st}^{d} to $L1_{tb}$ by $M1_{tb}$	1/(M-units·h)	0.0431	0.0791	2.0496×10^{-5}	0.1193
	k_{l2}	Induction rate of L_{st}^{ud} and L_{st}^{d} to $L2_{tb}$ by $M2_{tb}$	1/(M-units·h)	0.0369	FIXED	3.2730×10^{-5}	0.0946
	d_{ℓ}	Decay rate of $L1_{tb}$ and $L2_{tb}$	1/h	0.0594	FIXED	1.8227×10^{-4}	0.1634

PARAMETER		DESCRIPTION	UNITS	BASELINE VALUE	ESTIMATED VALUE	ESTIMATED MINIMUM	ESTIMATED MAXIMUM
Pathogen	k_{pg}	Growth rate of P_{tb}	1/h	0.4000	0.3674	0.0210	1.0058
	P^{∞}	Carrying capacity of P_{tb}	P-units	13.3333	15.9333	1.0503	36.6802
	k_{pb}	Phagocytosis rate of P_{tb} by the background immune response	1/(B-units·h)	0.6000	0.9612	0.0035	1.5088
	s_b	Recruitment rate of circulating background immune cells	B-units/h	0.0050	0.0096	5.2745×10^{-5}	0.0125
	μ_b	Decay rate of background immune cells	1/h	0.0020	FIXED	2.4398×10^{-6}	0.0054
	k_{bp}	Phagocytosis rate of cells in the background immune response by P_{tb}	1/(M-units·h)	0.0079	FIXED	1.1504×10^{-4}	0.0234
	k_{pn}	Phagocytosis rate of P_{tb} by N_{tb}	N-units/h	1.4596	2.5717	0.0061	4.2044
	k_{pm1}	Phagocytosis rate of P_{tb} by $M1_{tb}$	M-units/h	0.0947	FIXED	4.0218×10^{-4}	0.2570
	k_{pm2}	Phagocytosis rate of P_{tb} by $M2_{tb}$	M-units/h	0.0947	FIXED	2.3841×10^{-4}	0.2666

Notation:

- Dam_{tb} and Deb_{tb} have the same units- D is used to denote their units.

PARAMETER	DESCRIPTION	UNITS	BASELINE VALUE	ESTIMATED VALUE	ESTIMATED MINIMUM	ESTIMATED MAXIMUM
• N, M, F, L, and P denote the units of neutrophils (N_{st}^{ud}, N_{st}^{d}, and N_{tb}), macrophages ($\bar{M}_{st}^{ud}$, $\bar{M}_{st}^{d}$, $M1_{tb}$, and $M2_{tb}$), fibroblasts (F_{st}^{ud}, F_{st}^{d}, and F_{tb}), T lymphocytes (L_{st}^{ud}, L_{st}^{d}, $L1_{tb}$, and $L2_{tb}$), and pathogen (P_{tb}) respectively. • B denotes the units for the background immune response including mast cells and natural killer cells. • Gy denotes the units for radiation dose (Gray). • The cell survival parameters a and b do not have estimated values in the current model iteration.						

Section 3. Sensitivity Analysis

The development of models in systems biology involves varying amounts of simplification to capture as much of the dynamics as possible without overcomplicating the analysis. This, along with expected ambiguity in experimentally observed phenomena makes SA necessary. Difficulties associated with data availability for the present model have been discussed in a previous technical note (TN) ARA-HS-TN-22-016 (Creel, Hay, et al., 2022). Many SA methods exist (described in more detail in ARA-HS-TN-21-014 (Creel, 2021) and ARA-HS-TN-22-016 (Creel, Hay, et al., 2022)) but due to the lack of data, nonlinearity, and general complexity of the model, a global SA method was used to inform selection of a subset of parameters for estimation.

3.1 Methods

Due to its applicability to the present model as well as general popularity in the field, eFAST (using the approach demonstrated in DTRA-TR-21-063 R1 (Creel, Jennings, et al., 2022)) is the best method to assess and identify parameters for this model. For the LITBM, a slightly modified version of eFAST was used namely, MeFAST, a method developed by Dela and colleagues (Dela et al., 2022). The primary difference in methodologies is the inclusion of additional statistical tests during analyses, described later, to better determine parameter influence.

The model was assessed at five time points: $t = 24$, $t = 72$, $t = 168$, $t = 240$, and $t = 336$ hours, corresponding to days one, three, seven, ten, and fourteen, respectively. These time points were previously used in analysis of the STBM (Creel, Jennings, et al., 2022) and are common data points for collection in experimental models of thermal burn injury (Lateef et al., 2019). The model was also simulated for three different initial conditions, referred to as initial condition (IC) 1, IC2, and IC3 for the radiation dose. The three initial conditions are 1 Gy (IC1), 7 Gy (IC2), and 14 Gy (IC3). These values were used previously in numerical simulations during model development (Hay et al., 2022) and correspond to a low, medium, or high radiation exposure, respectively. All simulations and algorithms were executed in MATLAB (The MathWorks Inc., 2022).

3.1.1. Multi-test Extended Fourier Amplitude Sensitivity Test (MeFAST)

MeFAST is an improvement of the eFAST method by including additional statistical tests for the significance of the sensitivity indices. This method was developed recently by Dela and colleagues (Dela et al., 2022) to address concerns regarding the appropriateness of the previously used statistical tests for eFAST. The main output of the eFAST algorithm, S_{Ti}, representing the total sensitivity index for the ith parameter (Marino et al., 2008), relies on a statistical test, namely a two-sided t-test, to determine whether this value is significantly larger than random variation or accumulation of numerical error in the method. The use of a t-test is generally a good choice for determining statistical significance using both the mean and standard deviation to assess statistical significance which requires an assumption of normality in the data. When samples are large, normality is often assumed, but due to the large computational cost associated with running eFAST, these statistical tests are frequently performed on smaller sample sizes ($n < 30$). Without the assurance of normality, statistical tests may produce misleading results. Additionally, there is always a risk of false conclusions from statistical tests which can become of greater concern when many statistical tests are being performed. With a nearly 50%

increase in both the number of parameters and the number of outputs being assessed compared to the STBM, it makes sense to improve the method identifying influential parameters. MeFAST amends the single statistical test by performing multiple tests, improving the accuracy of the conclusions.

The method developed by Dela and colleagues uses three additional statistical tests, namely the Wilcoxon rank sum test, permutation test, and ANOVA followed by the Tukey procedure. The Wilcoxon and permutation tests are both non-parametric, making them useful when normality is not guaranteed. The Wilcoxon test works by ranking data from the two samples, summing the ranks, and comparing these sums among the samples (Mann & Whitney, 1947). It can also be interpreted as showing a difference in medians. For the permutation test, the test statistic under the null hypothesis is obtained by calculating all possible values of the test statistic under possible rearrangements of the data and is described as a form of resampling (Moore, 1999). Due to the similarities in the assumptions, the permutation test was not used in the present report. The ANOVA test is slightly more rigid, including an assumption of normality; however, it is useful when making multiple comparisons. The ANOVA test itself serves as a global test to determine whether any parameters have indices significantly different than the dummy parameter, and then the subsequent Tukey procedure identifies which parameters, if any, do produce statistically significant results. This is beneficial compared to the t-test since the individual tests are not subject to the Bonferroni correction (described in more detail in (Abdi, 2007; Benjamini & Hochberg, 1995)), which is sometimes overly conservative and would cause us to miss some parameters that may actually be influential. Additionally, the use of multiple statistical tests helps reduce the risk of false conclusions. For this report, we apply the original t-test proposed in Marino *et. al* (Marino et al., 2008), the Wilcoxon test as a non-parametric option allowing for the possibility of data that does not follow a normal distribution, and the ANOVA test with the Tukey comparison procedure to allow for a comparable test to the t-test without increased restrictions on the p-value. We consider a parameter's sensitivity index to be influential if its value is larger than that of the dummy parameter calculated by the eFAST method and is statistically significant in at least two of these three tests.

The full MeFAST method also includes a statistical test for choosing the values for the number of samples per search curve, N_s, and resampling number, N_r. For details on the use and significance of these values in the eFAST algorithm see (Creel, Jennings, et al., 2022; Dela et al., 2022; Marino et al., 2008). This process involves running eFAST for multiple values of N_s and N_r and comparing the sensitivity indices using a two-sample Kolmogorov-Smirnov test to determine the optimal values. Due to the computational cost of running this procedure, N_s and N_r were selected by running only a few values in increasing order and visually assessing stability of the calculated indices. Final SA results from this method were obtained using $N_s = 2000$ and $N_r = 32$, the largest sampling procedure tested. This results in 4,672,000 total iterations per initial condition.

3.1.2. Parameter Selection Algorithm

The MeFAST algorithm produces a total of 5,475 sensitivity indices for each initial condition which are used to select parameters for further estimation efforts based on relative importance. The model has a total of 73 parameters, so of the 5,475 total sensitivity indices, 75 are attributed to each parameter. The total of 75 for each parameter is obtained by calculating sensitivity indices for 15 model variables at each of the five time points mentioned above. Note that the 16$^{\text{th}}$ variable (F_{st}^{d}) was excluded from

sensitivity analysis since it has a closed form solution and thus sensitivity can be easily categorized by the two associated parameters. Details on the calculation of the closed form solution can be found in DTRA-TR-22-067 (Hay et al., 2022). The parameters in this equation, however, are still assessed for their effect on other model variables. To select a reduced subset of parameters for estimation, these 75 sensitivity indices for each parameter were used. Parameters were determined to be influential at a given time point and variable if the value for S_{T_i} was larger than the total sensitivity index for the dummy parameter and the p-value was less than 0.05 in at least two of the three statistical tests performed. Each method was performed at three possible radiation initial conditions to ensure that the parameter is influential in model outcome independent of the radiation dose. To implement the algorithm, six values were calculated for each parameter.

- $n_{1,all}$: the number of times the parameter was found to be statistically significant across all 75 sensitivity indices with IC1 for the MeFAST method
- $n_{2,all}$: the number of times the parameter was found to be statistically significant across all 75 sensitivity indices with IC2 for the MeFAST method
- $n_{3,all}$: the number of times the parameter was found to be statistically significant across all 75 sensitivity indices with IC3 for the MeFAST method
- $n_{1,DD}$: the number of times the parameter was found to be statistically significant for $Dam_{tb}(336)$ and $Deb_{tb}(336)$ with IC1 for the MeFAST method
- $n_{2,DD}$: the number of times the parameter was found to be statistically significant for $Dam_{tb}(336)$ and $Deb_{tb}(336)$ with IC2 for the MeFAST method
- $n_{3,DD}$: the number of times the parameter was found to be statistically significant for $Dam_{tb}(336)$ and $Deb_{tb}(336)$ with IC3 for the MeFAST method

Observe that by construction $n_{j,all} \leq 75$ and $n_{j,DD} = 0, 1, 2$ for $j = 1, 2, 3$.

The algorithm used to select parameters for estimation is given in Figure 1. A cut-off of at least 16 significant points was used in the algorithm for each parameter based on the results of each method. A value of 16 ensures that the parameter is sensitive in a least four of the model variables and at least two of the time points, since each variable has at most five time points and each time point spans 15 total variables. Note that the variable F_{st}^{d} is excluded since the solution for this equation (Equation (A.14), Appendix A) is only dependent on time and the two associated parameters, thus the variation in output is easily analyzed.

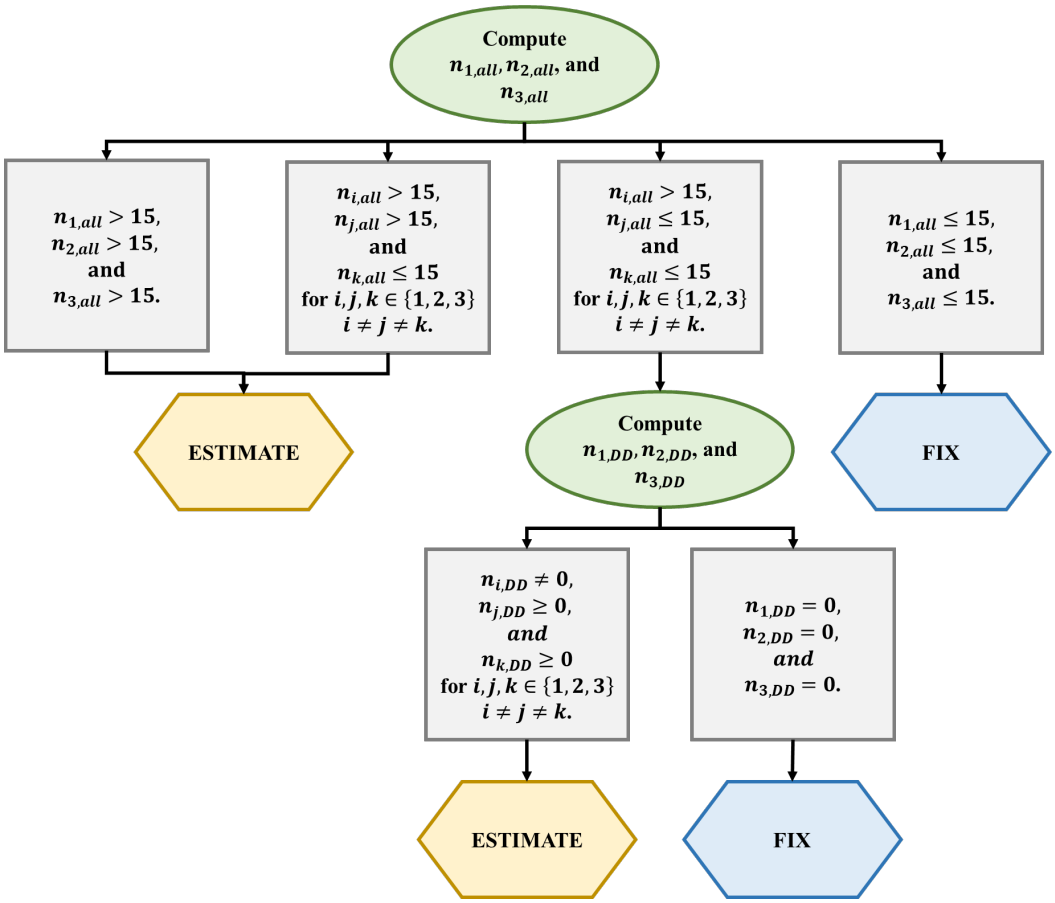

Figure 1. Flowchart of parameter selection algorithm to determine whether a parameter should be fixed or estimated. In the first step, if two or more of the initial conditions have significance counts across all the variables larger than 15, the parameter is estimated. If only one of the initial conditions produces a significance count across the variables larger than 15, the algorithm proceeds to the next step. In the next step significance counts for just the variables for damage and debris at the latest time point (14 days) are calculated. If these counts are positive for at least one of the initial conditions, then the parameter is estimated. Otherwise, the parameter is fixed. Finally, if all of the significance counts across all the variables are less than or equal to 15, then the parameter is fixed.

3.2 Results

The results generated from MeFAST are fed into the parameter selection algorithm to produce a subset of parameters used in the following section for parameter estimation. Parameters not chosen by the algorithm are fixed at their baseline values (given in Table 2). The SA identified the most influential parameters to be related to macrophage function, pathogen dynamics, and inhibition parameters. Parameters related to fibroblasts and lymphocytes were found to be least influential in model output.

3.2.1. Multi-test Extended Fourier Amplitude Sensitivity Test (MeFAST)

MeFAST produced an S_{Ti} value for each parameter, across each variable, for each time point assessed, and each initial condition (IC1, IC2, and IC3), so plots of the S_{Ti} values for each variable can be shown over time for each parameter. Due to the number of parameters, these plots are contained in Appendix B. As mentioned above, S_{Ti} values range between 0 and 1 where values closer to 1 indicate stronger

influence on model output. Plots with many large S_{Ti} values across multiple variables and time points can give an early idea of what parameters are most important allowing us to verify the algorithm results. Parameters that have larger values of S_{Ti} include d_{m1}, d_{mr}, γ_m, k_{pg}, $M1_1^\infty$, N_1^∞, P^∞, s_b, s_{lr}, s_{mr}, s_{nr}. Source rates (s_{lr}, s_{mr} and s_{nr}) are assumed to be highly influential in model output as they control the capacity for the inflammatory response. They were also identified as highly influential in the previous STBM (Creel, Jennings, et al., 2022). Manual simulations also indicated the importance of parameters related to pathogen (k_{pg}, P^∞ and s_b), inhibition ($M1_1^\infty$, N_1^∞), and macrophages (d_{m1} and d_{mr}).

3.2.2. Parameter Selection

The algorithm was implemented to choose which parameters should be estimated and which should be fixed using the results from MeFAST to guide selection. The results of this algorithm are presented in Table 3 organized by model processes.

Table 3. List of parameters to be estimated and fixed during the parameter estimation process as determined by the MeFAST-based selection algorithm.

PARAMETERS TO ESTIMATE	PARAMETERS TO FIX
Inhibition	
$N_1^\infty, M1_1^\infty, M2^\infty$	$Deb_{dam}^\infty, Deb_H, M1_2^\infty, F^\infty, L2_1^\infty, L2_2^\infty, N_H, M1_H$
Inhibition (radiation-related)	
$\gamma_n, \gamma_m, \omega_f$	$\gamma_f, \gamma_l, \omega_{m2}, \omega_{dam}$
Damage and Debris	
k_{dnp}, k_{dm1p}	$k_{dn}, \sigma_{dm1}, d_{deb}, \rho_{dam}, k_{df}, k_{dm2p}$
Neutrophils	
$k_{nd}, s_{nr}, k_{nm1p}, d_n$	$k_{np}, k_{nn}, k_{nm2p}, d_{nr}$
Macrophages	
$k_{m1d}, k_{m1n}, k_{m2m1}, s_{mr}, d_{mr}, d_{m1}, k_{m1p}$	$k_{m1l1}, k_{m1m1}, k_{m2m2}, k_{m2l2}, d_{mrd}, d_{m2}, \theta_{m1m2}$
T Lymphocytes	
k_{l1}	$s_{lr}, d_l, k_{l2}, d_{lr}, d_{lrd}$
Fibroblasts	
	$s_f, k_{ftb}^{ud}, k_{ftb}^d, k_f, \alpha_{dam}, d_f, \alpha_{m2}, d_{fr}, d_{frd}$
Pathogen	
$k_{pg}, P^\infty, k_{pb}, s_b, k_{bp}, k_{pn}$	μ_b, k_{pm1}, k_{pm2}

As expected, the algorithm selected many of the same parameters as in the STBM. Namely, identifying parameters involved in macrophage and neutrophil function, damage and debris, and inhibition. However, the LITBM model identified fewer terms involved in inhibition than the non-irradiated model, particularly those involved in inhibition from anti-inflammatory cells ($M2$ macrophages and $L2$ lymphocytes). Other minor differences are observed in the selection of parameters for neutrophil and macrophage function.

The main difference between the parameter chosen to be estimated for the LITBM and the STBM lies in the parameter chosen for lymphocytes. The LITBM only chose one parameter, k_{l1}, involved in lymphocyte function to be estimated which involves activation rates of the pro-inflammatory $L1$ lymphocytes. The STBM selected all lymphocyte parameters to be estimated; it is clear that these parameters did not appear to be as important in the present model. Additionally, no parameters involved in fibroblast processes were chosen to be estimated in the LITBM. In the STBM only α_{m2} was chosen, which is a constant parameter controlling the upregulation of fibroblasts by $M2$ macrophages. Generally, it seems both models found fibroblast parameters to be of low importance in determining model output.

Parameters that are novel to the present model are those involved in radiation-related inhibition and the pathogen. Selected radiation-related inhibition parameters included initial inhibition of neutrophils and macrophages from radiation damage in the surrounding tissue and inhibition of fibroblast proliferation resulting from cellular damage to fibroblasts. Selected pathogen parameters included the growth rate, carrying capacity, parameters involved in removal by antibodies, and removal of the pathogen by neutrophils. Early exploratory simulations indicated that pathogen parameters were important to model output since perturbations can result in sustained infection ($P_{tb}(t) > 0$ for all t). Sustained infection also results in sustained populations of inflammatory cells representing a diversion from the healed state. Overall, the parameter selection algorithm showed high sensitivity for 26 total parameters, representing 36% of the total parameter set. Parameter estimation methods presented in the following section will provide values for the identified parameters.

Section 4. Parameter Estimation

Due to data limitations and model complexity, systematic parameter estimation methods are required. Parameter estimation was performed only on the set of parameters selected to be estimated from the MeFAST results and parameter selection algorithm, ensuring computation effort is allocated properly to influential model parameters. All simulations and calculations were executed in MATLAB (The MathWorks Inc., 2022).

4.1 Methods

Brute-force with Latin-hypercube sampling (LHS) was used to generate potential parameter sets following the methods described for the parameterization of the STBM (Jennings et al., 2022b). Acceptability criteria was then used to determine whether the parameter sets reproduced biologically observed trends for the various initial conditions. Accepted parameter sets exhibited a wide range of model behavior similar to what would be observed across a population. Accepted parameter sets were then used to select a *representative set*, allowing for visualization of average model behavior.

4.1.1. Acceptability Criteria

Known qualitative results include healing dynamics in the wound space and dose-dependent delays in wound healing, immune cell infiltration, and macrophage polarization. Efforts were also made to ensure that the present model produces results consistent with the STBM in the absence of radiation. This is done by including previous estimates from the STBM for healing times of the superficial thermal burn ($Dam_{tb} = Deb_{tb} = 0.1$) and superficial partial thickness burn ($Dam_{tb} = Deb_{tb} = 0.9$). These are included as the second acceptability criteria (AC2). All criteria used in the selection of parameter sets are included in Table 4.

Table 4. Acceptability criteria for parameter combinations prescribed under LHS.

CRITERIA	BIOLOGICAL DESCRIPTION	MATHEMATICAL REPRESENTATION	REFS.
AC1	Debris must be removed before damaged tissue can be repaired (this is a natural result of the progression of the stages of wound healing)	• $\tau_{deb} < \tau_{dam}$	(Goldberg & Diegelmann, 2010; Schultz et al., 2011)
AC2	In the absence of radiation, the irradiated thermal burn model collapses to the thermal burn model, satisfying previous estimates for healing time	• For a superficial thickness burn ($Dam_{tb}(0) = Deb_{tb}(0) = 0.1$), ▪ $\tau_{dam} = 4.667 \pm 0.5$ days ▪ $\left\|\boldsymbol{X}_{0.1}^{tail} - \boldsymbol{X}^{*}\right\|_2 < 0.3$ ** • For a minor superficial partial thickness burn ($Dam_{tb}(0) = Deb_{tb}(0) = 0.9$), ▪ $\tau_{dam} = 7.833 \pm 0.5$ days ▪ $\left\|\boldsymbol{X}_{0.9}^{tail} - \boldsymbol{X}^{*}\right\|_2 < 0.3$ **	(Abazari et al., 2020; Evers et al., 2010; Jeschke et al., 2020; Peng et al., 2006; Reeves, 2018)
AC3	In the absence of radiation, superficial burns heal without scarring	• $\left\|\boldsymbol{X}_{0.1}^{tail} - \boldsymbol{X}^{*}\right\|_2 < 0.3$ • $\left\|\boldsymbol{X}_{0.9}^{tail} - \boldsymbol{X}^{*}\right\|_2 < 0.3$	(Finnerty et al., 2016)

CRITERIA	BIOLOGICAL DESCRIPTION	MATHEMATICAL REPRESENTATION	REFS.
AC4	Radiation delays wound healing in a dose-dependent manner	• $\tau_{0Gy} < \tau_{1Gy} < \tau_{7Gy} < \tau_{14Gy}$	(Chen et al., 2019; Iddins et al., 2022; Liu et al., 2005; United Nations Scientific Committee on the Effects of Atomic Radiation, 1982)
AC5	Damage to the surrounding tissue delays immune cell infiltration to the wound site	• $\tau_{0Gy}^{Nmax} < \tau_{1Gy}^{Nmax} < \tau_{7Gy}^{Nmax} < \tau_{14Gy}^{Nmax}$ • $\tau_{0Gy}^{Mmax} < \tau_{1Gy}^{Mmax} < \tau_{7Gy}^{Mmax} < \tau_{14Gy}^{Mmax}$ • $\tau_{0Gy}^{Lmax} < \tau_{1Gy}^{Lmax} < \tau_{7Gy}^{Lmax} < \tau_{14Gy}^{Lmax}$ • $\tau_{0Gy}^{Fmax} < \tau_{1Gy}^{Fmax} < \tau_{7Gy}^{Fmax} < \tau_{14Gy}^{Fmax}$	(Iddins et al., 2022; Vegesna et al., 1993)
AC6	Radiation induces macrophage polarization to the classically-activated ($M1_{tb}$) phenotype	• $\tau_{0Gy}^{M2} < \tau_{1Gy}^{M2} < \tau_{7Gy}^{M2} < \tau_{14Gy}^{M2}$	(Rödel et al., 2015)

Notation: Let τ_{dam} and τ_{deb} be the time points such that $Dam(\tau_{dam}) < 0.01$ and $Deb(\tau_{deb}) < 0.01$, respectively.

Let τ_{0Gy}, τ_{1Gy}, τ_{7Gy}, and τ_{14Gy} be the time points such that $Dam(\tau_{0Gy}) < 0.01$, $Dam(\tau_{1Gy}) < 0.01$, $Dam(\tau_{7Gy}) < 0.01$, and $Dam(\tau_{14Gy}) < 0.01$ for a thermal burn irradiated with 0 Gy, 1 Gy, 7 Gy, or 14 Gy, respectively.

Let $\tau_{iGy}^{Nmax}, \tau_{iGy}^{Mmax}, \tau_{iGy}^{Lmax}, \tau_{iGy}^{Fmax}$ for $i = 0, 1, 7, 14$ be the time points such that N_{tb}, $M1_{tb} + M2_{tb}$, $L1_{tb} + L2_{tb}$, and F_{tb}, respectively, reach their maximum values.

Let τ_{iGy}^{M2} for $i = 0, 1, 7, 14$ be the time points such that $\frac{M2_{tb}}{M1_{tb}} > 1$, thus the time points at which the concentration of alternatively-activated macrophages ($M2_{tb}$) is larger than the concentration of classically-activated macrophages ($M1_{tb}$).

** $\|\cdot\|_2$ represents the 2-norm of a matrix, which computes the maximum absolute row sum. $\boldsymbol{X}_{0.1}^{tail}$ and $\boldsymbol{X}_{0.9}^{tail}$ represent the "tail" numerical solution over $t \in [0, 100 * 24]$ (in hours) of all state variables under superficial thickness burn ($Dam_{tb}(0) = Deb_{tb}(0) = 0.1$) and superficial partial thickness burn ($Dam_{tb}(0) = Deb_{tb}(0) = 0.1$), respectively (see Table XX). The healed steady-state is that in which all state variables within the thermal burn, expect fibroblasts, are zero, i.e., $(Dam_{tb}^*, Deb_{tb}^*, N_{tb}^*, M1_{tb}^*, M2_{tb}^*, L1_{tb}^*, L2_{tb}^*, F_{tb}^*, P_{tb}^*)^T = \left(0,0,0,0,0,0,0, \frac{k_{ftb}^{ud}}{d_f - k_f} \cdot \frac{s_f}{k_{ftb}^{ud} + d_{fr}}, 0\right)^T$ where T denotes the transpose of a matrix. Thus, $\boldsymbol{X}^*$ is taken to be $(Dam_{tb}^*, Deb_{tb}^*, N_{tb}^*, M1_{tb}^*, M2_{tb}^*, L1_{tb}^*, L2_{tb}^*, F_{tb}^*, P_{tb}^*)^T$, whence $\left\|\boldsymbol{X}_{0.1}^{tail} - \boldsymbol{X}^*\right\|_2$ and $\left\|\boldsymbol{X}_{0.9}^{tail} - \boldsymbol{X}^*\right\|_2$.

4.1.2. Parameter Distributions and Sampling

Parameters were sampled on a uniform distribution over a prescribed interval since little is known about the parameter values and their respective distributions (Marino et al., 2008). Minimums and maximums of this interval were calculated for the sensitivity analysis and are available in Table 2. Some parameters also had additional restrictions based on biological relevance. For cells in the surrounding tissue, it is assumed that decay rates of damaged cells will be larger than decay rates of undamaged cells. Thus, the following inequalities are enforced for parameter sets where d_{mr}, d_{lr}, and d_{fr} are the decay rates of undamaged resting cells and d_{mr}^{d}, d_{lr}^{d}, and d_{fr}^{d} are the decay rates of resting damaged cells for macrophages, lymphocytes, and fibroblasts, respectively:

1. $d_{mr} < d_{mr}^{d}$
2. $d_{lr} < d_{lr}^{d}$
3. $d_{fr} < d_{fr}^{d}$

Note that only d_{mr} is estimated, so all others are set at their nominal values, satisfying the above inequalities. Some additional inequalities are set to ensure the existence and stability of the healed steady state. The healed steady state exists where all variables in the thermal burn compartment are zero except for F_{tb} which has a small positive value, described by Eq. 1 where $F_{tb}(0)$ represents the value of F_{tb} when $t = 0$ and k_{ftb}^{ud}, d_f, k_f, and d_{fr} are parameters associated with fibroblast function.

$$F_{tb}(0) = \frac{k_{ftb}^{ud}}{d_f - k_f} \cdot \frac{s_f}{k_{ftb}^{ud} + d_{fr}} \quad \text{(Eq. 1)}$$

Since all state variables are defined to be positive values, the steady state value only exists if $d_f - k_f > 0$, so the following inequality must also be satisfied.

4. $k_f < d_f$

These parameters were not chosen to be estimated and thus are set to their nominal values satisfying this inequality.

The parameter estimation of the STBM also included stability analysis and additional parameter restrictions to ensure stability of the healed state. Due to the increased complexity of this model, the stability analysis is not as conclusive. Some necessary inequalities are not identifiable without significant computational effort, so the majority of stability inequalities are excluded. However, inequality 4 above does support stability as well as inequality 5 for the pathogen growth rate where k_{pg}, k_{pb}, s_b, and μ_b are all parameters involved in pathogen dynamics. The restriction on pathogen growth is well defined across multiple math models (Cooper et al., 2015; Reynolds et al., 2006). While they do not ensure stability of the healed state, parameters are sampled satisfying these inequalities to maximize the number of plausible parameter sets produced.

5. $k_{pg} < \frac{k_{pb} s_b}{\mu_b}$

4.1.3. Representative Set

The process of choosing parameter sets for an accepted set produces many plausible parameter sets exhibiting various model behaviors and outcomes. To get an idea of average model behavior, a representative set was chosen following the procedure previously defined for the STBM and other models in mathematical biology (Cooper et al., 2015; Jennings et al., 2022b). Following the previous approach, the mean at each time point across all the accepted parameter combinations is computed for each state variable using the weighted mean sum squared error[1] (MSE) averaged across the variables and initial conditions. Previous implementations defined the representative set by selecting the set with the minimum MSE. A similar process for identifying parameter sets with small MSE was performed for this model, but additional steps were taken to ensure the representative set also offered the best fit of each individual model variable. Since variable scales differ greatly, minimizing the MSE may sacrifice the fit of a variable with smaller overall values for variables with larger overall values that contribute higher residuals to the MSE. To help improve the fit of these variables with smaller scales, the coefficient of determination (R^2)[2] values were also used to guide the selection of the representative set. The parameter sets with MSE values in the bottom 5% of the accepted sets were chosen to be ranked by R^2 values and the representative set was selected by taking the highest ranked set. Since overall MSE varied minimally within the bottom 5%, the selected representative set only slightly compromises on MSE but greatly improves overall fit for some variables. This was verified qualitatively by comparing plots of the two sets and quantitatively by comparing R^2 values. Since select cell populations are currently being investigated for their role in clinical outcomes, it is in the best interest to ensure the representative set accurately models these individual variables.

[1] Let y denote the state variable of the model. Here, weighted mean sum squared error is defined as

$$\frac{1}{N_T}\left(\sum_{i=1}^{N_T}\frac{\left[y_j(t_i)-y_{mean}(t_i)\right]^2}{\sigma_i^2}\right)$$

where N_T is the total number of time points; $y_j(t_i)$ is the model predicted value at time point t_i under the jth parameter combination; $y_{mean}(t_i)$ is the mean of y at time point t_i across all parameter combinations in the accepted set; and σ_i^2 is the variance of y at time point t_i across all parameter combinations in the accepted set.

[2] The coefficient of determination (R^2) is a measure of how well the predicted data explains the variation in the actual outcome. For the present model, the individual model outputs from a given parameter set represents the predicted data and the mean data across the time points represents the actual outcome. The coefficient of determination is calculated by

$$R^2 = 1 - \frac{SS_{Residual}}{SS_{Total}}$$

where $SS_{Residual}$ is the sum of square residuals between the predicted data and the actual data and SS_{Total} is the total variation in the model. Generally, values of R^2 closer to 1 indicate a better fit.

4.2 Results

A total of 400,000 parameter sets were generated by LHS, simulated, and run through the acceptability criteria. Parameter sets were placed in the accepted set if they satisfied all the criteria.

4.2.1. Accepted Parameter Combinations

A total of 22,469 parameter sets were accepted by the criteria. Half violin plots for the parameters showing the overall distributions of the parameters from the resulting accepted sets are presented in Figure 2. Most parameter estimates are relatively uniform across the plausible parameter space. This indicates that the desired dynamics can be observed under many different parameter combinations. The presence of nonlinearities and parameter interactions allows for this to occur. Some parameters do have skewed distributions, indicating preference towards certain values. The parameter s_{mr} is skewed right, indicating higher occurrence in the lower range of this parameter; however, larger values do still exist in the accepted set. Other parameters with slightly skewed distributions include d_n, d_{mr}, k_{pg}, and s_b.

(a)

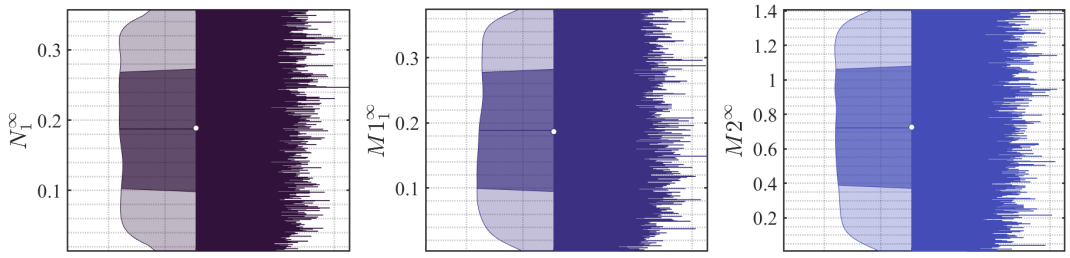

(b)

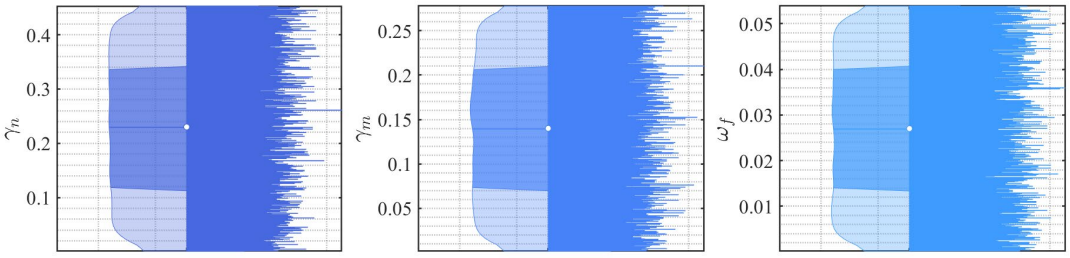

(c)

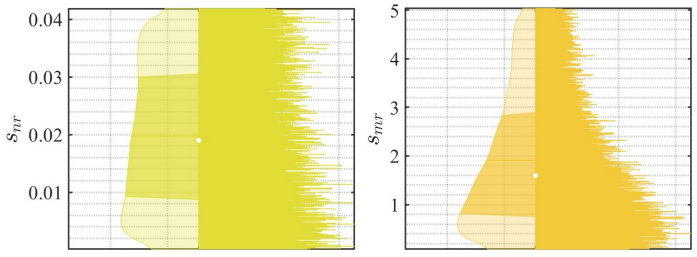

(d)

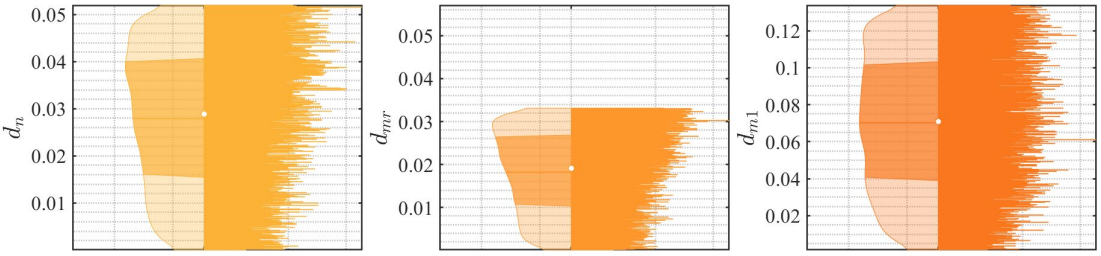

(e)

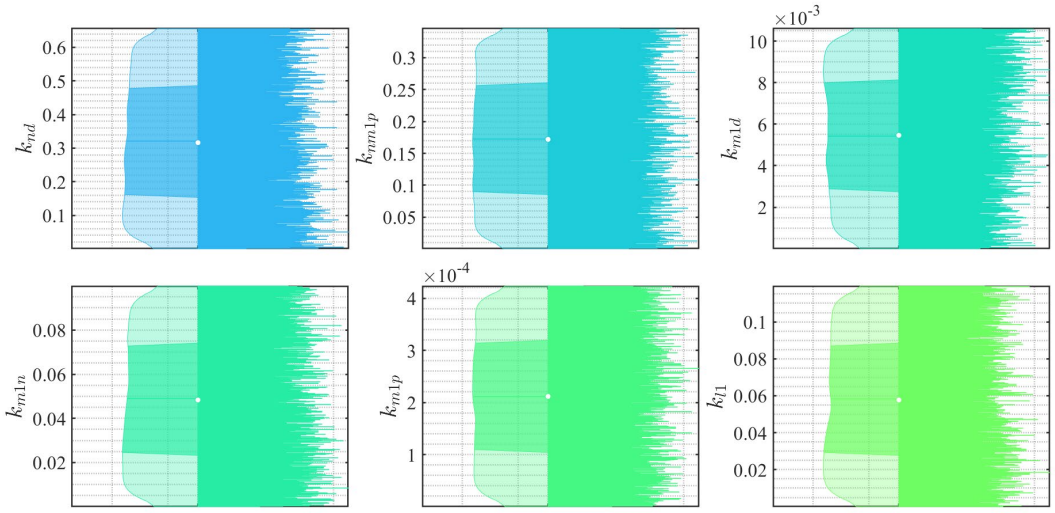

(f)

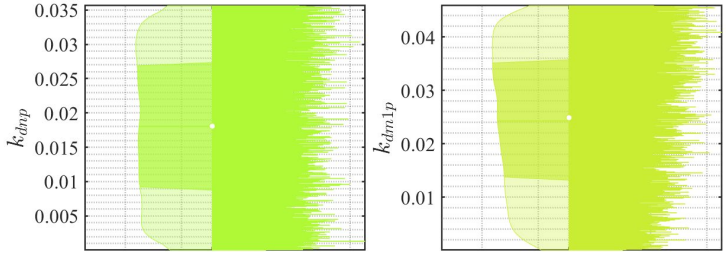

(g)

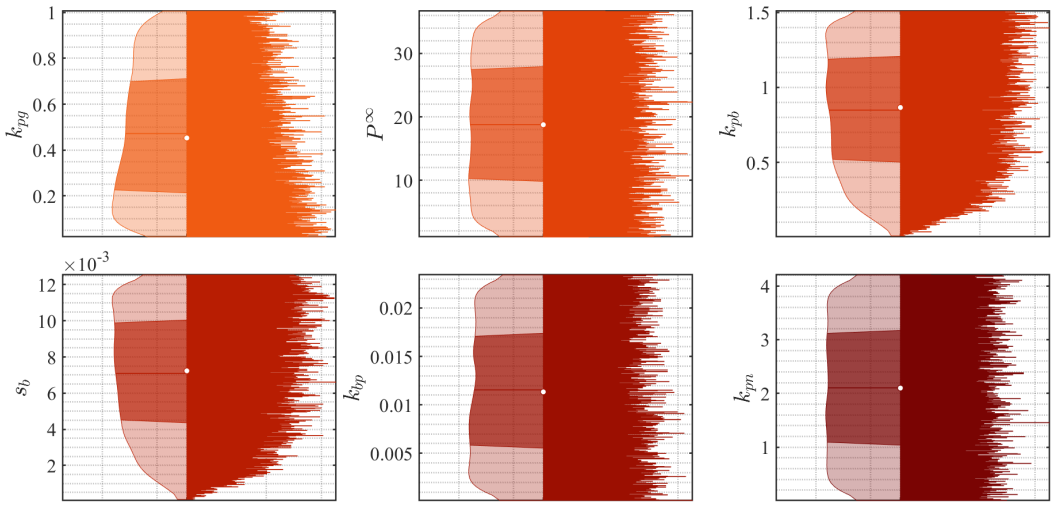

Figure 2. Half-violin plots for the estimated parameter values describing (a) inhibition, (b) radiation-related inhibition, (c) inflammatory cell source rates, (d) inflammatory cell decay rate, (e) pro-inflammatory activation rates, (f) phagocytosis of debris at the wound site, and (g) pathogen dynamics at the wound site. The left-hand side represents a traditional violin plot with the features of a boxplot where the darker shaded region shows the interquartile range with the median marked by the darker line. The mean is represented on the plot by an open circle. The right-hand side shows a standard histogram representation of the parameter estimates.

To exercise model behavior, 100 parameter sets were randomly selected from the accepted sets and simulated on the same plot (Figure 3-Figure 4). The variation observed in the surrounding tissue variables can be directly attributed to the estimated parameters. Some of the parameters (resting cell source rates and decay rates) directly control the initial conditions and carrying capacity for their respective variables. Differing outcomes in the burn compartment correspond with differences in healing times and pathogen population. The variables Dam_{tb} and Deb_{tb}, which indicate healing time, show high variation in resolution time which would likely be observed across a population as healing times vary between individuals. Additionally, there is a significant amount of variation in the variable P_{tb} including the capacity for sustained infection ($P_{tb}(t) > 0$ for all t) which also results in sustained inflammation ($N_{tb}(t)$, $M1_{tb}(t)$, $L1_{tb}(t) > 0$ for all t). The possibility of infection is known to be possible in injuries combined with irradiation (Ledney & Elliott, 2010; Pellmar & Ledney, 2005).

(a) IC1

(b) IC2

(c) IC3

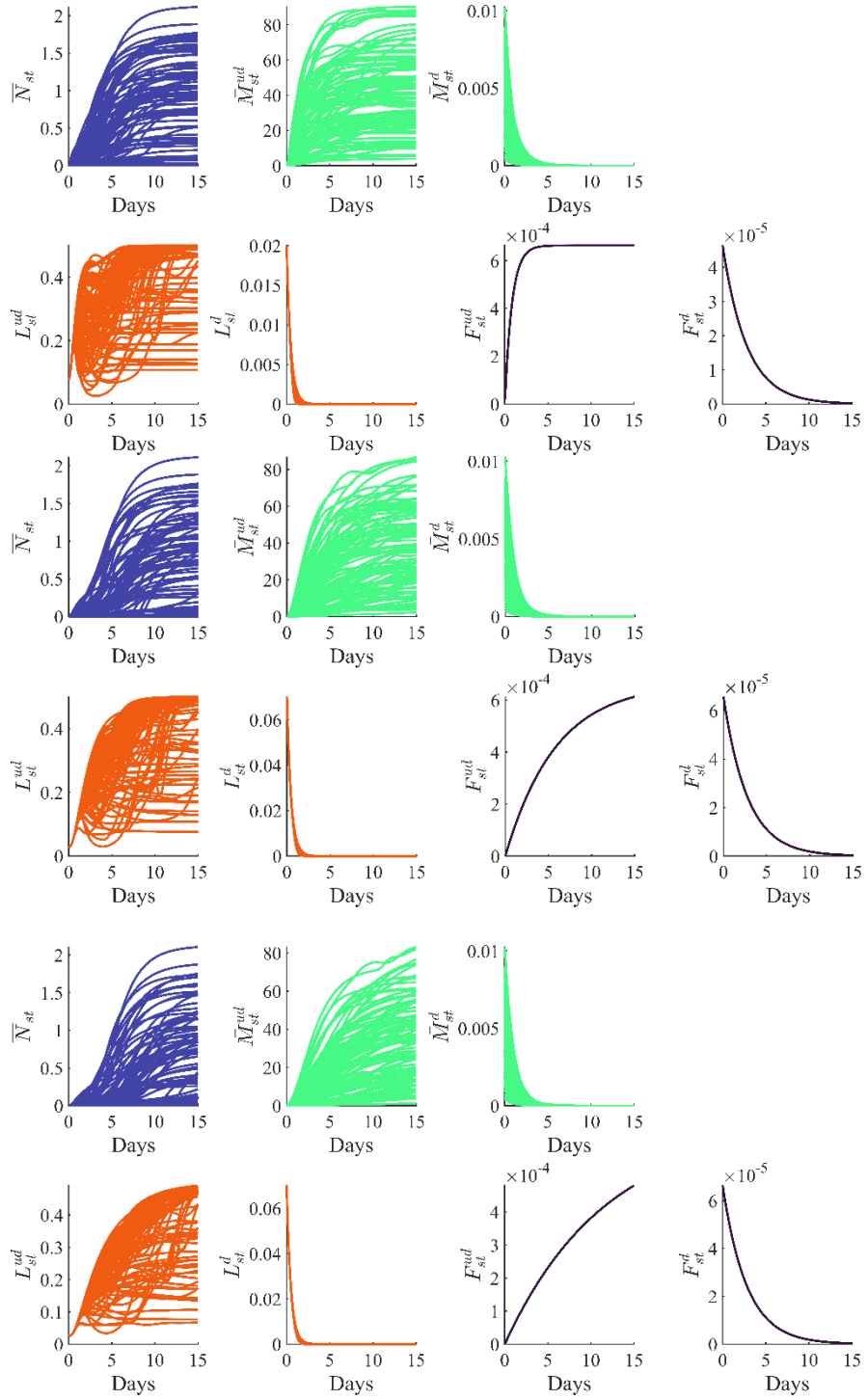

Figure 3. Example dynamics in the surrounding tissue compartment predicted by the TDPM for (a) IC1, (b) IC2, and (c) IC3. The accepted set was randomly sampled and simulated 100 times to show diverse model behavior achieved by the accepted sets. The increase in radiation dose from IC1 to IC3 results in a change in dynamics wherein the return to homeostasis (indicated by a plateau) is correspondingly delayed.

(a) IC1

(b) IC2

(c) IC3

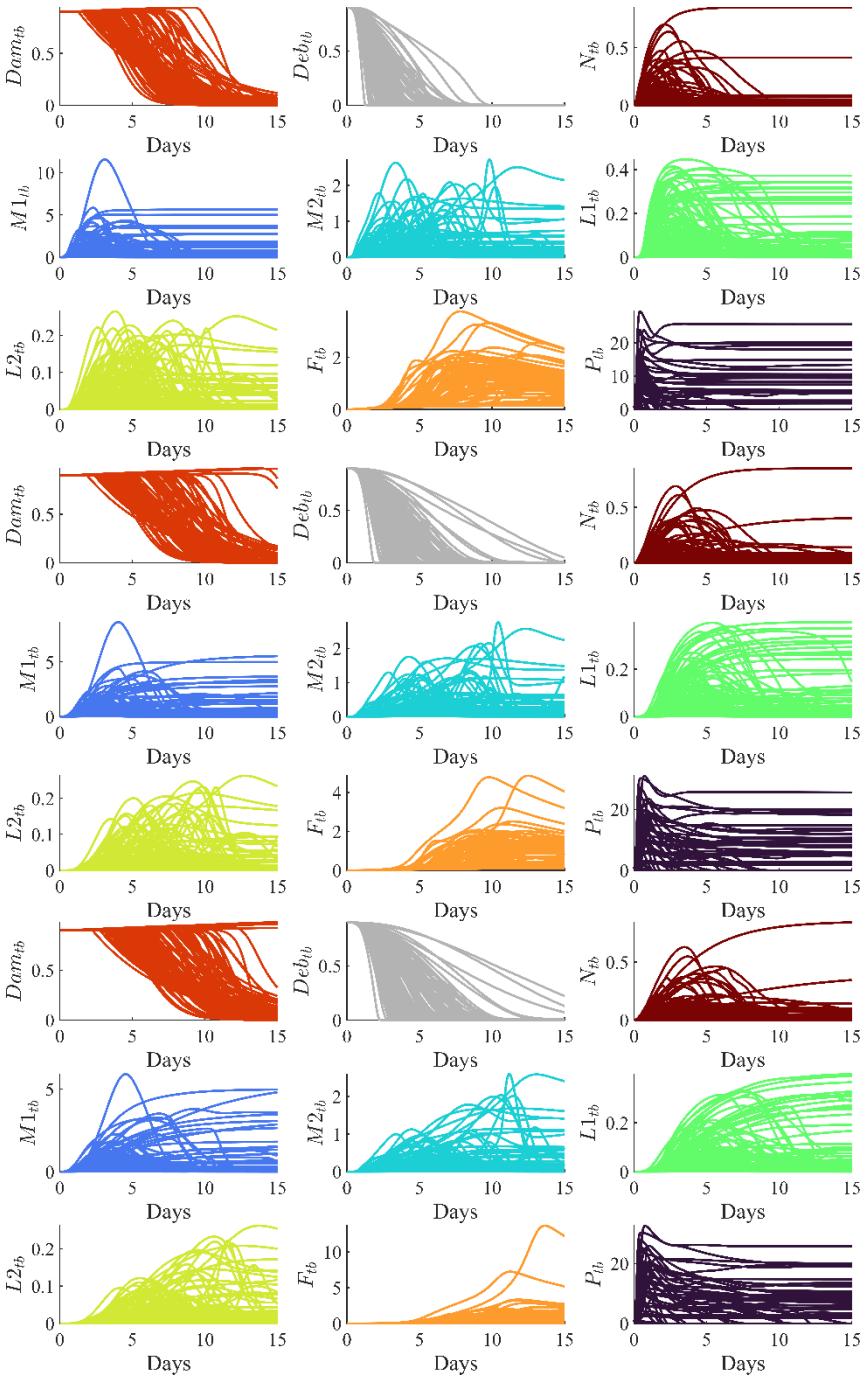

Figure 4. Example dynamics in the thermal burn compartment predicted by the TDPM for (a) IC1, (b) IC2, and (c) IC3. The accepted set was randomly sampled and simulated 100 times to show the diverse model behavior generated by the accepted sets. The increase in radiation dose from IC1 to IC3 results in significant delays in healing times (evidenced by Dam_{tb}), and delays in inflammatory infiltration (shown in variables N_{tb}, $M1_{tb}$, $M2_{tb}$, $L1_{tb}$, and $L2_{tb}$) and fibroblast infiltration. Note that the variable Dam_{tb} indicates a healed wound when its value is less than 0.01.

4.2.2. Representative Set

The representative set was chosen by comparing each of the 22,469 accepted sets with the temporal mean calculated for each variable across all the model simulations. Plots of the representative set compared to the temporal mean for each initial condition are shown in Figure 5 and Figure 6. Visual comparison of the mean response and representative sets shows values close to the temporal mean with similar curvature. For plots where the actual value of the variable differs from the mean response (i.e. $\bar{M}_{st}^{ud}$, $L1_{tb}$, etc.) the general shape of the curve is still consistent with that of the mean response. This is supported by the R^2 values in Table 5 and Table 6. The majority of the variables have R^2 values larger than 0.8, representing good explanation of the mean response by the representative set.

(a) IC1

(b) IC2

(c) IC3

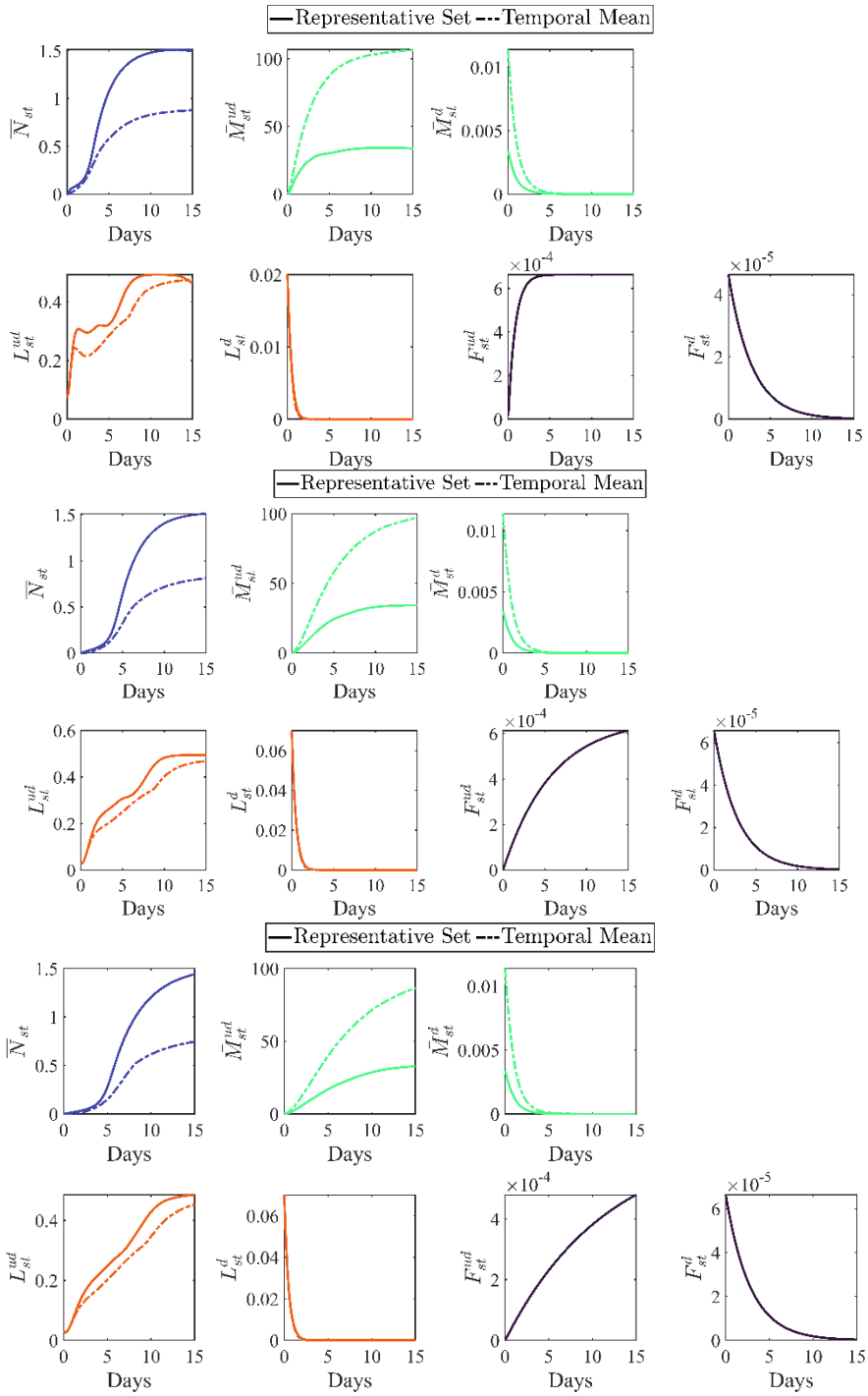

Figure 5. Comparison of dynamics in the surrounding tissue compartment predicted by the representative set (solid lines) and temporal means (dashed lines) for (a) IC1, (b) IC2, and (c) IC3. Overall fit is consistent across initial conditions indicating that the representative set fits the mean response well for varying levels of radiation. The plots show that the representative set produces results close in value for variables for fibroblasts and lymphocytes. As neutrophils and macrophages are heavily dependent on the parameters being estimated, there are differences in the actual value. However, the general curvature matches that of the temporal mean.

(a) IC1

(b) IC2

(c) IC3

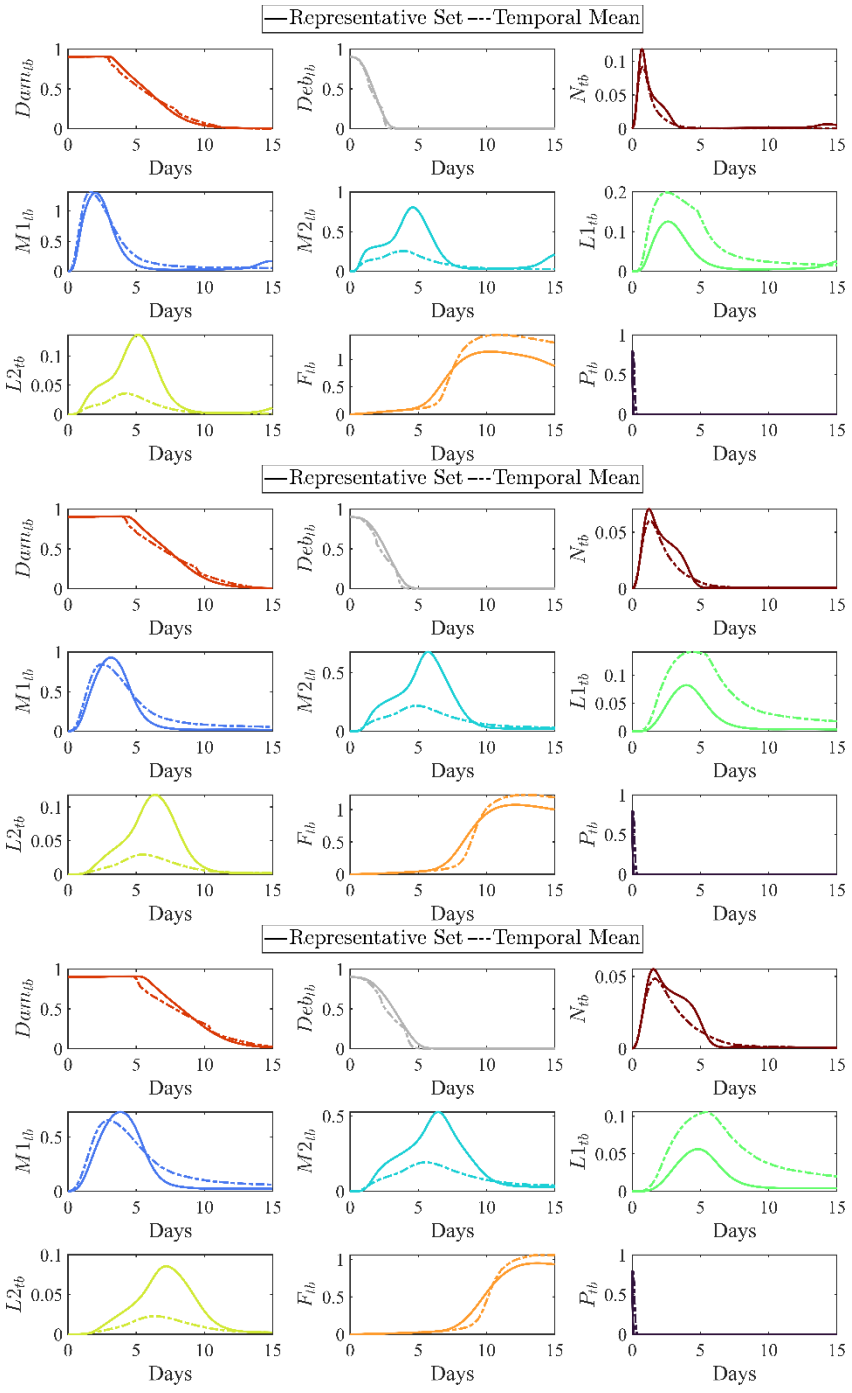

Figure 6. Comparison of dynamics in the thermal burn compartment predicted by the representative set (solid lines) and temporal means (dashed lines) for (a) IC1, (b) IC2, and (c) IC3. The overall fit is consistent across the initial conditions indicating that the representative set represents the temporal mean for various levels of radiation. The representative set is close to the temporal mean in value for the variables describing damage, neutrophils, M1 macrophages, fibroblasts, and pathogen. While the remaining variables show some difference in actual value, similar curvature is still shared particularly in the placement of peaks.

Table 5. R^2 values of the representative set compared to the temporal mean for state variables in the surrounding tissue compartment.

Initial Conditions	State Variable (Surrounding Tissue)						
	$\bar{N}_{st}$	$\bar{M}_{st}^{ud}$	$\bar{M}_{st}^{d}$	L_{st}^{ud}	L_{st}^{d}	F_{st}^{ud}	F_{st}^{d}
IC1	0.9939	0.9713	0.9999	0.9198	0.9980	1.0000	1
IC2	0.9973	0.9876	0.9999	0.9716	0.9995	1.0000	1
IC3	0.9984	0.9971	0.9998	0.9867	0.9998	1.0000	1

Table 6. R^2 values of the representative set compared to the temporal mean for state variables in the thermal burn compartment.

Initial Conditions	State Variable (Thermal Burn)								
	Dam_{tb}	Deb_{tb}	N_{tb}	$M1_{tb}$	$M2_{tb}$	$L1_{tb}$	$L2_{tb}$	F_{tb}	P_{tb}
IC1	0.9920	0.9954	0.9711	0.9646	0.8092	0.8622	0.8681	0.9651	0.3873
IC2	0.9874	0.9905	0.9622	0.9492	0.8692	0.8652	0.8906	0.9681	0.3727
IC3	0.9802	0.9853	0.9526	0.9263	0.8911	0.8607	0.8984	0.9763	0.3709

Figure 7 shows plots of the model variables normalized between 0 and 1 and plotted over each other to show the progression of wound phases and compare between the initial conditions. Comparing between the thermal burn variables, the delay in the various phases of wound healing is clear from the placement of the peaks for the inflammatory cells and the fibroblasts. The delays in clearance of damage and debris are also clear between the initial conditions.

(a) IC1

(b) IC2

(c) IC3

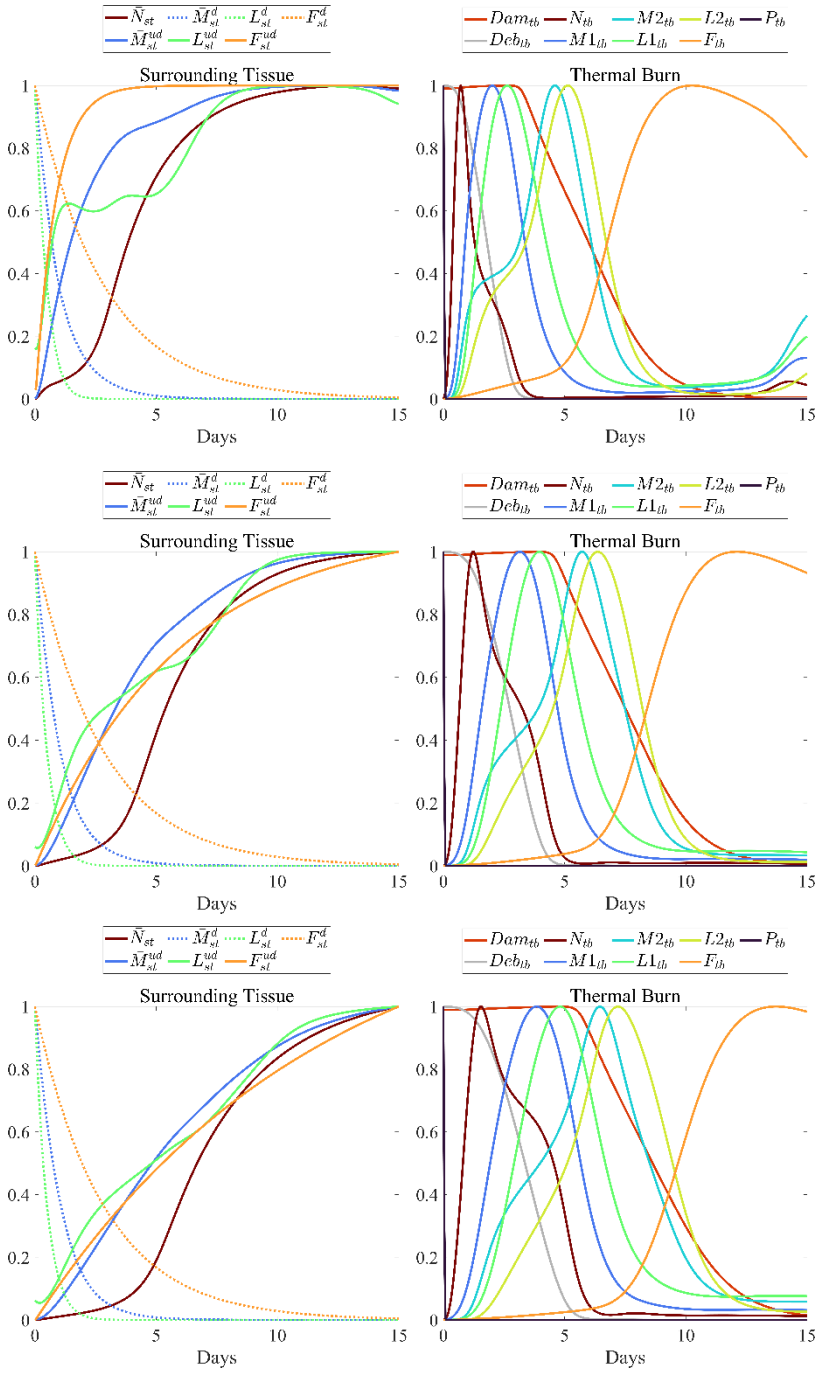

Figure 7. Normalized time-series predictions of the TDPM using the representative set for (a) IC1, (b) IC2, and (c) IC3. The right-hand plots show the variables in the surrounding tissue compartment and the left-hand plots show the variables in the thermal burn compartment. The variables are normalized to represent delays in maximum values of variables across the initial conditions and compare between pro-inflammatory cells (N_{tb}, $M1_{tb}$, and $L1_{tb}$) and anti-inflammatory cells ($M2_{tb}$ and $L2_{tb}$). As expected, pro-inflammatory cells are in decline as anti-inflammatory cells peak. Additionally, fibroblasts reach maximum values after the inflammatory response has resolved as expected in normal wound healing.

Section 5. Discussion

The individual injuries associated with this model (superficial thermal burn and localized radiation exposure) are not typically severe on their own. However, combined injuries typically exhibit synergistic effects resulting in a combined injury with greater effects than the sum of the individual injuries (Reeves, 2018). Combined injuries are generally associated with greater magnitude of health effects, complications, and impaired wound healing. Most recent models developed by ARA have focused on combined injury due to these synergistic effects and overall prevalence in NUDET events (DiCarlo et al., 2008; Palmer et al., 2011; Pellmar & Ledney, 2005) . The present model focuses on survivable injuries requiring little to no medical intervention as there are currently no well-defined methods for predicting performance decrement for these types of injuries. More severe injuries will likely result in complete decay of performance or even death whereas the present injury model has the capacity for varying degrees of performance decrement for varying amounts of time.

Despite the prevalence of combined injury, little to no data exists for this type of injury, so a formal parameter estimation paired with sensitivity analysis was necessary to produce plausible parameter sets. Sensitivity analysis identified a set of 26 influential parameters out of the 73 total model parameters to estimate, greatly reducing the number of parameters necessary for sampling and estimation efforts. Influential parameters were primarily those involved in macrophage dynamics, inhibition, and the pathogen. Macrophage dynamics are often identified as important drivers of wound outcome in other mathematical models (Minucci et al., 2021; Torres et al., 2019). Pathogen dynamics were newly introduced for this model and are a hallmark of radiation injury. Ionizing radiation exposure is associated with risk of infection for both localized (Hill et al., 2004) and whole-body exposure (Carter et al., 2016; Elliott et al., 1990; Landauer et al., 2001; Ran et al., 2003), supporting its importance in the model. Parameters involved in inhibition were also assumed to be influential from early model simulations where manual perturbation of these parameters produced large deviations in model output. The parameterization of the STBM also identified macrophage parameters and inhibition parameters as highly influential. The main difference between the parameterization results of the STBM and the LITBM is the estimation of lymphocyte parameters. All lymphocyte parameters were chosen to be estimated in the STBM whereas only one parameter was chosen for the LITBM. One explanation may be that the presence of pathogen upregulates the activation of the innate inflammatory cells (neutrophils and macrophages), thus there is less need for the adaptive immune response from lymphocytes for clearing damage and debris. Some populations of T lymphocytes do phagocytize bacteria (i.e. cytotoxic T cells) (Barry & Bleackley, 2002); however, these populations are excluded from the LITBM. Due to this observation, future models may consider either including more populations of T cells to get a better picture of overall importance or consider removing them entirely if they do not contribute significantly to changes in model dynamics.

The final steps of parameter estimation included the selection of a representative set to best exhibit average model behavior. The representative set reproduced expected delays in wound healing and immune cell infiltration in a dose dependent manor. Statistical measures of model fit using R^2 also produced generally high values across the model variables indicating a good explanation of the mean response by the representative set.

To implement this parameterized model in HENRE, future work includes initial condition mapping for the insult-to-outcome pipeline. Initial condition mapping for the LITBM is currently in the final stages of development. Additional research into connecting physiological state variables to clinical outcomes and performance decrement is underway, to be fully realized in conjunction with the introduction of systemic models of combined injury. Whole body radiation exposure is more likely than the local irradiation described in the model presented here but presents additional challenges. The LITBM purposefully serves as an intermediate step to ensure consistently accurate model development and implementation while expanding the combined injury mechanistic modeling framework using TDPMs. Systemic models, leveraging and modifying legacy models of the hematopoietic system, are in development to build on this work.

In summary, this parameterized time-dependent physiological model of a locally irradiated thermal burn represents the first combined injury within the wound healing framework and is a crucial step towards a systems-level model of combined injury effects that will inform measures of clinical outcomes and performance decrement for combined injury in the event of a nuclear detonation. Implementation of this parameterized model into HENRE will immediately provide quantification of delay in predicted wound healing times and insight into pathophysiological responses that affect clinical outcomes. Future development work will be focused on systemic modeling to support growth of the combined injury analyses available in HENRE to support medical planning and estimates of combat power.

Section 6. References

Abazari, M., Ghaffari, A., Rashidzadeh, H., Badeleh, S. M., & Maleki, Y. (2020). A systematic review on classification, identification, and healing process of burn wound healing. *International Journal of Lower Extremity Wounds*, 1–13.

Abdi, H. (2007). Bonferroni and Šidák corrections for multiple comparisons. *Encyclopedia of Measurement and Statistics*, *3*, 103–107.

Barry, M., & Bleackley, R. C. (2002). Cytotoxic T lymphocytes: All roads lead to death. *Nature Reviews Immunology*, *2*(6), 401–409. https://doi.org/10.1038/nri819

Benjamini, Y., & Hochberg, Y. (1995). Controlling the False Discovery Rate: A Practical and Powerful Approach to Multiple Testing. *Journal of the Royal Statistical Society: Series B (Methodological)*, *57*(1), 289–300. https://doi.org/10.1111/j.2517-6161.1995.tb02031.x

Carter, S. R., Chen, M. M., Palmer, J. L., Wang, L., Ramirez, L., Plackett, T. P., Gamelli, R. L., & Kovacs, E. J. (2016). Neutrophil Accumulation in the Small Intestine Contributes to Local Tissue Destruction Following Combined Radiation and Burn Injury. *Journal of Burn Care & Research*, *37*(2), 97–105. https://doi.org/10.1097/BCR.0000000000000220

Chen, Y., Zhang, Q., Wu, Y., Branch-Brooks, C. D., & Butler, C. E. (2019). Short-term influences of radiation on musculofascial healing in a laparotomy rat model. *Scientific Reports*, *9*(1), Article 1. https://doi.org/10.1038/s41598-019-48201-5

Cooper, R. L., Segal, R. A., Diegelmann, R. F., & Reynolds, A. M. (2015). Modeling the effects of systemic mediators on the inflammatory phase of wound healing. *Journal of Theoretical Biology*, *367*, 86–99. https://doi.org/10.1016/j.jtbi.2014.11.008

Creel, A. (2021). *Global Sensitivity Analysis for Mathematical Models in Biology* (ARA-HS-TN-21-014-A). Applied Research Associates, Inc., Arlington, VA.

Creel, A., Hay, Q., & Jennings, R. (2022). *Preliminary Sensitivity Results for a Time-Dependent Physiological Model of Irradiated Thermal Burns* (ARA-HS-TN-22-016-A). Applied Research Associates, Inc., Arlington, VA.

Creel, A., Jennings, R., & Reynolds, A. (2022). *Sensitivity Analysis for a Time-Dependent Physiological Model of Superficial Thermal Burns* (DTRA-TR-21-063 R1). Defense Threat Reduction Agency, Fort Belvoir, VA.

Dela, A., Shtylla, B., & de Pillis, L. (2022). Multi-method global sensitivity analysis of mathematical models. *Journal of Theoretical Biology*, *546*, 111159. https://doi.org/10.1016/j.jtbi.2022.111159

DiCarlo, A. L., Hatchett, R. J., Kaminski, J. M., Ledney, G. D., Pellmar, T. C., Okunieff, P., & Ramakrishnan, N. (2008). Medical Countermeasures for Radiation Combined Injury: Radiation with Burn, Blast, Trauma and/or Sepsis. Report of an NIAID Workshop, March 26–27, 2007. *Radiation Research*, *169*(6), 712–721. https://doi.org/10.1667/RR1295.1

Elliott, T. B., Brook, I., & Stiefel, S. M. (1990). Quantitative study of wound infection in irradiated mice. *International Journal of Radiation Biology*, *58*(2), 341–350. https://doi.org/10.1080/09553009014551671

Evers, L. H., Bhavsar, D., & Mailänder, P. (2010). The biology of burn injury. *Experimental Dermatology*, *19*(9), 777–783. https://doi.org/10.1111/j.1600-0625.2010.01105.x

Finnerty, C. C., Jeschke, M. G., Branski, L. K., Barret, J. P., Dziewulski, P., & Herndon, D. N. (2016). Hypertrophic scarring: The greatest unmet challenge following burn injury. *Lancet (London, England)*, *388*(10052), 1427–1436. https://doi.org/10.1016/S0140-6736(16)31406-4

Goldberg, S. R., & Diegelmann, R. F. (2010). Wound Healing Primer. *Surgical Clinics of North America*, *90*(6), 1133–1146. https://doi.org/10.1016/j.suc.2010.08.003

Hay, Q., Jennings, R., Reynolds, A. M., & Creel, A. (2022). *A TDPM of Healing Initiated by an Irradiated Superficial Thermal Burn* (DTRA-TR-22-067). Defense Threat Reduction Agency, Fort Belvoir, VA.

Hill, A., Hanson, M., Bogle, M. A., & Duvic, M. (2004). Severe Radiation Dermatitis is Related to Staphylococcus Aureus. *American Journal of Clinical Oncology*, *27*(4), 361. https://doi.org/10.1097/01.COC.0000071418.12121.C2

Iddins, C. J., DiCarlo, A. L., Ervin, M. D., Herrera-Reyes, E., & Goans, R. E. (2022). Cutaneous and Local Radiation Injuries. *Journal of Radiological Protection : Official Journal of the Society for Radiological Protection*, *42*(1), 10.1088/1361-6498/ac241a. https://doi.org/10.1088/1361-6498/ac241a

Iijima, S. (1982). Pathology of atomic bomb casualties. *Acta Pathologica Japonica*, *32 Suppl 2*, 237–270.

Jennings, R., Creel, A., & Reynolds, A. (2022a). *A Time-Dependent Physiological Model of Innate and Adaptive Immune Responses Activated by Superficial Thermal Burns* (DTRA-TR-21-032 R1). Defense Threat Reduction Agency, Fort Belvoir, VA.

Jennings, R., Creel, A., & Reynolds, A. (2022b). *Estimation of Inflammation and Repair Parameters for a Superficial Thermal Burn* (DTRA-TR-22-026). Defense Threat Reduction Agency, Fort Belvoir, VA.

Jeschke, M. G., van Baar, M. E., Choudhry, M. A., Chung, K. K., Gibran, N. S., & Logsetty, S. (2020). Burn injury. *Nature Reviews. Disease Primers*, *6*(1), 11. https://doi.org/10.1038/s41572-020-0145-5

Kishi, H. S. (2000). Effects of the "special bomb": Recollections of a neurosurgeon in Hiroshima, August 8-15, 1945. *Neurosurgery*, *47*(2), 441–445; discussion 445-6. https://doi.org/10.1097/00006123-200008000-00034

Landauer, M. R., Elliott, T. B., King, G. L., Bouhaouala, S. S., Wilhelmsen, C. L., Ferrell, J. L., Wang, P. S., Chap, A. D., & Knudson, G. B. (2001). Performance Decrement after Combined Exposure to Ionizing Radiation and Shigella sonnei. *Military Medicine*, *166*(suppl_2), 71–73. https://doi.org/10.1093/milmed/166.suppl_2.71

Lateef, Z., Stuart, G., Jones, N., Mercer, A., Fleming, S., & Wise, L. (2019). The Cutaneous Inflammatory Response to Thermal Burn Injury in a Murine Model. *International Journal of Molecular Sciences*, *20*(3), Article 3. https://doi.org/10.3390/ijms20030538

Ledney, G. D., & Elliott, T. B. (2010). Combined injury: Factors with potential to impact radiation dose assessments. *Health Physics*, *98*(2), 145–152. https://doi.org/10.1097/01.HP.0000348466.09978.77

Ledney, G. D., Madonna, G. S., Elliott, T. B., Moore, M. M., & Jackson, W. 3rd. (1991). Therapy of infections in mice irradiated in mixed neutron/photon fields and inflicted with wound trauma: A review of current work. *Radiation Research*, *128*(1 Suppl), S18-28.

Liu, X., Liu, J.-Z., Zhang, E., Li, P., Zhou, P., Cheng, T.-M., & Zhou, Y.-G. (2005). Impaired Wound Healing after Local Soft X-Ray Irradiation in Rat Skin: Time Course Study of Pathology, Proliferation, Cell Cycle, and Apoptosis. *Journal of Trauma and Acute Care Surgery*, *59*(3), 682. https://doi.org/10.1097/01.ta.0000177674.55388.40

Mann, H. B., & Whitney, D. R. (1947). On a Test of Whether one of Two Random Variables is Stochastically Larger than the Other. *The Annals of Mathematical Statistics*, *18*(1), 50–60. https://doi.org/10.1214/aoms/1177730491

Marino, S., Hogue, I. B., Ray, C. J., & Kirschner, D. E. (2008). A Methodology For Performing Global Uncertainty And Sensitivity Analysis In Systems Biology. *Journal of Theoretical Biology*, *254*(1), 178–196. https://doi.org/10.1016/j.jtbi.2008.04.011

Minucci, S., Heise, R. L., Valentine, M. S., Kamga Gninzeko, F. J., & Reynolds, A. M. (2021). Mathematical modeling of ventilator-induced lung inflammation. *Journal of Theoretical Biology*, *526*, 110738. https://doi.org/10.1016/j.jtbi.2021.110738

Moore, J. H. (1999). Bootstrapping, permutation testing and the method of surrogate data. *Physics in Medicine and Biology*, *44*(6), L11–L12. https://doi.org/10.1088/0031-9155/44/6/101

Palmer, J. L., Deburghgraeve, C. R., Bird, M. D., Hauer-Jensen, M., & Kovacs, E. J. (2011). Development of a Combined Radiation and Burn Injury Model. *Journal of Burn Care & Research : Official Publication of the American Burn Association*, *32*(2), 317–323. https://doi.org/10.1097/BCR.0b013e31820aafa9

Pellmar, T. C., & Ledney, G. D. (2005). *Combined Injury: Radiation in Combination with Trauma, Infectious Disease, or Chemical Exposures*. d

Peng, D., Huang, W., Ai, S., & Wang, S. (2006). Clinical significance of leukocyte infiltrative response in deep wound of patients with major burns. *Burns*, *32*(8), 946–950. https://doi.org/10.1016/j.burns.2006.03.003

Ran, X., Cheng, T., Lin, Y., Qu, J., Liu, D., Al, G., Yan, G., Wang, W., & Xu, R. (2003). Dose-effect relationships in total body irradiation on the healing of cutaneous wounds. *Chinese Medical Journal*, *116*(06), 878–882. https://doi.org/10.3760/cma.j.issn.0366-6999.2003.06.118

Reeves, G. I. (2018). Chapter 14: Effects on Personnel. In *EM-1: Capabilities of Nuclear Weapons*.

Reynolds, A., Rubin, J., Clermont, G., Day, J., Vodovotz, Y., & Bard Ermentrout, G. (2006). A reduced mathematical model of the acute inflammatory response: I. Derivation of model and analysis of anti-inflammation. *Journal of Theoretical Biology*, *242*(1), 220–236. https://doi.org/10.1016/j.jtbi.2006.02.016

Rödel, F., Frey, B., Multhoff, G., & Gaipl, U. (2015). Contribution of the immune system to bystander and non-targeted effects of ionizing radiation. *Cancer Letters*, *356*(1), 105–113. https://doi.org/10.1016/j.canlet.2013.09.015

Schultz, G. S., Chin, G. A., Moldawer, L., & Diegelmann, R. F. (2011). Principles of Wound Healing. In *Mechanisms of Vascular Disease: A Reference Book for Vascular Specialists*. University of Adelaide Press. https://www.ncbi.nlm.nih.gov/books/NBK534261/

The MathWorks Inc. (2022). *MATLAB version: 9.12.0 (R2022a) Update 2* [Computer software]. The MathWorks Inc. https://www.mathworks.com

Torres, M., Wang, J., Yannie, P. J., Ghosh, S., Segal, R. A., & Reynolds, A. M. (2019). Identifying important parameters in the inflammatory process with a mathematical model of immune cell

influx and macrophage polarization. *PLOS Computational Biology*, *15*(7), e1007172. https://doi.org/10.1371/journal.pcbi.1007172

United Nations Scientific Committee on the Effects of Atomic Radiation. (1982). *Ionizing Radiation, Sources and Biological Effects, United Nations Scientific Committee on the Effects of Atomic Radiation (UNSCEAR) 1982 Report: Report to the General Assembly, with Scientific Annexes*. United Nations. https://doi.org/10.18356/34127272-en

Vegesna, V., Withers, R. H., Holly, E. F., & McBride, W. H. (1993). The Effect of Local and Systemic Irradiation on Impairment of Wound Healing in Mice. *Radiation Research*, *135*(3), 431–433.

Wang, C. (2014). Assessment and Physiology of Burns. In C. S. Scher (Ed.), *Anesthesia for Trauma: New Evidence and New Challenges* (pp. 271–289). Springer. https://doi.org/10.1007/978-1-4939-0909-4_13

Appendix A. Model Equations

$$\frac{dDam_{tb}}{dt} = k_{dn}\Omega_H(\Omega_i(N_{tb}; L2_{tb}, L2_2^{\infty}), 6, N_H) + k_{dm1}\Omega_H(\Omega_i(M1_{tb}; L2_{tb}, L2_2^{\infty}), 6, M1_H) - \rho_{dam}\Omega_i(Dam_{tb}; Deb_{tb}, Deb_{dam}^{\infty}) - \Omega_i\left(F_{tb}; F_{st}^{d}, \omega_{dam}\right)k_{df}\Omega_i(Dam_{tb}; Deb_{tb}, Deb_{dam}^{\infty}) \quad (A.1)$$

$$\frac{dDeb_{tb}}{dt} = k_{dn}\Omega_H(\Omega_i(N_{tb}; L2_{tb}, L2_2^{\infty}), 6, N_H) + k_{dm1}\Omega_H(\Omega_i(M1_{tb}; L2_{tb}, L2_2^{\infty}), 6, M1_H) - k_{dnp}N_{tb}\Omega_H(Deb_{tb}, 1, Deb_H) - k_{dm1p}\Omega_i(M1_{tb}; N_{tb}, N_1^{\infty})\Omega_H(Deb_{tb}, 1, Deb_H) - k_{dm2p}\Omega_i(M2_{tb}; N_{tb}, N_1^{\infty})\Omega_H(Deb_{tb}, 1, Deb_H) - d_{deb}Deb_{tb} \quad (A.2)$$

$$\frac{d\bar{N}_{st}^{ud}}{dt} = v(t, Dose_{rad}; \gamma_n)s_{nr} - R_n\bar{N}_{st}^{ud} - d_{nr}\bar{N}_{st}^{ud} \quad (A.3)$$

$$\frac{dN_{tb}}{dt} = R_n\bar{N}_{st}^{ud} - k_{nm1p}N_{tb}\Omega_i(M1_{tb}; N_{tb}, N_1^{\infty}) - k_{nm2p}N_{tb}\Omega_i(M2_{tb}; N_{tb}, N_1^{\infty}) - d_nN_{tb} \quad (A.4)$$

$$\frac{d\bar{M}_{st}^{ud}}{dt} = v(t, Dose_{rad}; \gamma_m)s_{mr} - R_{m1}\bar{M}_{st}^{ud} - \Omega_i\left(R_{m2}; \bar{M}_{st}^{d}, \omega_{m2}\right)\bar{M}_{st}^{ud} - d_{mr}^{ud}\bar{M}_{st}^{ud} \quad (A.5)$$

$$\frac{d\bar{M}_{st}^{d}}{dt} = -R_{m1}\bar{M}_{st}^{d} - \Omega_i\left(R_{m2}; \bar{M}_{st}^{d}, \omega_{m2}\right)\bar{M}_{st}^{d} - d_{mr}^{d}\bar{M}_{st}^{d} \quad (A.6)$$

$$\frac{dM1_{tb}}{dt} = R_{m1}\left(\bar{M}_{st}^{ud} + \bar{M}_{st}^{d}\right) - \theta_{m1m2}\left[k_{nm1p}N_{tb}\Omega_i(M1_{tb}; N_{tb}, N_1^{\infty})\right] - d_{m1}M1_{tb} \quad (A.7)$$

$$\frac{dM2_{tb}}{dt} = \Omega_i\left(R_{m2}; \bar{M}_{st}^{d}, \omega_{m2}\right)\left(\bar{M}_{st}^{ud} + \bar{M}_{st}^{d}\right) + \theta_{m1m2}\left[k_{nm1p}N_{tb}\Omega_i(M1_{tb}; N_{tb}, N_1^{\infty})\right] - d_{m2}M2_{tb} \quad (A.8)$$

$$\frac{dL_{st}^{ud}}{dt} = v(t, Dose_{rad}; \gamma_l)s_{lr} - R_{l1}L_{st}^{ud} - R_{l2}L_{st}^{ud} - d_{lr}^{ud}L_{st}^{ud} \quad (A.9)$$

$$\frac{dL_{st}^{d}}{dt} = -R_{l1}L_{st}^{d} - R_{l2}L_{st}^{d} - d_{lr}^{d}L_{st}^{d} \quad (A.10)$$

$$\frac{dL1_{tb}}{dt} = R_{l1}L_{st}^{ud} + R_{l1}L_{st}^{d} - d_lL1_{tb} \quad (A.11)$$

$$\frac{dL2_{tb}}{dt} = R_{l2}L_{st}^{ud} + R_{l2}L_{st}^{d} - d_lL2_{tb} \quad (A.12)$$

$$\frac{dF_{st}^{ud}}{dt} = v\left(t, Dose_{rad}; \gamma_f\right) s_f - k_{sttb}^{ud} F_{st}^{ud} - d_{fr}^{ud} F_{st}^{ud} \tag{A.13}$$

$$\frac{dF_{st}^{d}}{dt} = -k_{sttb}^{d} F_{st}^{d} - d_{fr}^{d} F_{st}^{d} \tag{A.14}$$

$$\begin{aligned}\frac{dF_{tb}}{dt} = {} & k_{sttb}^{ud} F_{st}^{ud} + k_{sttb}^{d} F_{st}^{d} \\ & + \Omega_i\left(1; F_{st}^{d}, \omega_f\right)\Omega_i(F_{tb}; N_{tb}, N_2^{\infty}, M1_{tb}, M1_2^{\infty})\left(k_f \right. \\ & \left. + \alpha_{dam} Dam_{tb} + \alpha_{m2} M2_{tb}\right) - d_f F_{tb}\end{aligned} \tag{A.15}$$

$$\begin{aligned}\frac{dP_{tb}}{dt} = {} & k_{pg} P_{tb}\left(1 - \frac{P_{tb}}{P^{\infty}}\right) - \frac{k_{pb} s_b P_{tb}}{\mu_b + k_{bp} P_{tb}} - k_{pn} P_{tb} N_{tb} - k_{pm1} P_{tb} \Omega_i(M1_{tb}; N_{tb}, N_1^{\infty}) \\ & - k_{pm2} P_{tb} \Omega_i(M2_{tb}; N_{tb}, N_1^{\infty}).\end{aligned} \tag{A.16}$$

where

$$\Omega_i(X; Y_1, Y_1^{\infty}, \ldots, Y_m, Y_m^{\infty}) = \frac{X}{1 + ©+\ldots+\left(\frac{Y_m}{Y_m^{\infty}}\right)^2} \tag{A.17}$$

$$\Omega_H(X, n, X_H) = \frac{X^n}{X_H^n + X^n} \tag{A.18}$$

$$v(t, Dose_{rad}; \gamma) = \begin{cases} 1, & Dose_{rad} = 0 \\ 1 - exp\left(-\dfrac{\gamma}{Dose_{rad}} t\right), & Dose_{rad} > 0 \end{cases} \tag{A.19}$$

$$R_n = \Omega_i\left(k_{nd} Deb_{tb} + k_{np} P_{tb} + k_{nn} N_{tb}; M2_{tb}, M2^{\infty}, L2_{tb}, L2_1^{\infty}\right) \tag{A.20}$$

$$s_{nr} = \bar{\eta}_{bvtb} \overline{N}_{bv}. \tag{A.21}$$

$$\begin{aligned}R_{m1} = \Omega_i\big(k_{m1d} Deb_{tb} + k_{m1p} P_{tb} + k_{m1n} N_{tb} + k_{m1m1} M1_{tb} \\ + k_{m1l1} L1_{tb}; M2_{tb}, M2^{\infty}, L2_{tb}, L2_1^{\infty}\big)\end{aligned} \tag{A.22}$$

$$R_{m2} = \Omega_i(k_{m2m1} M1_{tb} + k_{m2m2} M2 + k_{m2l2} L2; N_{tb}, N_1^{\infty}, M1_{tb}, M1_1^{\infty}, F_{tb}, F^{\infty}) \tag{A.23}$$

$$s_{mr} = \overline{\mu}_{bvtb} \overline{M}_{bv} \tag{A.24}$$

$$R_{l1} = \Omega_i(k_{l1} M1_{tb}; L2_{tb}, L2_1^{\infty}) \tag{A.25}$$

$$R_{l2} = \Omega_i(k_{l2} M2_{tb}; F_{tb}, F^{\infty}) \tag{A.26}$$

$$s_{lr} = \lambda_{bvtb} L_{bv} \tag{A.27}$$

$$s_f = k_{ct} F_{ct}. \tag{A.28}$$

Appendix B. Plots of S_{Ti} Over Time for Each Parameter and Variable

Plots show total sensitivity indices for each parameter (indicated on the y-axis) across all 75 sensitivity indices for (a) IC1, radiation dose of 1 Gy, (b) IC2, radiation dose of 7 Gy, (c) IC3, radiation dose of 14 Gy. Plots with many values closer to 1 indicate candidate influential parameters.

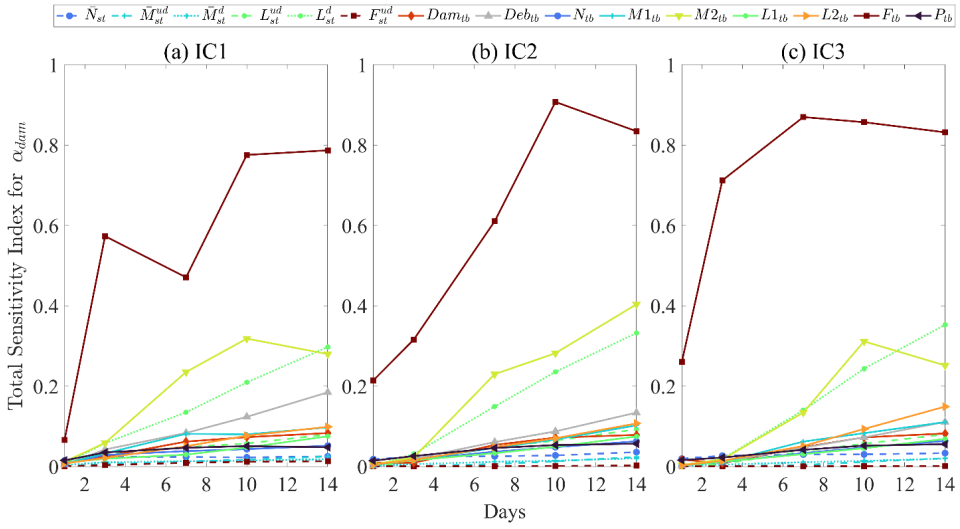

(B.1)

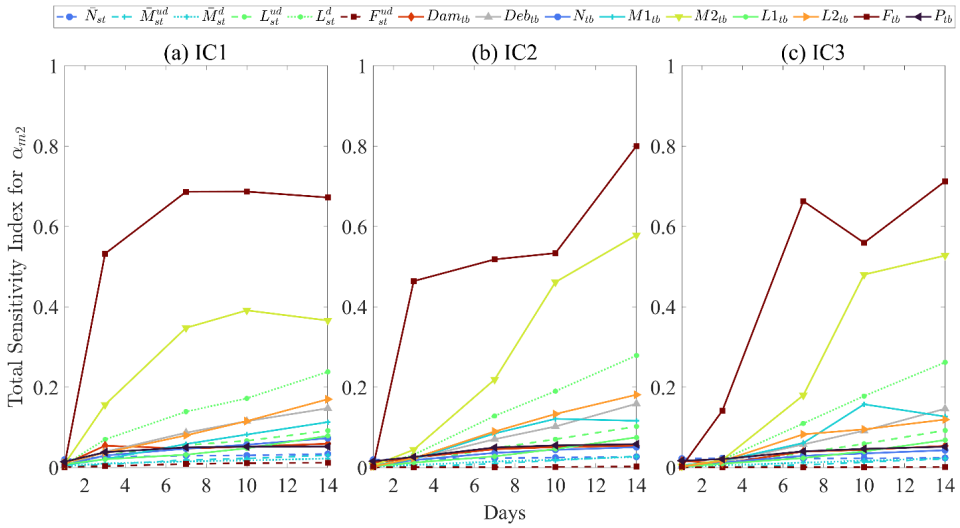

(B.2)

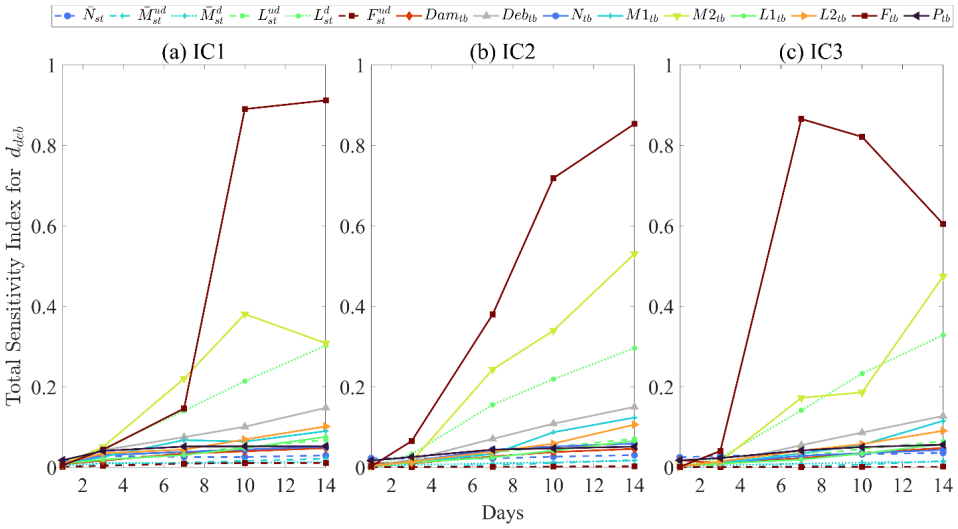
$\bar{N}_{st}$ $\bar{M}^{ud}_{st}$ $\bar{M}^{d}_{st}$ L^{ud}_{st} L^{d}_{st} F^{ud}_{st} Dam_{tb} Deb_{tb} N_{tb} $M1_{tb}$ $M2_{tb}$ $L1_{tb}$ $L2_{tb}$ F_{tb} P_{tb}
(a) IC1
(b) IC2
(c) IC3
Total Sensitivity Index for d_{dcb}
Days

(B.3)

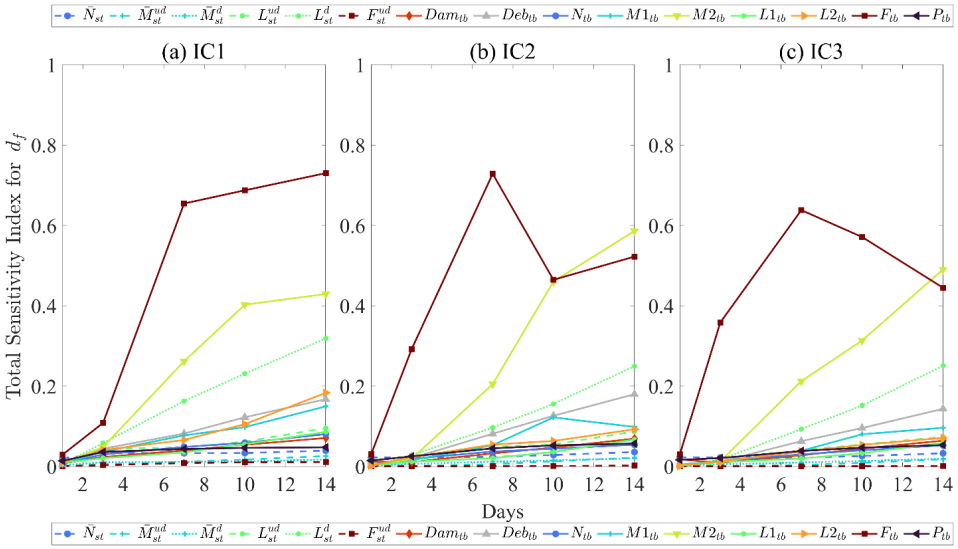
$\bar{N}_{st}$ $\bar{M}^{ud}_{st}$ $\bar{M}^{d}_{st}$ L^{ud}_{st} L^{d}_{st} F^{ud}_{st} Dam_{tb} Deb_{tb} N_{tb} $M1_{tb}$ $M2_{tb}$ $L1_{tb}$ $L2_{tb}$ F_{tb} P_{tb}
(a) IC1
(b) IC2
(c) IC3
Total Sensitivity Index for d_f
Days

(B.4)

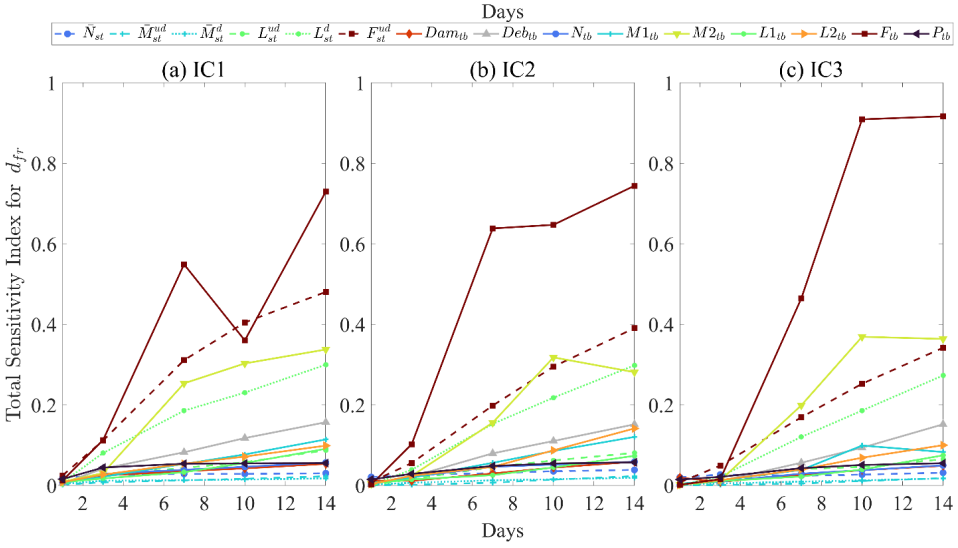
$\bar{N}_{st}$ $\bar{M}^{ud}_{st}$ $\bar{M}^{d}_{st}$ L^{ud}_{st} L^{d}_{st} F^{ud}_{st} Dam_{tb} Deb_{tb} N_{tb} $M1_{tb}$ $M2_{tb}$ $L1_{tb}$ $L2_{tb}$ F_{tb} P_{tb}
(a) IC1
(b) IC2
(c) IC3
Total Sensitivity Index for d_{fr}
Days

(B.5)

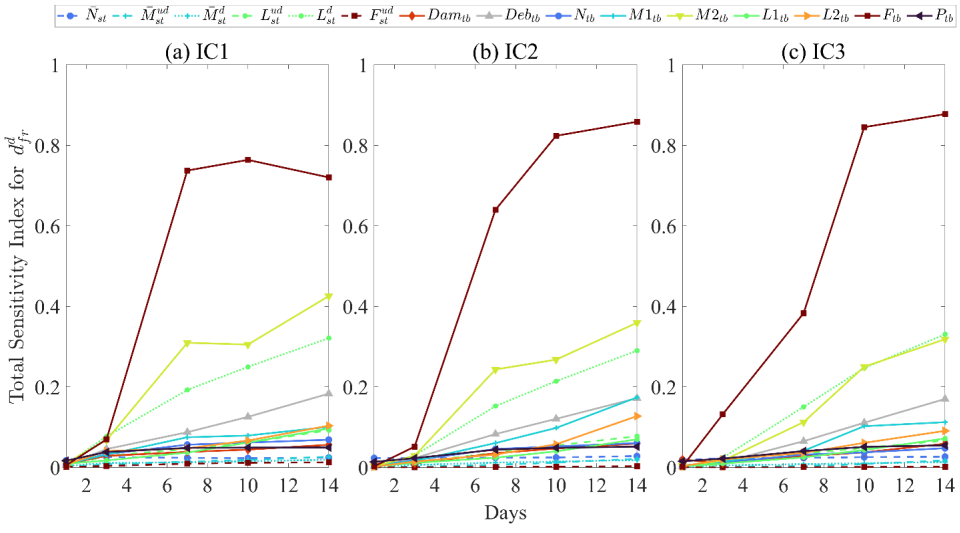
$\bar{N}_{st}$ $\bar{M}^{ud}_{st}$ $\bar{M}^{d}_{st}$ L^{ud}_{st} L^{d}_{st} F^{ud}_{st} Dam_{tb} Deb_{tb} N_{tb} $M1_{tb}$ $M2_{tb}$ $L1_{tb}$ $L2_{tb}$ F_{tb} P_{tb}
(a) IC1
(b) IC2
(c) IC3
Total Sensitivity Index for d^{d}_{fr}
Days

(B.6)

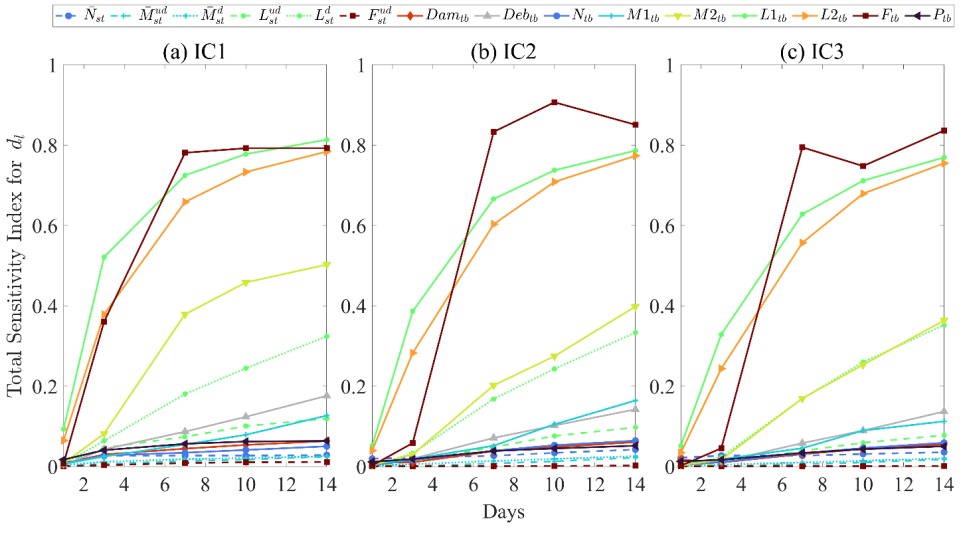
$\bar{N}_{st}$ $\bar{M}^{ud}_{st}$ $\bar{M}^{d}_{st}$ L^{ud}_{st} L^{d}_{st} F^{ud}_{st} Dam_{tb} Deb_{tb} N_{tb} $M1_{tb}$ $M2_{tb}$ $L1_{tb}$ $L2_{tb}$ F_{tb} P_{tb}
(a) IC1
(b) IC2
(c) IC3
Total Sensitivity Index for d_{l}
Days

(B.7)

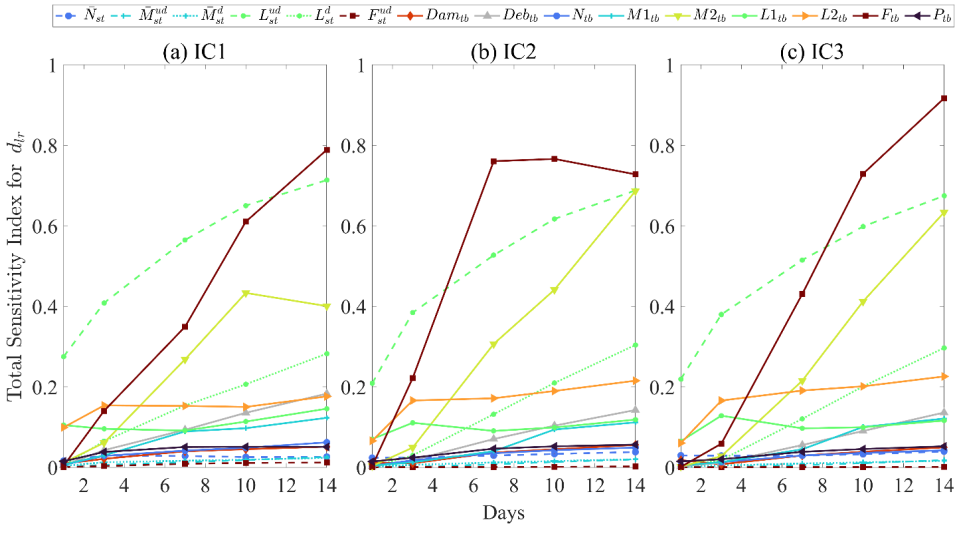
$\bar{N}_{st}$ $\bar{M}^{ud}_{st}$ $\bar{M}^{d}_{st}$ L^{ud}_{st} L^{d}_{st} F^{ud}_{st} Dam_{tb} Deb_{tb} N_{tb} $M1_{tb}$ $M2_{tb}$ $L1_{tb}$ $L2_{tb}$ F_{tb} P_{tb}
(a) IC1
(b) IC2
(c) IC3
Total Sensitivity Index for d_{lr}
Days

(B.8)

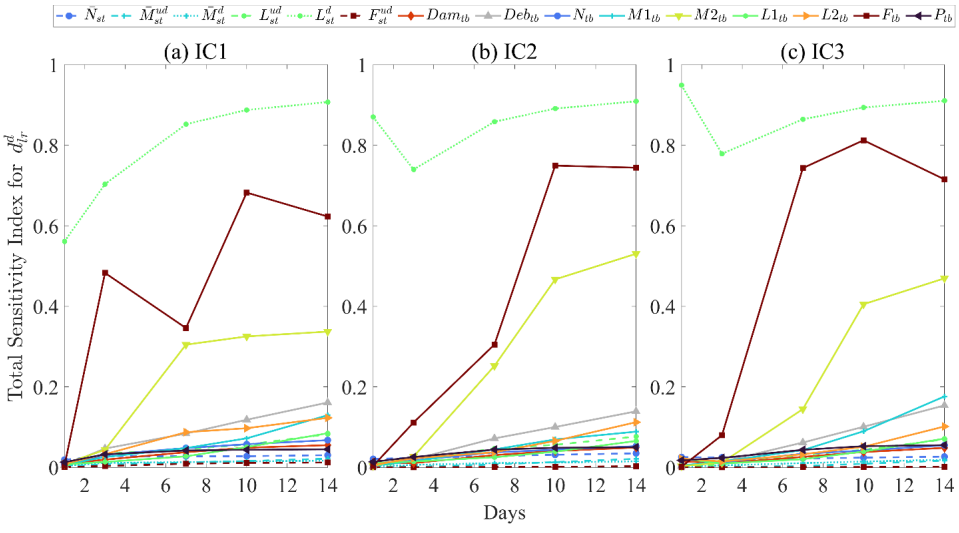
$\bar{N}_{st}$ $\bar{M}^{ud}_{st}$ $\bar{M}^{d}_{st}$ L^{ud}_{st} L^{d}_{st} F^{ud}_{st} Dam_{tb} Deb_{tb} N_{tb} $M1_{tb}$ $M2_{tb}$ $L1_{tb}$ $L2_{tb}$ F_{tb} P_{tb}
(a) IC1
(b) IC2
(c) IC3
Total Sensitivity Index for d^{d}_{tr}
Days

(B.9)

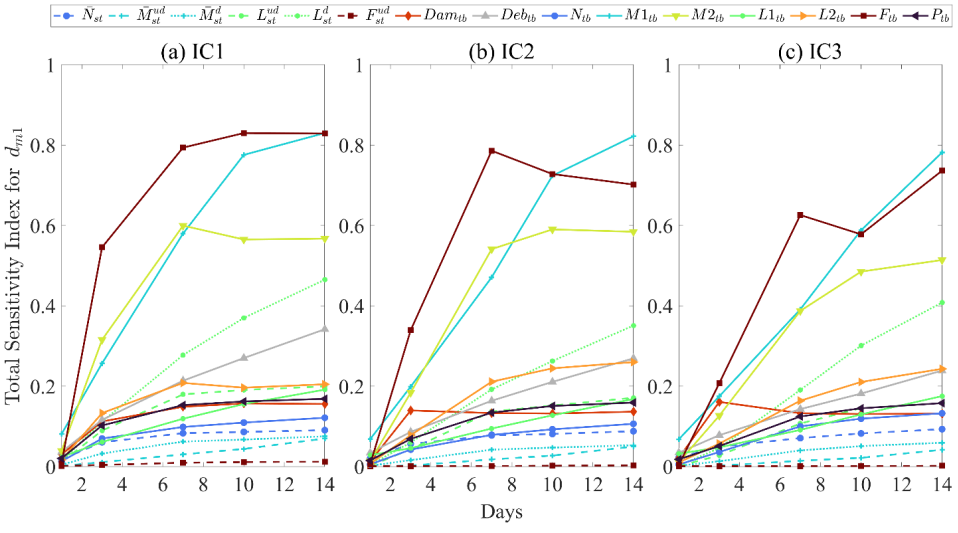
$\bar{N}_{st}$ $\bar{M}^{ud}_{st}$ $\bar{M}^{d}_{st}$ L^{ud}_{st} L^{d}_{st} F^{ud}_{st} Dam_{tb} Deb_{tb} N_{tb} $M1_{tb}$ $M2_{tb}$ $L1_{tb}$ $L2_{tb}$ F_{tb} P_{tb}
(a) IC1
(b) IC2
(c) IC3
Total Sensitivity Index for d_{m1}
Days

(B.10)

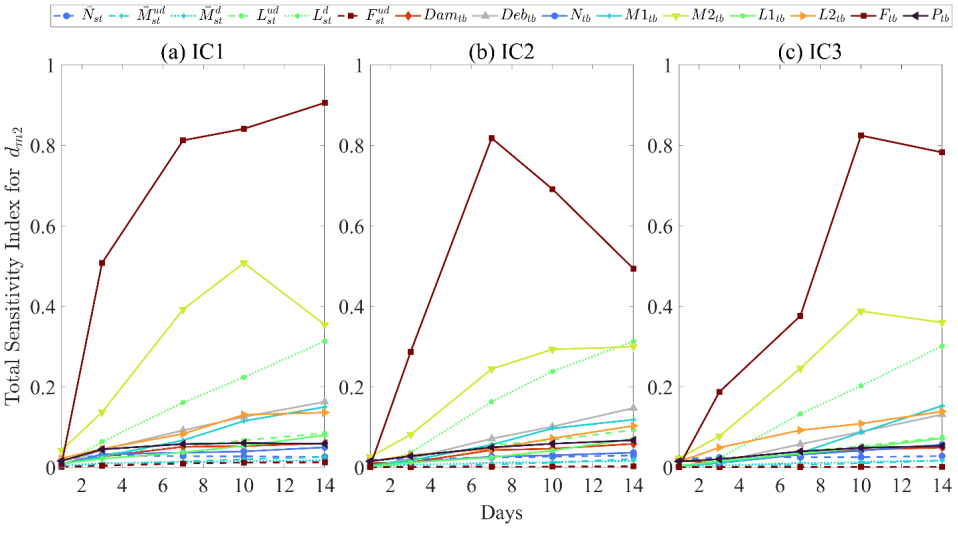
$\bar{N}_{st}$ $\bar{M}^{ud}_{st}$ $\bar{M}^{d}_{st}$ L^{ud}_{st} L^{d}_{st} F^{ud}_{st} Dam_{tb} Deb_{tb} N_{tb} $M1_{tb}$ $M2_{tb}$ $L1_{tb}$ $L2_{tb}$ F_{tb} P_{tb}
(a) IC1
(b) IC2
(c) IC3
Total Sensitivity Index for d_{m2}
Days

(B.11)

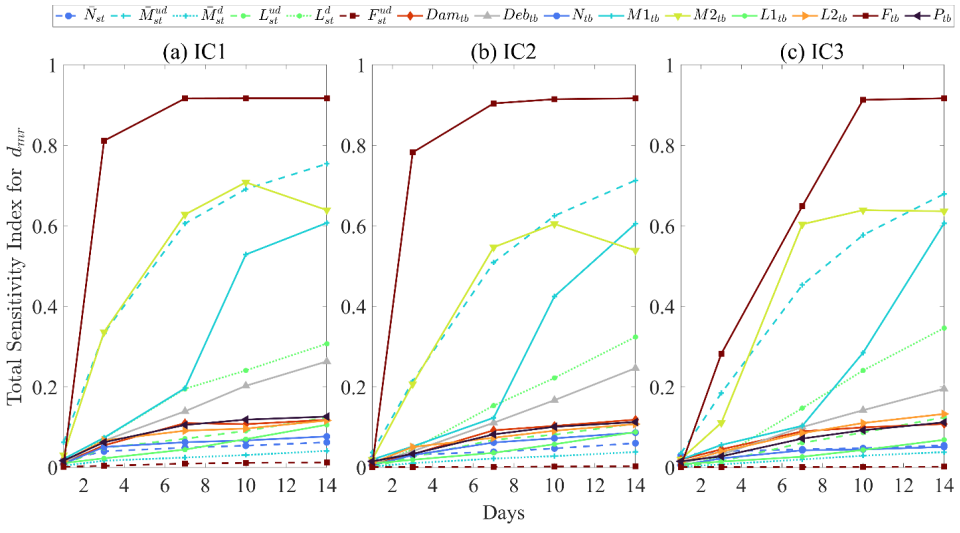
$\bar{N}_{st}$ $\bar{M}^{ud}_{st}$ $\bar{M}^{d}_{st}$ L^{ud}_{st} L^{d}_{st} F^{ud}_{st} Dam_{tb} Deb_{tb} N_{tb} $M1_{tb}$ $M2_{tb}$ $L1_{tb}$ $L2_{tb}$ F_{tb} P_{tb}
(a) IC1
(b) IC2
(c) IC3
Total Sensitivity Index for d_{mr}
Days

(B.12)

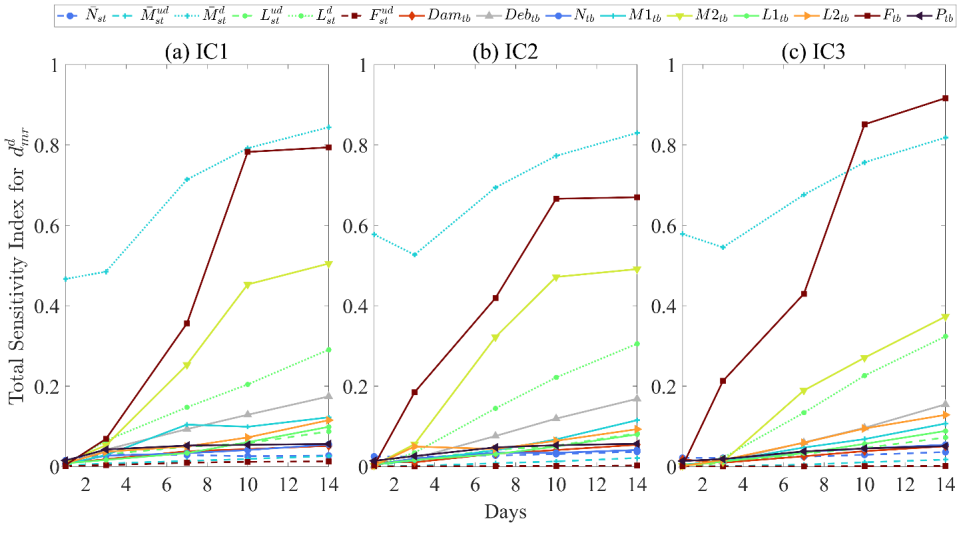
$\bar{N}_{st}$ $\bar{M}^{ud}_{st}$ $\bar{M}^{d}_{st}$ L^{ud}_{st} L^{d}_{st} F^{ud}_{st} Dam_{tb} Deb_{tb} N_{tb} $M1_{tb}$ $M2_{tb}$ $L1_{tb}$ $L2_{tb}$ F_{tb} P_{tb}
(a) IC1
(b) IC2
(c) IC3
Total Sensitivity Index for d^{d}_{mr}
Days

(B.13)

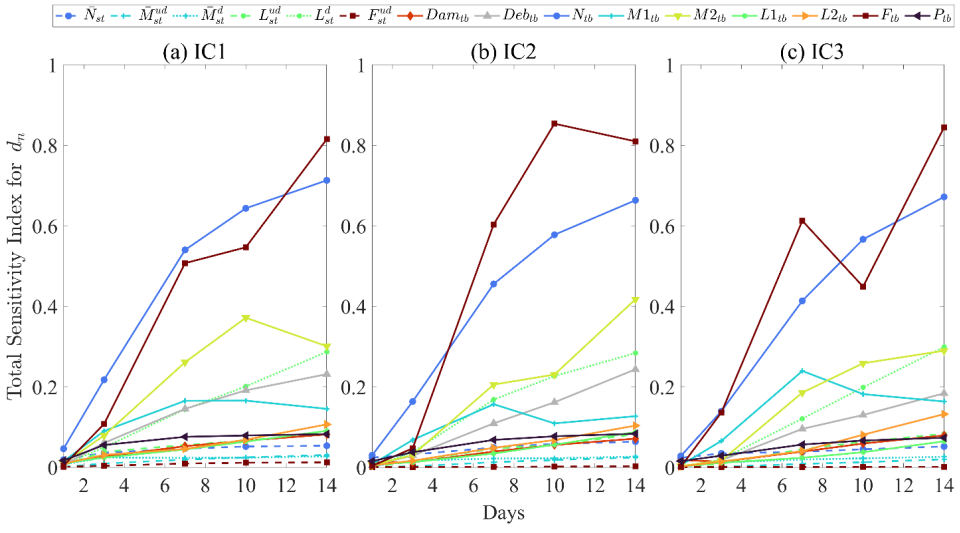
$\bar{N}_{st}$ $\bar{M}^{ud}_{st}$ $\bar{M}^{d}_{st}$ L^{ud}_{st} L^{d}_{st} F^{ud}_{st} Dam_{tb} Deb_{tb} N_{tb} $M1_{tb}$ $M2_{tb}$ $L1_{tb}$ $L2_{tb}$ F_{tb} P_{tb}
(a) IC1
(b) IC2
(c) IC3
Total Sensitivity Index for d_{n}
Days

(B.14)

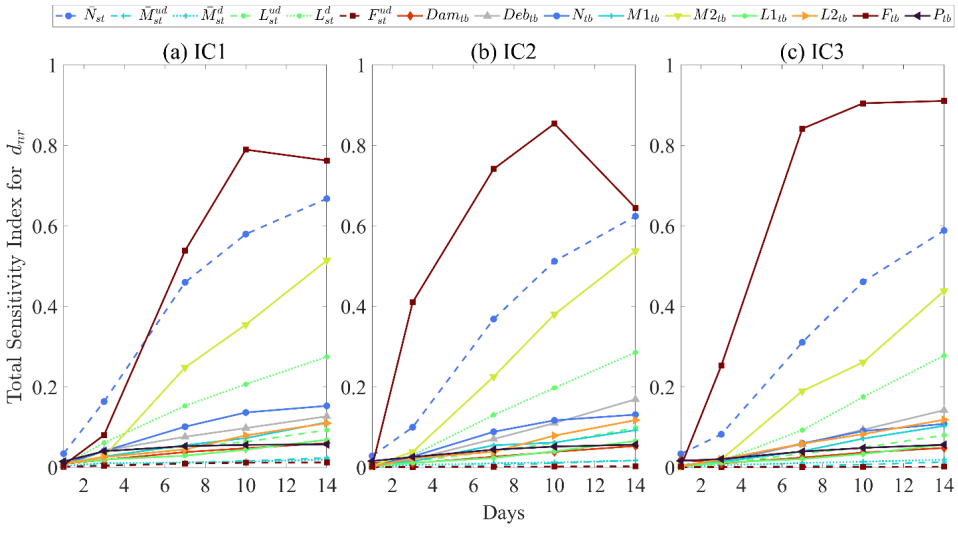
$\bar{N}_{st}$ $\bar{M}^{ud}_{st}$ $\bar{M}^{d}_{st}$ L^{ud}_{st} L^{d}_{st} F^{ud}_{st} Dam_{tb} Deb_{tb} N_{tb} $M1_{tb}$ $M2_{tb}$ $L1_{tb}$ $L2_{tb}$ F_{tb} P_{tb}
(a) IC1
(b) IC2
(c) IC3
Total Sensitivity Index for d_{nr}
Days

(B.15)

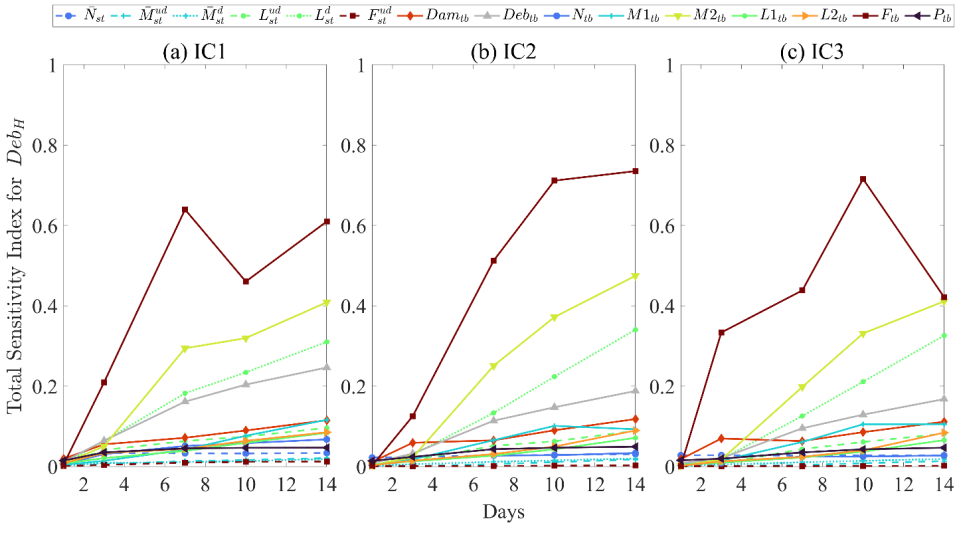
$\bar{N}_{st}$ $\bar{M}^{ud}_{st}$ $\bar{M}^{d}_{st}$ L^{ud}_{st} L^{d}_{st} F^{ud}_{st} Dam_{tb} Deb_{tb} N_{tb} $M1_{tb}$ $M2_{tb}$ $L1_{tb}$ $L2_{tb}$ F_{tb} P_{tb}
(a) IC1
(b) IC2
(c) IC3
Total Sensitivity Index for Deb_H
Days

(B.16)

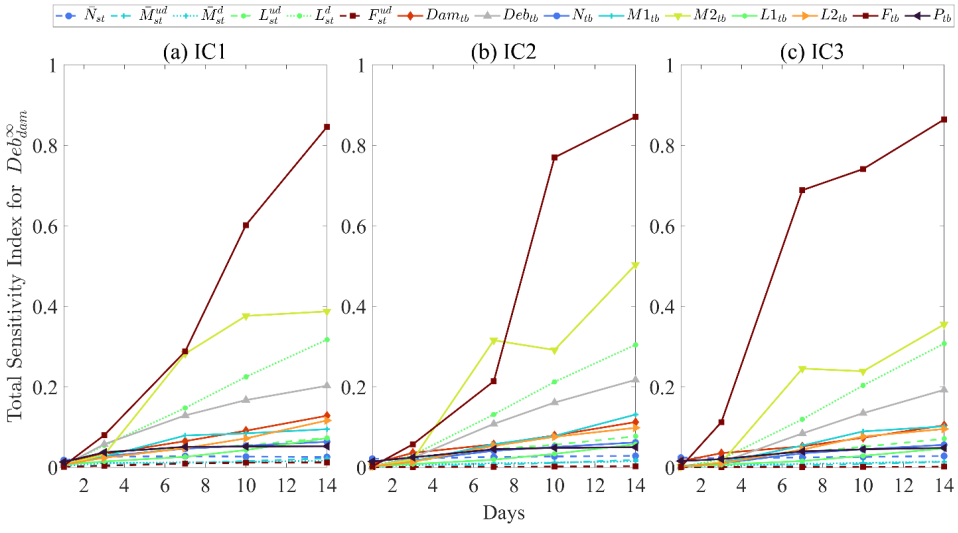
$\bar{N}_{st}$ $\bar{M}^{ud}_{st}$ $\bar{M}^{d}_{st}$ L^{ud}_{st} L^{d}_{st} F^{ud}_{st} Dam_{tb} Deb_{tb} N_{tb} $M1_{tb}$ $M2_{tb}$ $L1_{tb}$ $L2_{tb}$ F_{tb} P_{tb}
(a) IC1
(b) IC2
(c) IC3
Total Sensitivity Index for Deb^{∞}_{dam}
Days

(B.17)

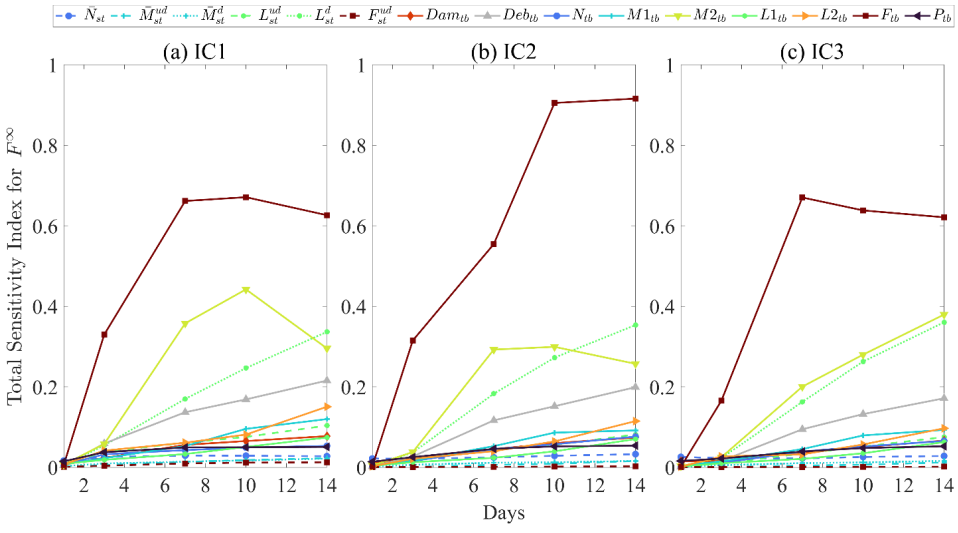
$\bar{N}_{st}$ $\bar{M}^{ud}_{st}$ $\bar{M}^{d}_{st}$ L^{ud}_{st} L^{d}_{st} F^{ud}_{st} Dam_{tb} Deb_{tb} N_{tb} $M1_{tb}$ $M2_{tb}$ $L1_{tb}$ $L2_{tb}$ F_{tb} P_{tb}
(a) IC1
(b) IC2
(c) IC3
Total Sensitivity Index for F^{∞}
Days

(B.18)

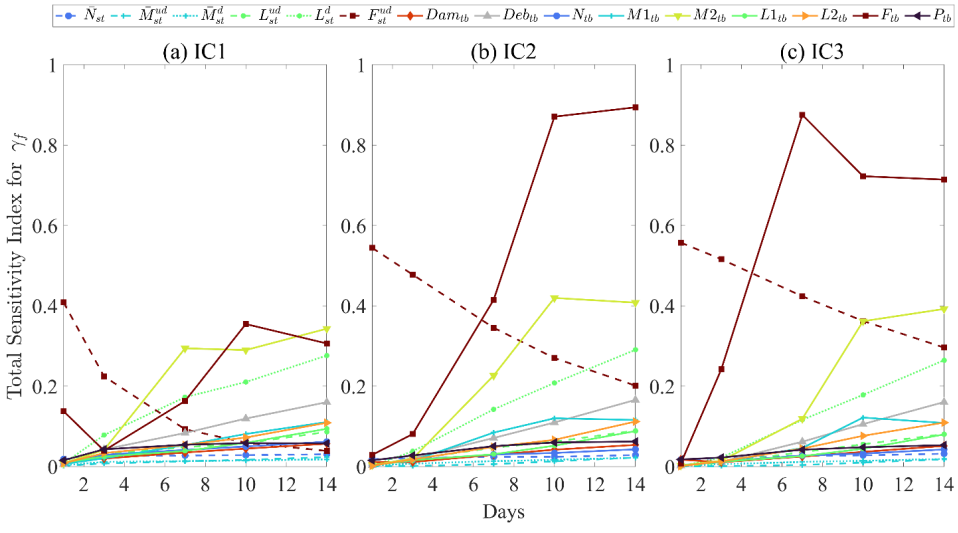
$\bar{N}_{st}$ $\bar{M}^{ud}_{st}$ $\bar{M}^{d}_{st}$ L^{ud}_{st} L^{d}_{st} F^{ud}_{st} Dam_{tb} Deb_{tb} N_{tb} $M1_{tb}$ $M2_{tb}$ $L1_{tb}$ $L2_{tb}$ F_{tb} P_{tb}
(a) IC1
(b) IC2
(c) IC3
Total Sensitivity Index for γ_f
Days

(B.19)

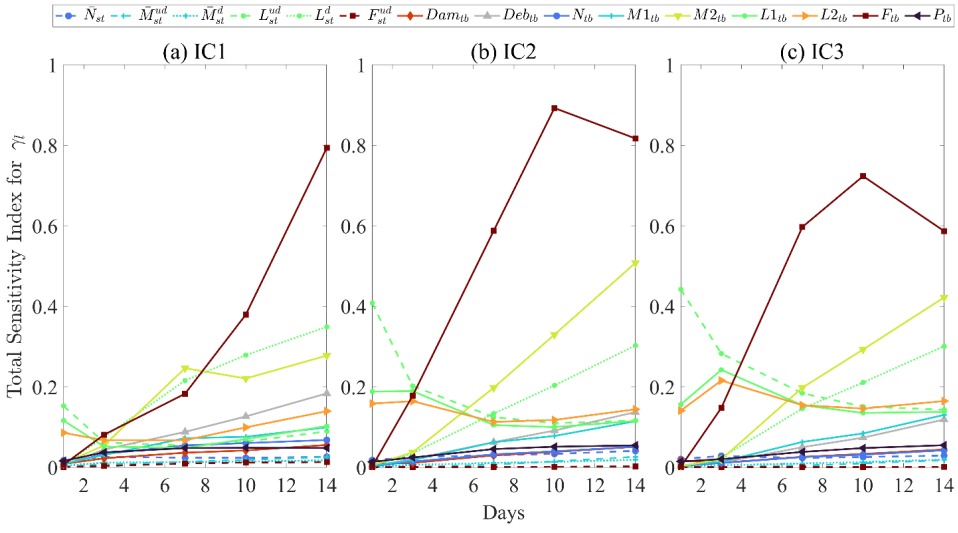
$\bar{N}_{st}$ $\bar{M}^{ud}_{st}$ $\bar{M}^{d}_{st}$ L^{ud}_{st} L^{d}_{st} F^{ud}_{st} Dam_{tb} Deb_{tb} N_{tb} $M1_{tb}$ $M2_{tb}$ $L1_{tb}$ $L2_{tb}$ F_{tb} P_{tb}
(a) IC1
(b) IC2
(c) IC3
Total Sensitivity Index for γ_l
Days

(B.20)

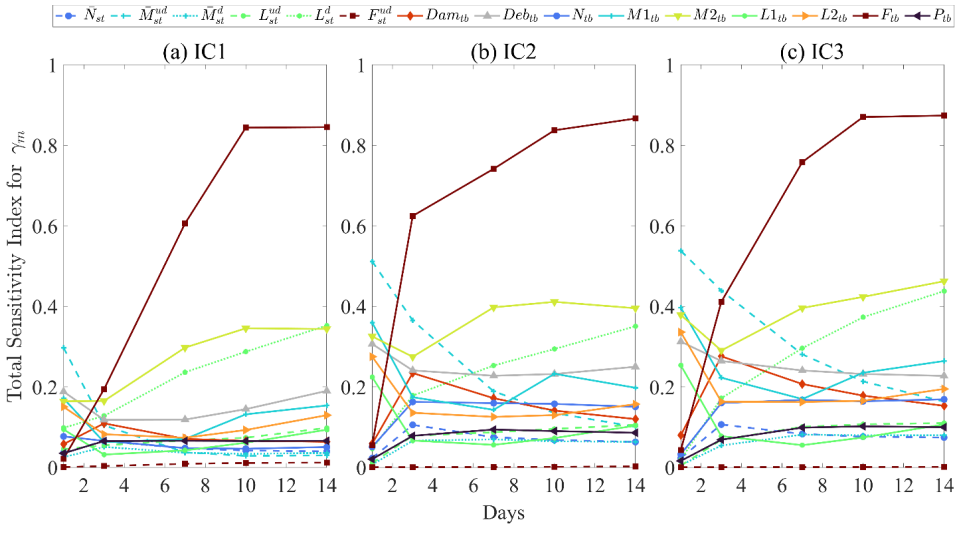
$\bar{N}_{st}$ $\bar{M}^{ud}_{st}$ $\bar{M}^{d}_{st}$ L^{ud}_{st} L^{d}_{st} F^{ud}_{st} Dam_{tb} Deb_{tb} N_{tb} $M1_{tb}$ $M2_{tb}$ $L1_{tb}$ $L2_{tb}$ F_{tb} P_{tb}
(a) IC1
(b) IC2
(c) IC3
Total Sensitivity Index for γ_m
Days

(B.21)

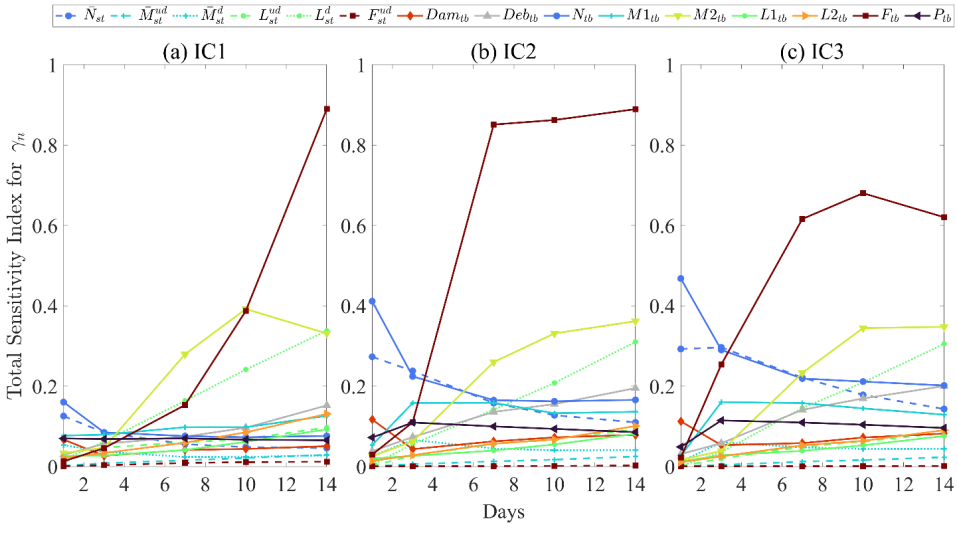
$\bar{N}_{st}$ $\bar{M}^{ud}_{st}$ $\bar{M}^{d}_{st}$ L^{ud}_{st} L^{d}_{st} F^{ud}_{st} Dam_{tb} Deb_{tb} N_{tb} $M1_{tb}$ $M2_{tb}$ $L1_{tb}$ $L2_{tb}$ F_{tb} P_{tb}
(a) IC1
(b) IC2
(c) IC3
Total Sensitivity Index for γ_n
Days

(B.22)

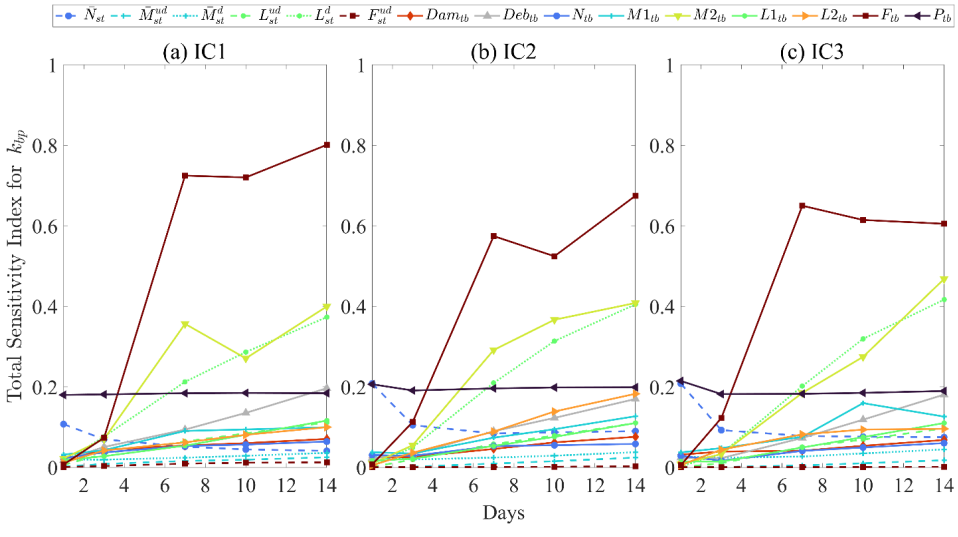
$\bar{N}_{st}$ $\bar{M}^{ud}_{st}$ $\bar{M}^{d}_{st}$ L^{ud}_{st} L^{d}_{st} F^{ud}_{st} Dam_{tb} Deb_{tb} N_{tb} $M1_{tb}$ $M2_{tb}$ $L1_{tb}$ $L2_{tb}$ F_{tb} P_{tb}
(a) IC1
(b) IC2
(c) IC3
Total Sensitivity Index for k_{bp}
Days

(B.23)

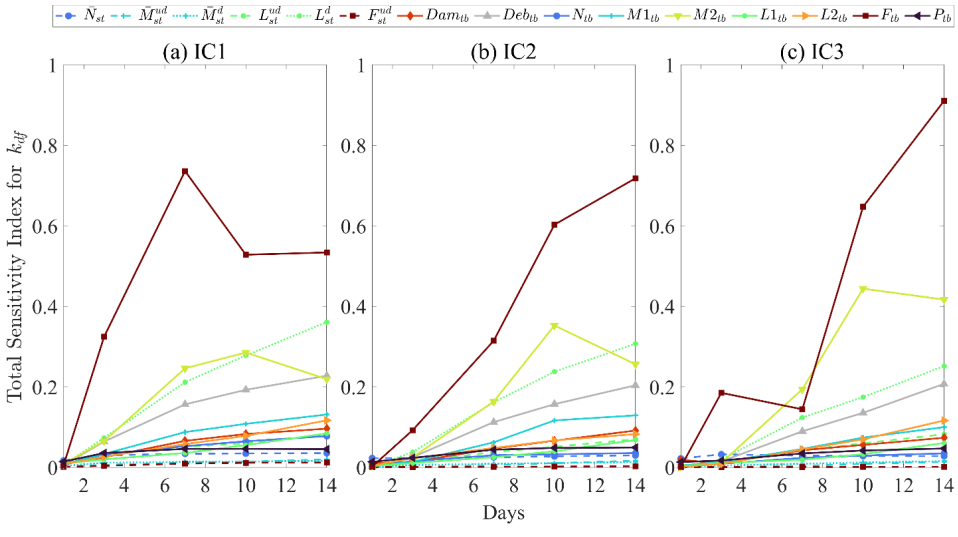
$\bar{N}_{st}$ $\bar{M}^{ud}_{st}$ $\bar{M}^{d}_{st}$ L^{ud}_{st} L^{d}_{st} F^{ud}_{st} Dam_{tb} Deb_{tb} N_{tb} $M1_{tb}$ $M2_{tb}$ $L1_{tb}$ $L2_{tb}$ F_{tb} P_{tb}
(a) IC1
(b) IC2
(c) IC3
Total Sensitivity Index for k_{df}
Days

(B.24)

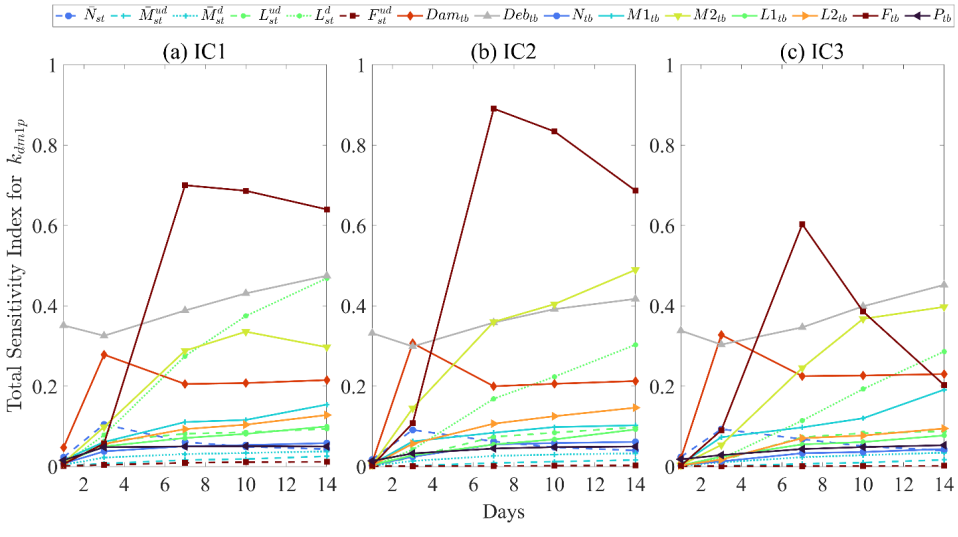
$\bar{N}_{st}$ $\bar{M}^{ud}_{st}$ $\bar{M}^{d}_{st}$ L^{ud}_{st} L^{d}_{st} F^{ud}_{st} Dam_{tb} Deb_{tb} N_{tb} $M1_{tb}$ $M2_{tb}$ $L1_{tb}$ $L2_{tb}$ F_{tb} P_{tb}
(a) IC1
(b) IC2
(c) IC3
Total Sensitivity Index for k_{dm1p}
Days

(B.25)

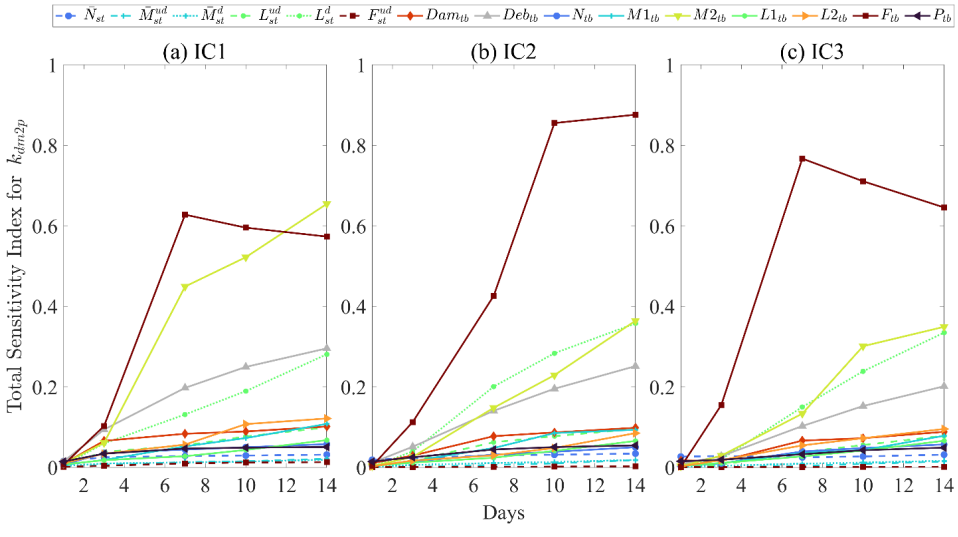
$\bar{N}_{st}$ $\bar{M}^{ud}_{st}$ $\bar{M}^{d}_{st}$ L^{ud}_{st} L^{d}_{st} F^{ud}_{st} Dam_{tb} Deb_{tb} N_{tb} $M1_{tb}$ $M2_{tb}$ $L1_{tb}$ $L2_{tb}$ F_{tb} P_{tb}
(a) IC1
(b) IC2
(c) IC3
Total Sensitivity Index for k_{dm2p}
Days

(B.26)

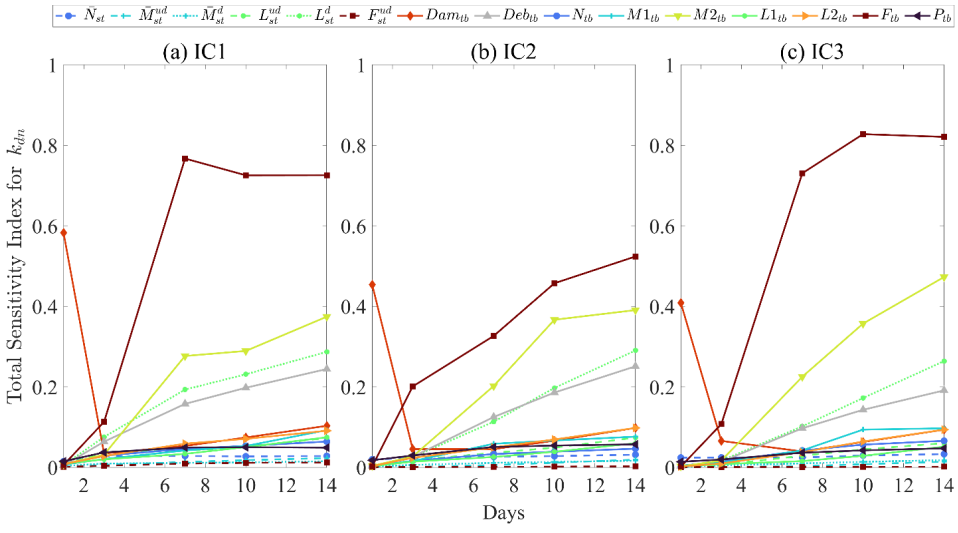
$\bar{N}_{st}$ $\bar{M}^{ud}_{st}$ $\bar{M}^{d}_{st}$ L^{ud}_{st} L^{d}_{st} F^{ud}_{st} Dam_{tb} Deb_{tb} N_{tb} $M1_{tb}$ $M2_{tb}$ $L1_{tb}$ $L2_{tb}$ F_{tb} P_{tb}
(a) IC1
(b) IC2
(c) IC3
Total Sensitivity Index for k_{dn}
Days

(B.27)

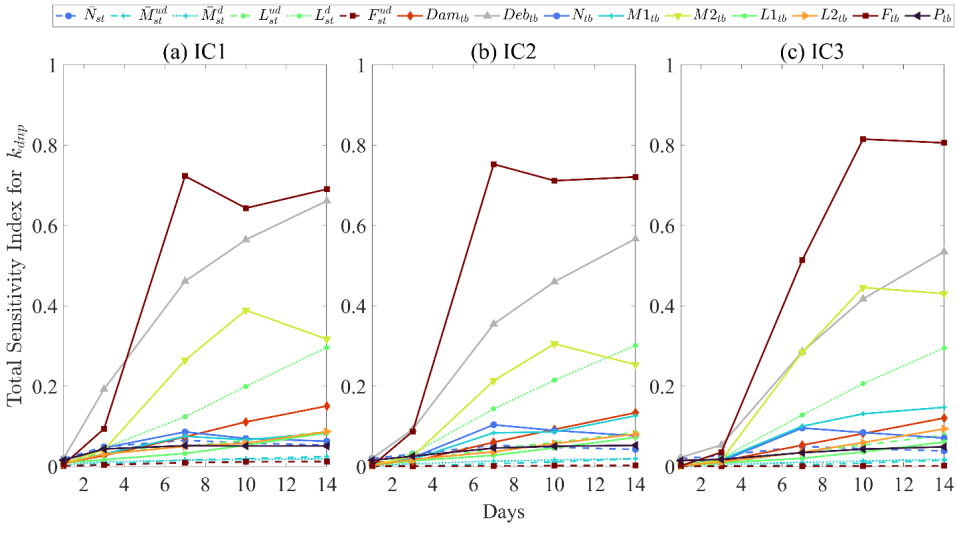
$\bar{N}_{st}$ $\bar{M}^{ud}_{st}$ $\bar{M}^{d}_{st}$ L^{ud}_{st} L^{d}_{st} F^{ud}_{st} Dam_{tb} Deb_{tb} N_{tb} $M1_{tb}$ $M2_{tb}$ $L1_{tb}$ $L2_{tb}$ F_{tb} P_{tb}
(a) IC1
(b) IC2
(c) IC3
Total Sensitivity Index for k_{dnp}
Days

(B.28)

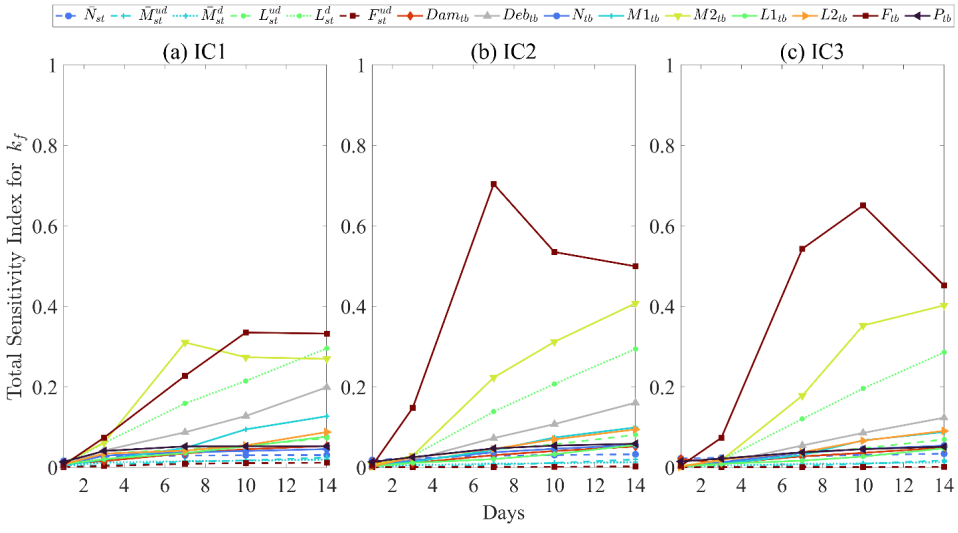
$\bar{N}_{st}$ $\bar{M}^{ud}_{st}$ $\bar{M}^{d}_{st}$ L^{ud}_{st} L^{d}_{st} F^{ud}_{st} Dam_{tb} Deb_{tb} N_{tb} $M1_{tb}$ $M2_{tb}$ $L1_{tb}$ $L2_{tb}$ F_{tb} P_{tb}
(a) IC1
(b) IC2
(c) IC3
Total Sensitivity Index for k_f
Days

(B.29)

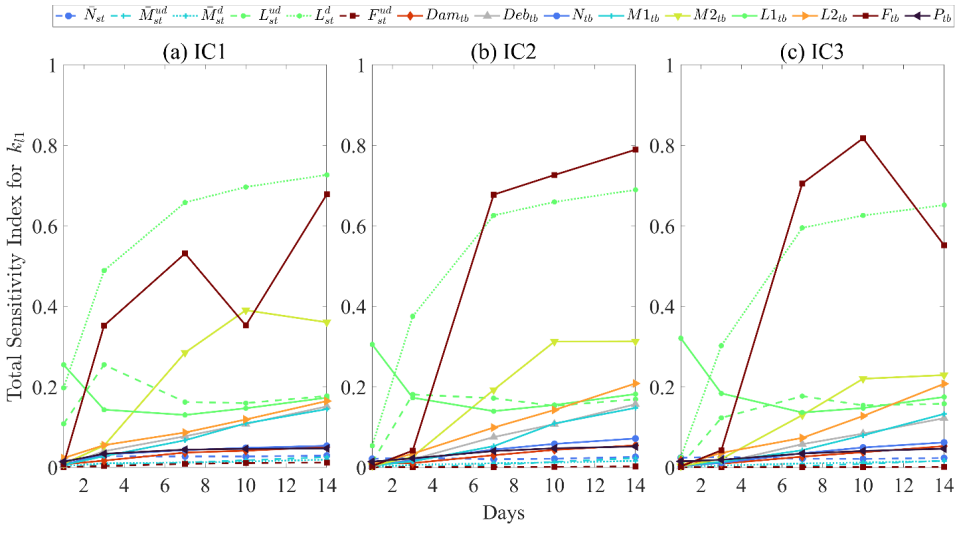
$\bar{N}_{st}$ $\bar{M}^{ud}_{st}$ $\bar{M}^{d}_{st}$ L^{ud}_{st} L^{d}_{st} F^{ud}_{st} Dam_{tb} Deb_{tb} N_{tb} $M1_{tb}$ $M2_{tb}$ $L1_{tb}$ $L2_{tb}$ F_{tb} P_{tb}
(a) IC1
(b) IC2
(c) IC3
Total Sensitivity Index for k_{l1}
Days

(B.30)

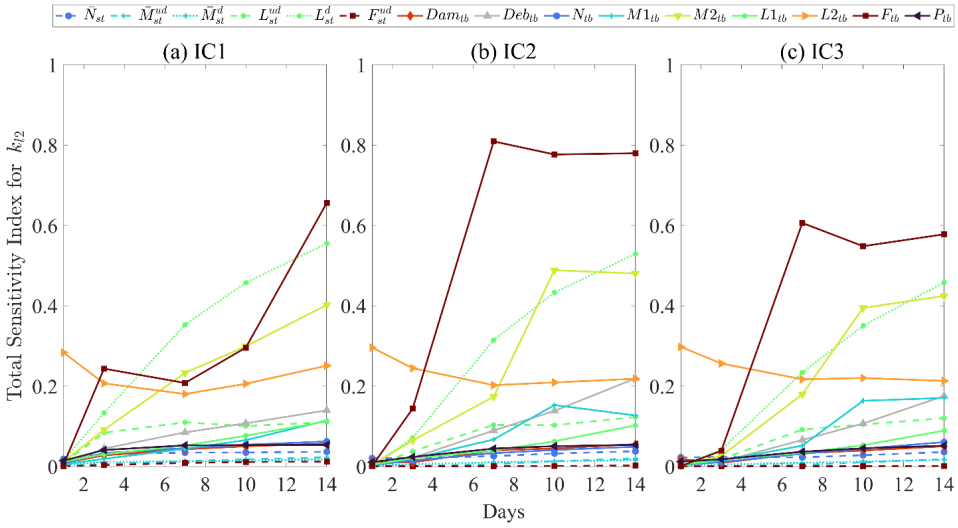
$\bar{N}_{st}$ $\bar{M}^{ud}_{st}$ $\bar{M}^{d}_{st}$ L^{ud}_{st} L^{d}_{st} F^{ud}_{st} Dam_{tb} Deb_{tb} N_{tb} $M1_{tb}$ $M2_{tb}$ $L1_{tb}$ $L2_{tb}$ F_{tb} P_{tb}
(a) IC1
(b) IC2
(c) IC3
Total Sensitivity Index for k_{l2}
Days

(B.31)

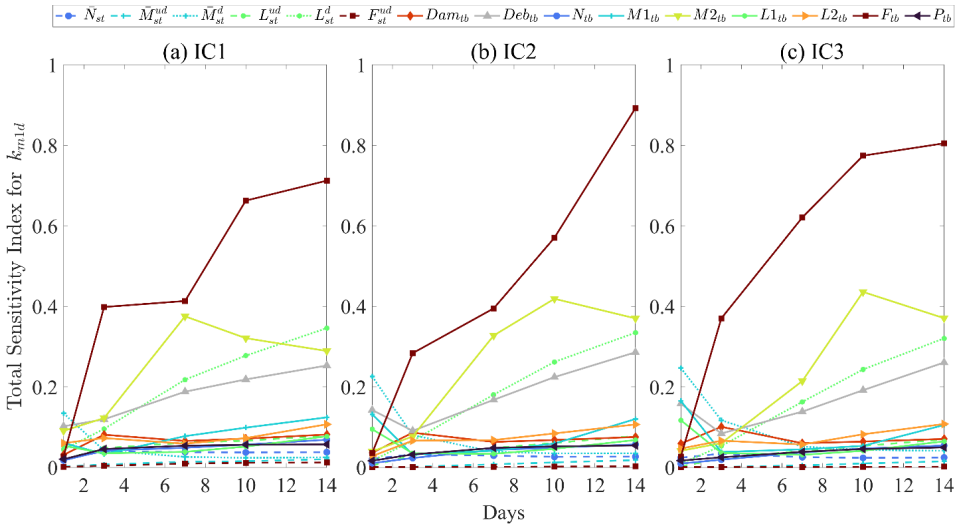
$\bar{N}_{st}$ $\bar{M}^{ud}_{st}$ $\bar{M}^{d}_{st}$ L^{ud}_{st} L^{d}_{st} F^{ud}_{st} Dam_{tb} Deb_{tb} N_{tb} $M1_{tb}$ $M2_{tb}$ $L1_{tb}$ $L2_{tb}$ F_{tb} P_{tb}
(a) IC1
(b) IC2
(c) IC3
Total Sensitivity Index for k_{m1d}
Days

(B.32)

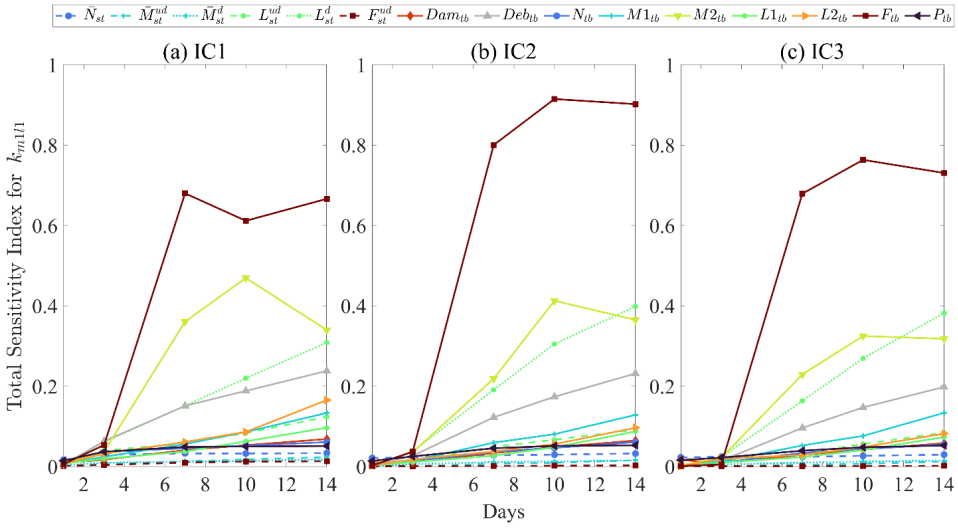
$\bar{N}_{st}$ $\bar{M}^{ud}_{st}$ $\bar{M}^{d}_{st}$ L^{ud}_{st} L^{d}_{st} F^{ud}_{st} Dam_{tb} Deb_{tb} N_{tb} $M1_{tb}$ $M2_{tb}$ $L1_{tb}$ $L2_{tb}$ F_{tb} P_{tb}
(a) IC1
(b) IC2
(c) IC3
Total Sensitivity Index for k_{m1l}
Days

(B.33)

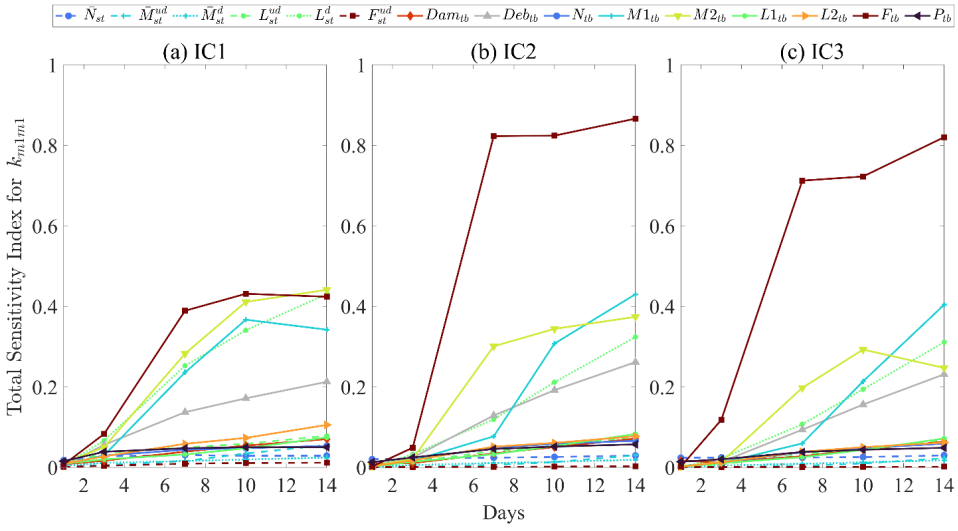
$\bar{N}_{st}$ $\bar{M}^{ud}_{st}$ $\bar{M}^{d}_{st}$ L^{ud}_{st} L^{d}_{st} F^{ud}_{st} Dam_{tb} Deb_{tb} N_{tb} $M1_{tb}$ $M2_{tb}$ $L1_{tb}$ $L2_{tb}$ F_{tb} P_{tb}
(a) IC1
(b) IC2
(c) IC3
Total Sensitivity Index for k_{m1m1}
Days

(B.34)

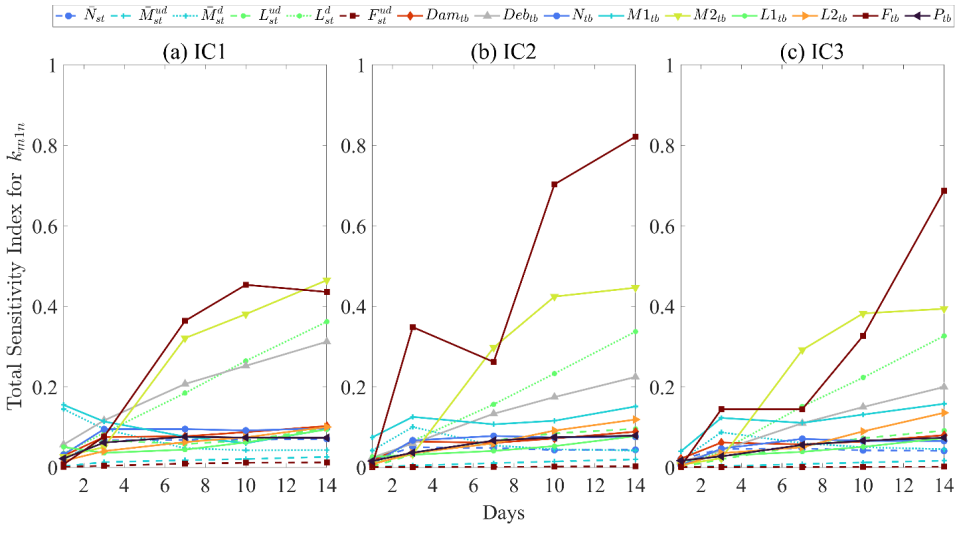
$\bar{N}_{st}$ $\bar{M}^{ud}_{st}$ $\bar{M}^{d}_{st}$ L^{ud}_{st} L^{d}_{st} F^{ud}_{st} Dam_{tb} Deb_{tb} N_{tb} $M1_{tb}$ $M2_{tb}$ $L1_{tb}$ $L2_{tb}$ F_{tb} P_{tb}
(a) IC1
(b) IC2
(c) IC3
Total Sensitivity Index for k_{m1n}
Days

(B.35)

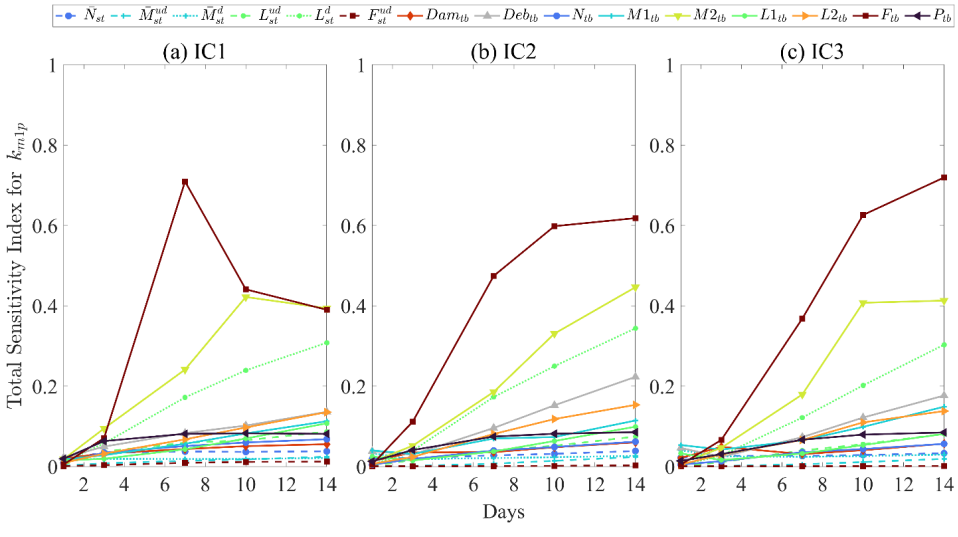
$\bar{N}_{st}$ $\bar{M}^{ud}_{st}$ $\bar{M}^{d}_{st}$ L^{ud}_{st} L^{d}_{st} F^{ud}_{st} Dam_{tb} Deb_{tb} N_{tb} $M1_{tb}$ $M2_{tb}$ $L1_{tb}$ $L2_{tb}$ F_{tb} P_{tb}
(a) IC1
(b) IC2
(c) IC3
Total Sensitivity Index for k_{m1p}
Days

(B.36)

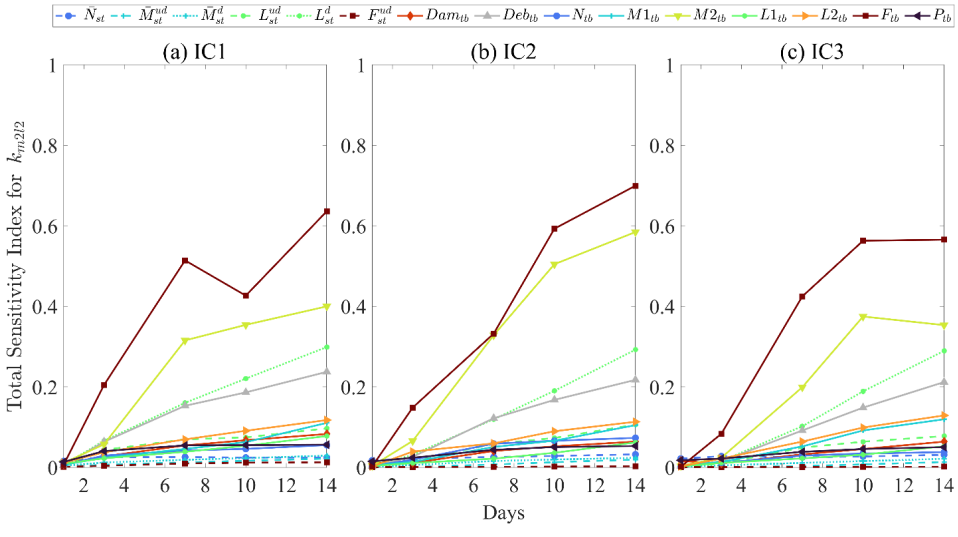
$\bar{N}_{st}$ $\bar{M}^{ud}_{st}$ $\bar{M}^{d}_{st}$ L^{ud}_{st} L^{d}_{st} F^{ud}_{st} Dam_{tb} Deb_{tb} N_{tb} $M1_{tb}$ $M2_{tb}$ $L1_{tb}$ $L2_{tb}$ F_{tb} P_{tb}
(a) IC1
(b) IC2
(c) IC3
Total Sensitivity Index for k_{m2p2}
Days

(B.37)

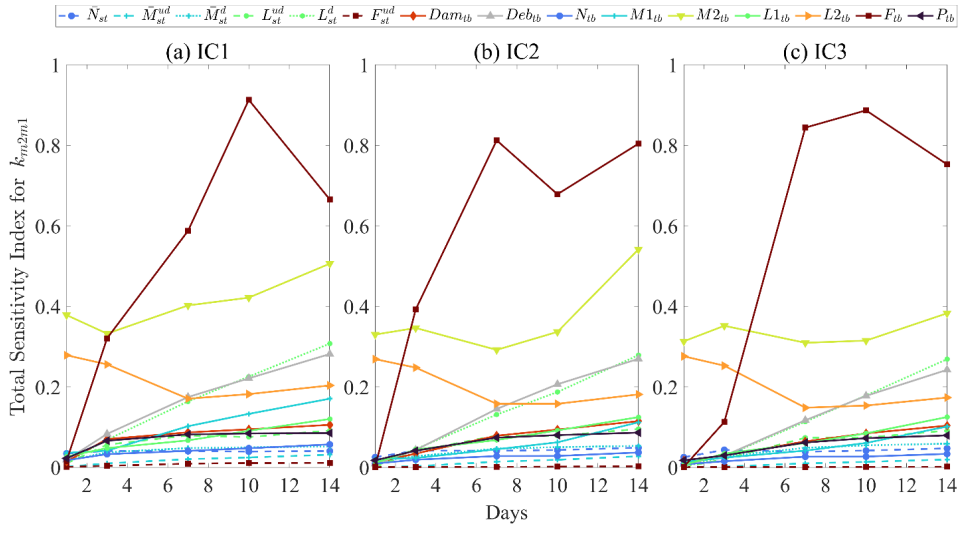
$\bar{N}_{st}$ $\bar{M}^{ud}_{st}$ $\bar{M}^{d}_{st}$ L^{ud}_{st} L^{d}_{st} F^{ud}_{st} Dam_{tb} Deb_{tb} N_{tb} $M1_{tb}$ $M2_{tb}$ $L1_{tb}$ $L2_{tb}$ F_{tb} P_{tb}
(a) IC1
(b) IC2
(c) IC3
Total Sensitivity Index for k_{m2m1}
Days

(B.38)

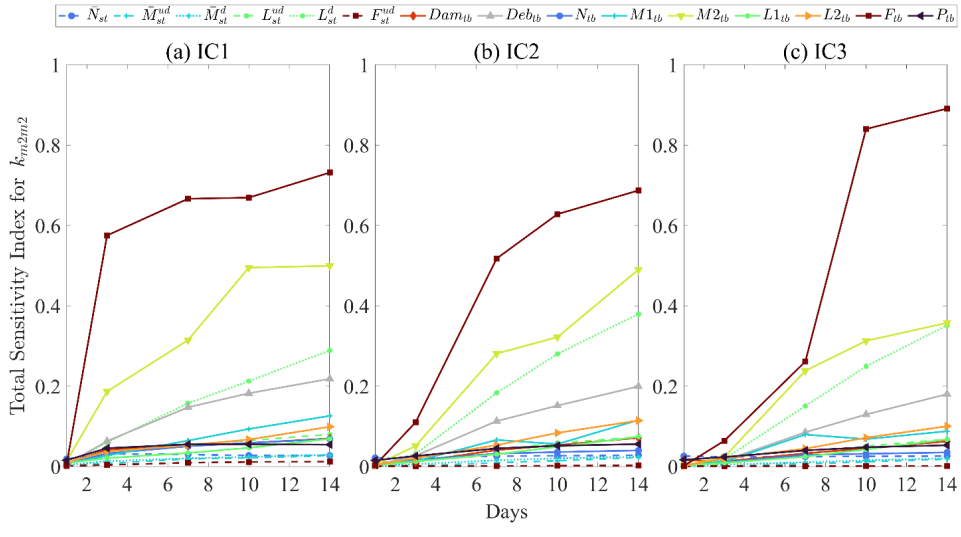
$\bar{N}_{st}$ $\bar{M}^{ud}_{st}$ $\bar{M}^{d}_{st}$ L^{ud}_{st} L^{d}_{st} F^{ud}_{st} Dam_{tb} Deb_{tb} N_{tb} $M1_{tb}$ $M2_{tb}$ $L1_{tb}$ $L2_{tb}$ F_{tb} P_{tb}
(a) IC1
(b) IC2
(c) IC3
Total Sensitivity Index for k_{m2m2}
Days

(B.39)

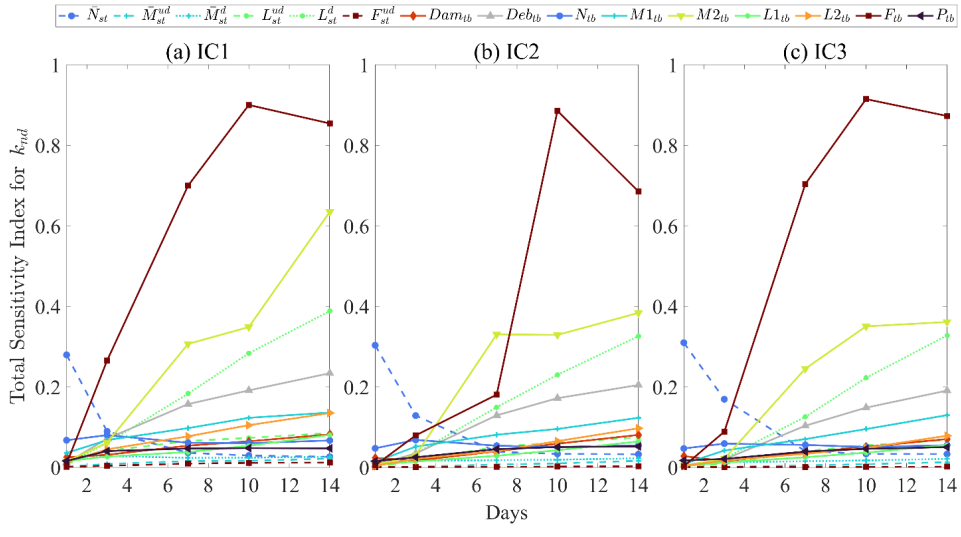
$\bar{N}_{st}$ $\bar{M}^{ud}_{st}$ $\bar{M}^{d}_{st}$ L^{ud}_{st} L^{d}_{st} F^{ud}_{st} Dam_{tb} Deb_{tb} N_{tb} $M1_{tb}$ $M2_{tb}$ $L1_{tb}$ $L2_{tb}$ F_{tb} P_{tb}
(a) IC1
(b) IC2
(c) IC3
Total Sensitivity Index for k_{md}
Days

(B.40)

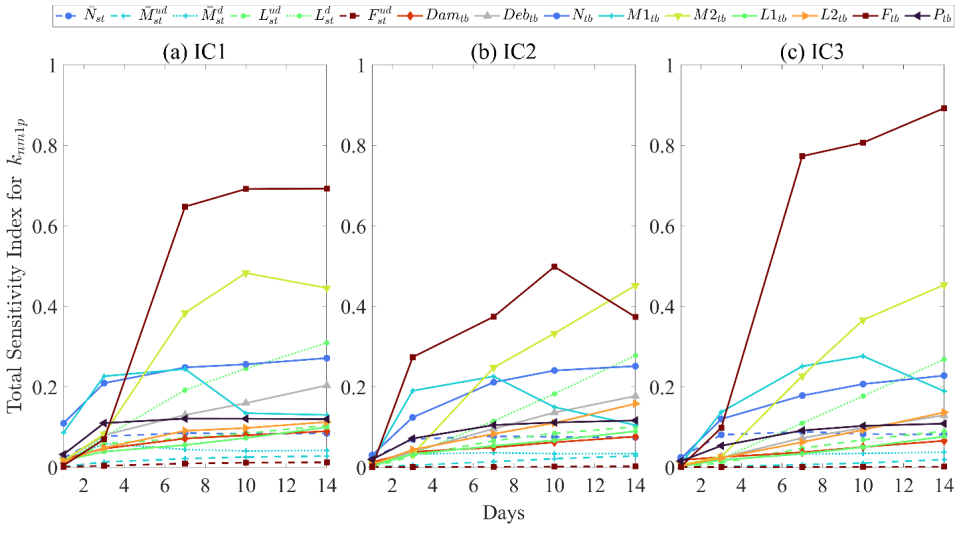
$\bar{N}_{st}$ $\bar{M}^{ud}_{st}$ $\bar{M}^{d}_{st}$ L^{ud}_{st} L^{d}_{st} F^{ud}_{st} Dam_{tb} Deb_{tb} N_{tb} $M1_{tb}$ $M2_{tb}$ $L1_{tb}$ $L2_{tb}$ F_{tb} P_{tb}
(a) IC1
(b) IC2
(c) IC3
Total Sensitivity Index for k_{nm1p}
Days

(B.41)

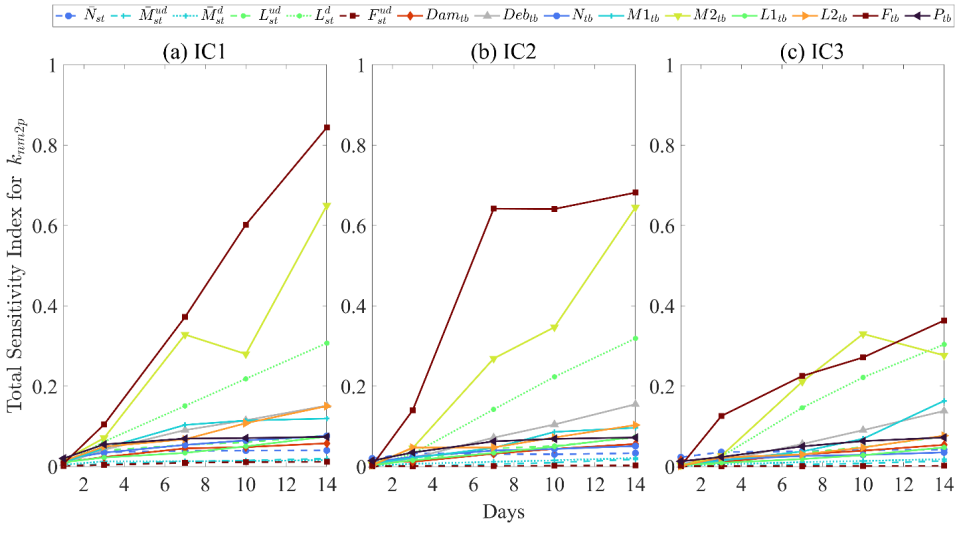
$\bar{N}_{st}$ $\bar{M}^{ud}_{st}$ $\bar{M}^{d}_{st}$ L^{ud}_{st} L^{d}_{st} F^{ud}_{st} Dam_{tb} Deb_{tb} N_{tb} $M1_{tb}$ $M2_{tb}$ $L1_{tb}$ $L2_{tb}$ F_{tb} P_{tb}
(a) IC1
(b) IC2
(c) IC3
Total Sensitivity Index for k_{nm2p}
Days

(B.42)

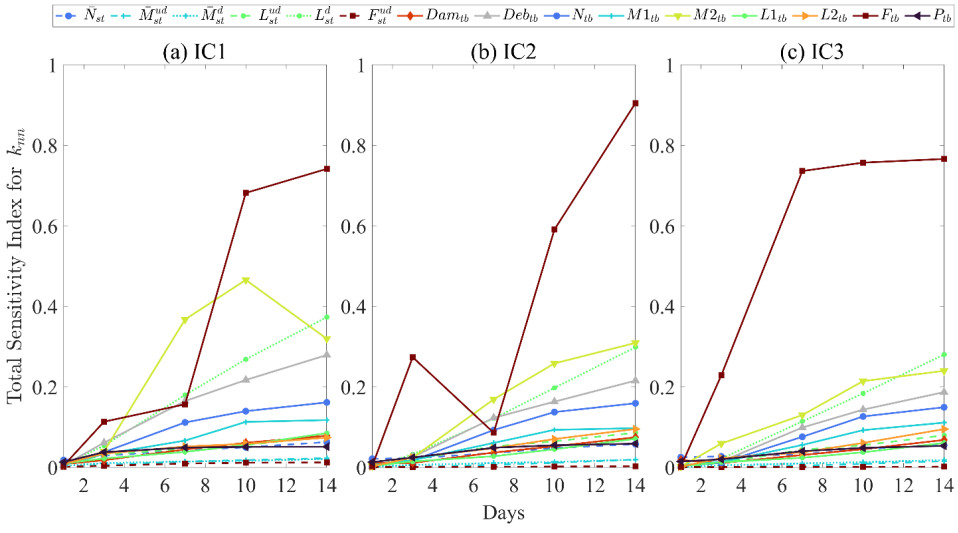
$\bar{N}_{st}$ $\bar{M}^{ud}_{st}$ $\bar{M}^{d}_{st}$ L^{ud}_{st} L^{d}_{st} F^{ud}_{st} Dam_{tb} Deb_{tb} N_{tb} $M1_{tb}$ $M2_{tb}$ $L1_{tb}$ $L2_{tb}$ F_{tb} P_{tb}
(a) IC1
(b) IC2
(c) IC3
Total Sensitivity Index for k_{nm}
Days

(B.43)

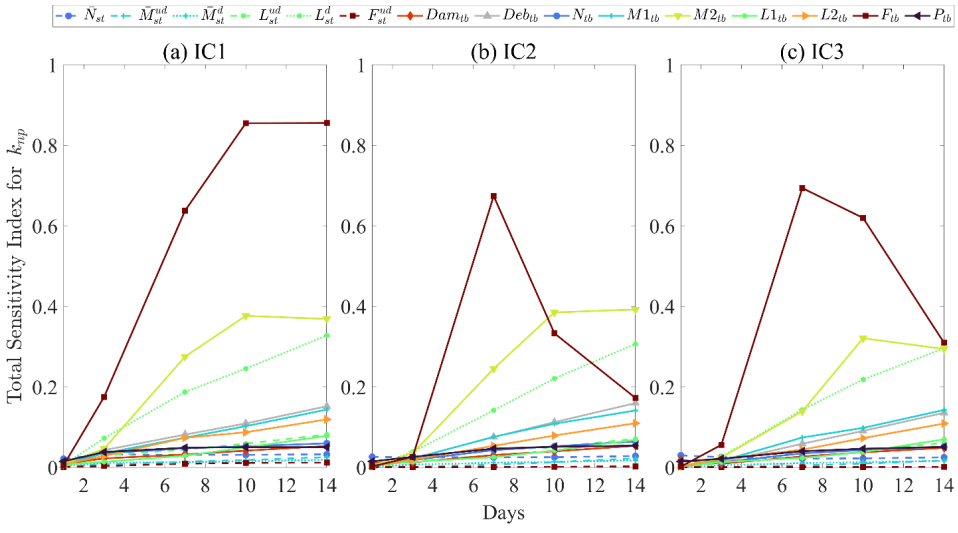
$\bar{N}_{st}$ $\bar{M}^{ud}_{st}$ $\bar{M}^{d}_{st}$ L^{ud}_{st} L^{d}_{st} F^{ud}_{st} Dam_{tb} Deb_{tb} N_{tb} $M1_{tb}$ $M2_{tb}$ $L1_{tb}$ $L2_{tb}$ F_{tb} P_{tb}
(a) IC1
(b) IC2
(c) IC3
Total Sensitivity Index for k_{np}
Days

(B.44)

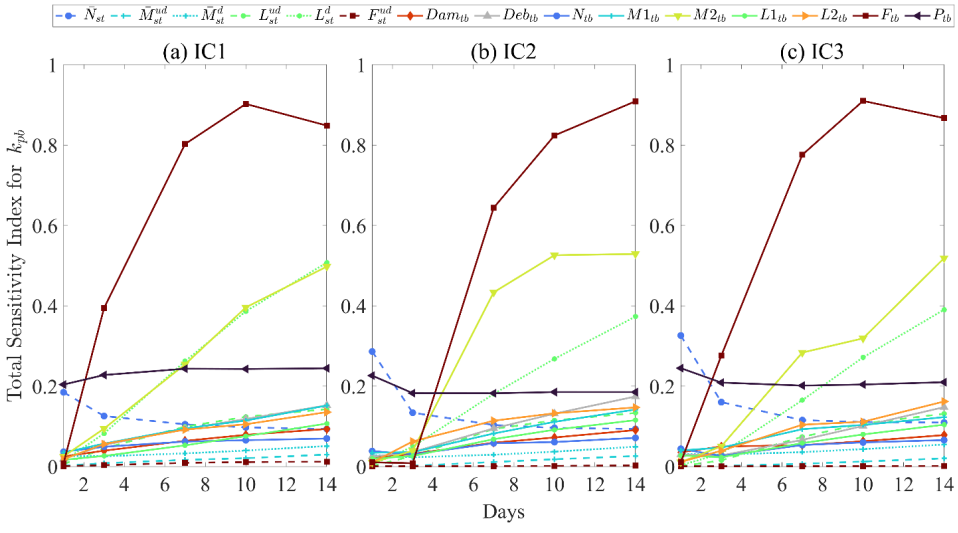
$\bar{N}_{st}$ $\bar{M}^{ud}_{st}$ $\bar{M}^{d}_{st}$ L^{ud}_{st} L^{d}_{st} F^{ud}_{st} Dam_{tb} Deb_{tb} N_{tb} $M1_{tb}$ $M2_{tb}$ $L1_{tb}$ $L2_{tb}$ F_{tb} P_{tb}
(a) IC1
(b) IC2
(c) IC3
Total Sensitivity Index for k_{pb}
Days

(B.45)

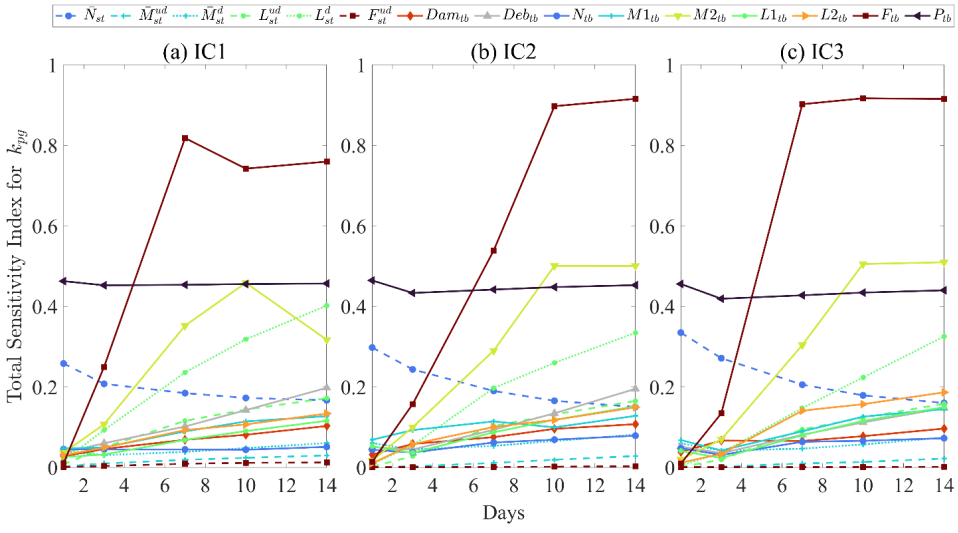
$\bar{N}_{st}$ $\bar{M}^{ud}_{st}$ $\bar{M}^{d}_{st}$ L^{ud}_{st} L^{d}_{st} F^{ud}_{st} Dam_{tb} Deb_{tb} N_{tb} $M1_{tb}$ $M2_{tb}$ $L1_{tb}$ $L2_{tb}$ F_{tb} P_{tb}
(a) IC1
(b) IC2
(c) IC3
Total Sensitivity Index for k_{pg}
Days

(B.46)

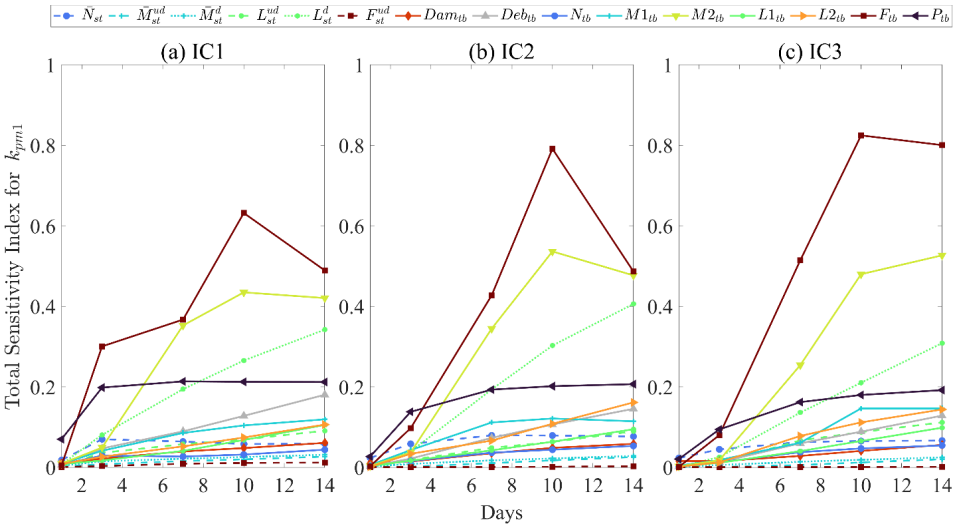
$\bar{N}_{st}$ $\bar{M}^{ud}_{st}$ $\bar{M}^{d}_{st}$ L^{ud}_{st} L^{d}_{st} F^{ud}_{st} Dam_{tb} Deb_{tb} N_{tb} $M1_{tb}$ $M2_{tb}$ $L1_{tb}$ $L2_{tb}$ F_{tb} P_{tb}
(a) IC1
(b) IC2
(c) IC3
Total Sensitivity Index for k_{pm1}
Days

(B.47)

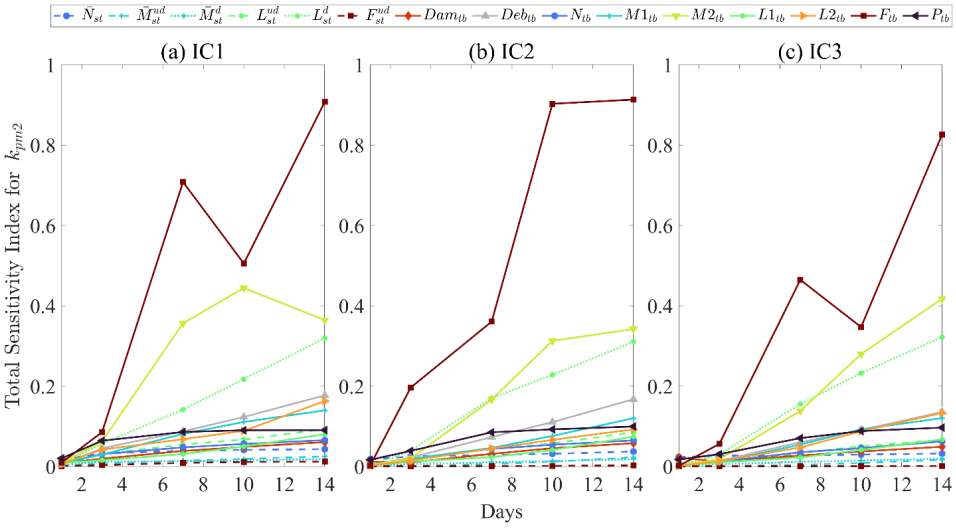
$\bar{N}_{st}$ $\bar{M}^{ud}_{st}$ $\bar{M}^{d}_{st}$ L^{ud}_{st} L^{d}_{st} F^{ud}_{st} Dam_{tb} Deb_{tb} N_{tb} $M1_{tb}$ $M2_{tb}$ $L1_{tb}$ $L2_{tb}$ F_{tb} P_{tb}
(a) IC1
(b) IC2
(c) IC3
Total Sensitivity Index for k_{pm2}
Days

(B.48)

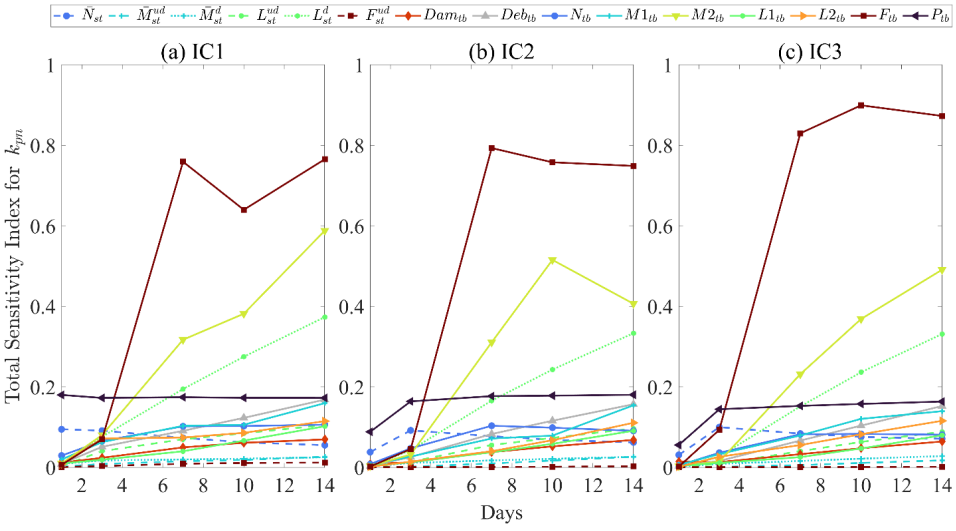
$\bar{N}_{st}$ $\bar{M}^{ud}_{st}$ $\bar{M}^{d}_{st}$ L^{ud}_{st} L^{d}_{st} F^{ud}_{st} Dam_{tb} Deb_{tb} N_{tb} $M1_{tb}$ $M2_{tb}$ $L1_{tb}$ $L2_{tb}$ F_{tb} P_{tb}
(a) IC1
(b) IC2
(c) IC3
Total Sensitivity Index for k_{pm}
Days

(B.49)

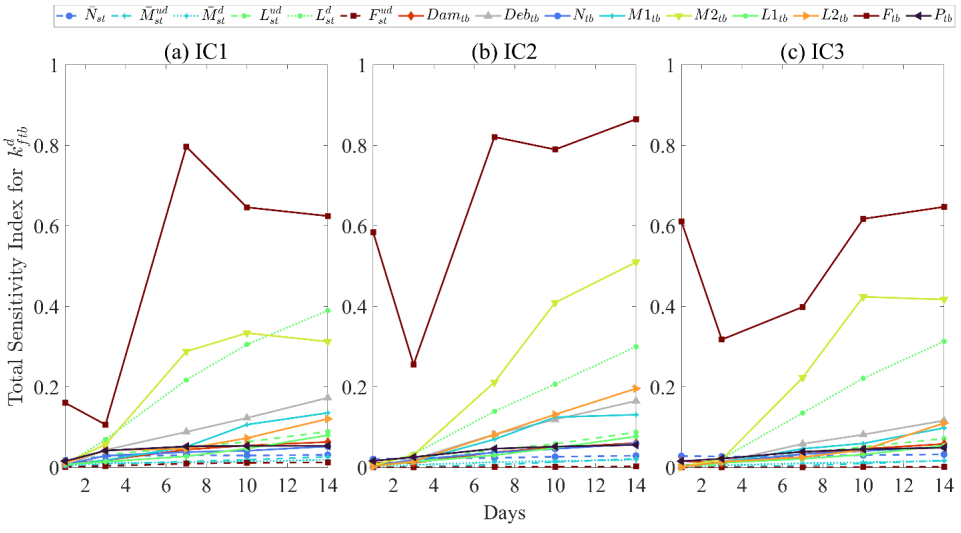
$\bar{N}_{st}$ $\bar{M}^{ud}_{st}$ $\bar{M}^{d}_{st}$ L^{ud}_{st} L^{d}_{st} F^{ud}_{st} Dam_{tb} Deb_{tb} N_{tb} $M1_{tb}$ $M2_{tb}$ $L1_{tb}$ $L2_{tb}$ F_{tb} P_{tb}
(a) IC1
(b) IC2
(c) IC3
Total Sensitivity Index for k^{d}_{ftb}
Days

(B.50)

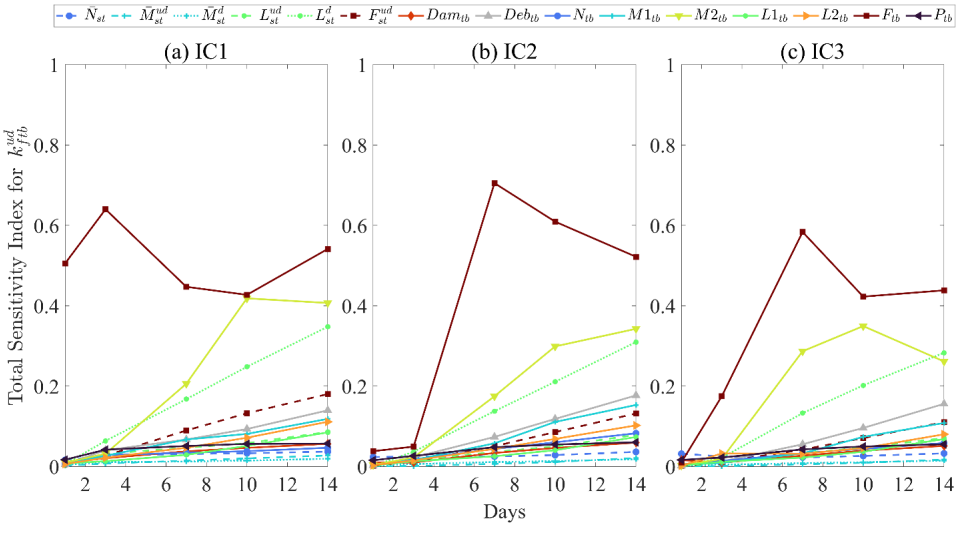
$\bar{N}_{st}$ $\bar{M}^{ud}_{st}$ $\bar{M}^{d}_{st}$ L^{ud}_{st} L^{d}_{st} F^{ud}_{st} Dam_{tb} Deb_{tb} N_{tb} $M1_{tb}$ $M2_{tb}$ $L1_{tb}$ $L2_{tb}$ F_{tb} P_{tb}
(a) IC1
(b) IC2
(c) IC3
Total Sensitivity Index for k^{ud}_{ftb}
Days

(B.51)

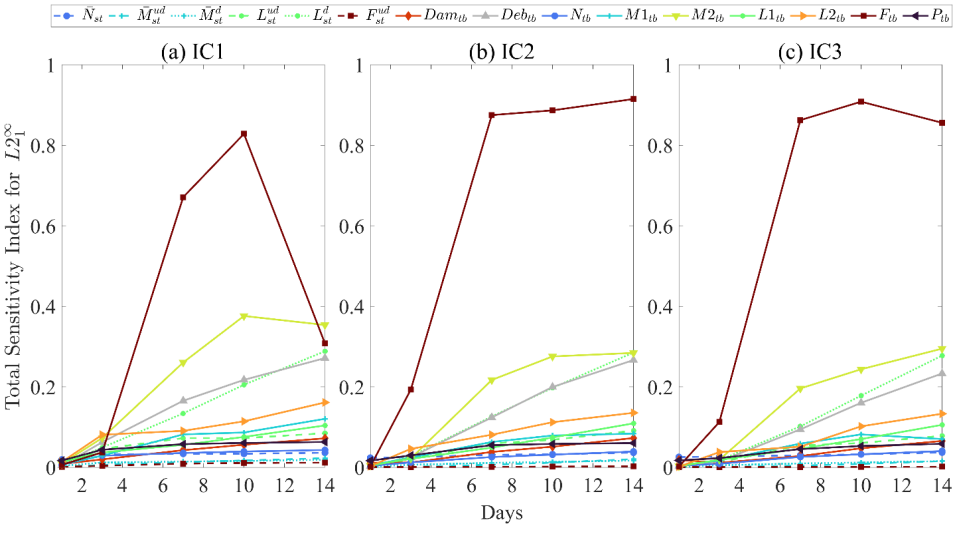
$\bar{N}_{st}$ $\bar{M}^{ud}_{st}$ $\bar{M}^{d}_{st}$ L^{ud}_{st} L^{d}_{st} F^{ud}_{st} Dam_{tb} Deb_{tb} N_{tb} $M1_{tb}$ $M2_{tb}$ $L1_{tb}$ $L2_{tb}$ F_{tb} P_{tb}
(a) IC1
(b) IC2
(c) IC3
Total Sensitivity Index for $L2^{\infty}_{1}$
Days

(B.52)

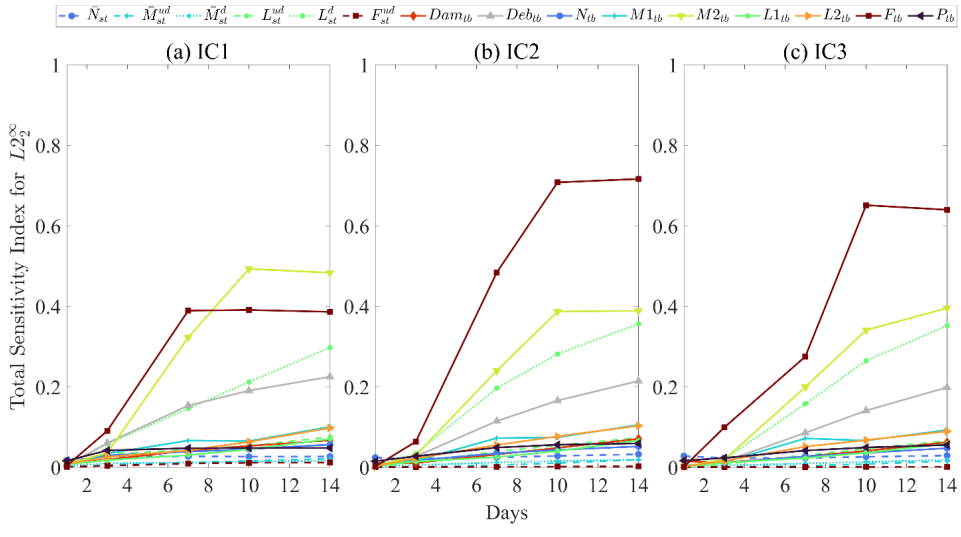
$\bar{N}_{st}$ $\bar{M}^{ud}_{st}$ $\bar{M}^{d}_{st}$ L^{ud}_{st} L^{d}_{st} F^{ud}_{st} Dam_{tb} Deb_{tb} N_{tb} $M1_{tb}$ $M2_{tb}$ $L1_{tb}$ $L2_{tb}$ F_{tb} P_{tb}
(a) IC1
(b) IC2
(c) IC3
Total Sensitivity Index for $L2^{\infty}_{2}$
Days

(B.53)

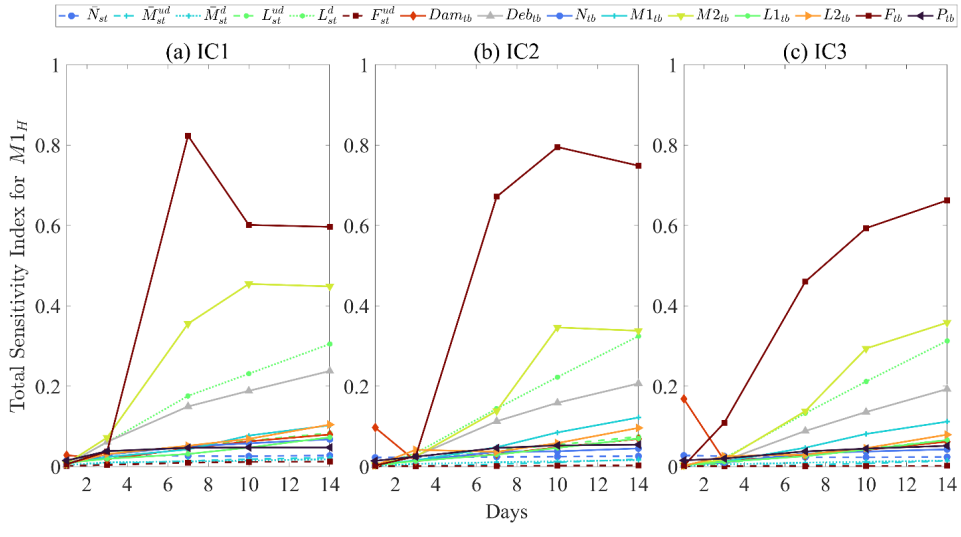
$\bar{N}_{st}$ $\bar{M}^{ud}_{st}$ $\bar{M}^{d}_{st}$ L^{ud}_{st} L^{d}_{st} F^{ud}_{st} Dam_{tb} Deb_{tb} N_{tb} $M1_{tb}$ $M2_{tb}$ $L1_{tb}$ $L2_{tb}$ F_{tb} P_{tb}
(a) IC1
(b) IC2
(c) IC3
Total Sensitivity Index for $M1_{H}$
Days

(B.54)

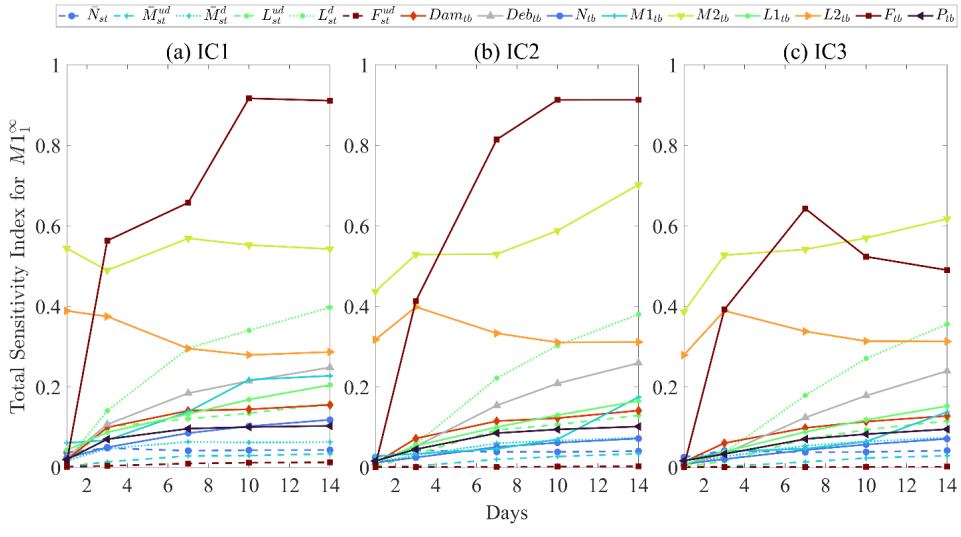
$\bar{N}_{st}$ $\bar{M}^{ud}_{st}$ $\bar{M}^{d}_{st}$ L^{ud}_{st} L^{d}_{st} F^{ud}_{st} Dam_{tb} Deb_{tb} N_{tb} $M1_{tb}$ $M2_{tb}$ $L1_{tb}$ $L2_{tb}$ F_{tb} P_{tb}
(a) IC1
(b) IC2
(c) IC3
Total Sensitivity Index for $M1^{\infty}_{1}$
Days

(B.55)

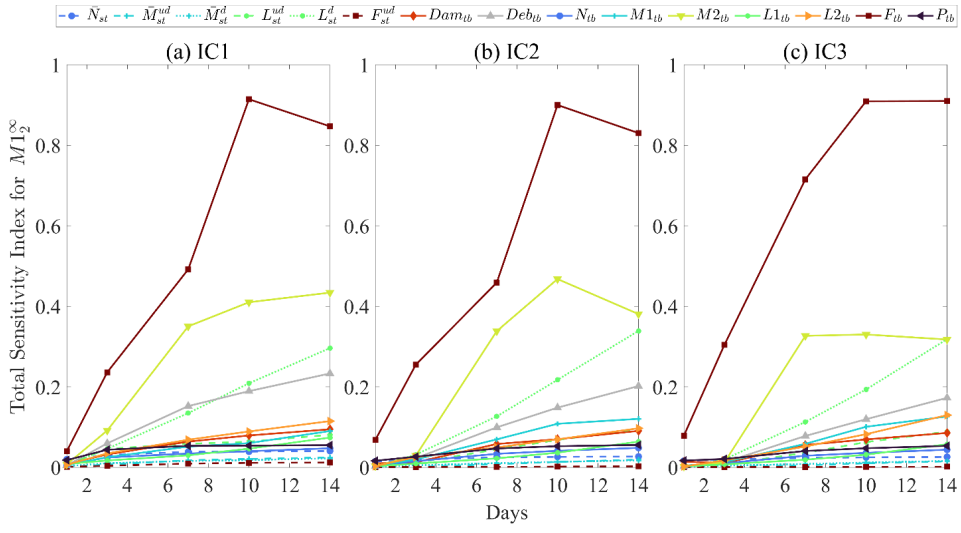
$\bar{N}_{st}$ $\bar{M}^{ud}_{st}$ $\bar{M}^{d}_{st}$ L^{ud}_{st} L^{d}_{st} F^{ud}_{st} Dam_{tb} Deb_{tb} N_{tb} $M1_{tb}$ $M2_{tb}$ $L1_{tb}$ $L2_{tb}$ F_{tb} P_{tb}
(a) IC1
(b) IC2
(c) IC3
Total Sensitivity Index for $M1_2^{\infty}$
Days

(B.56)

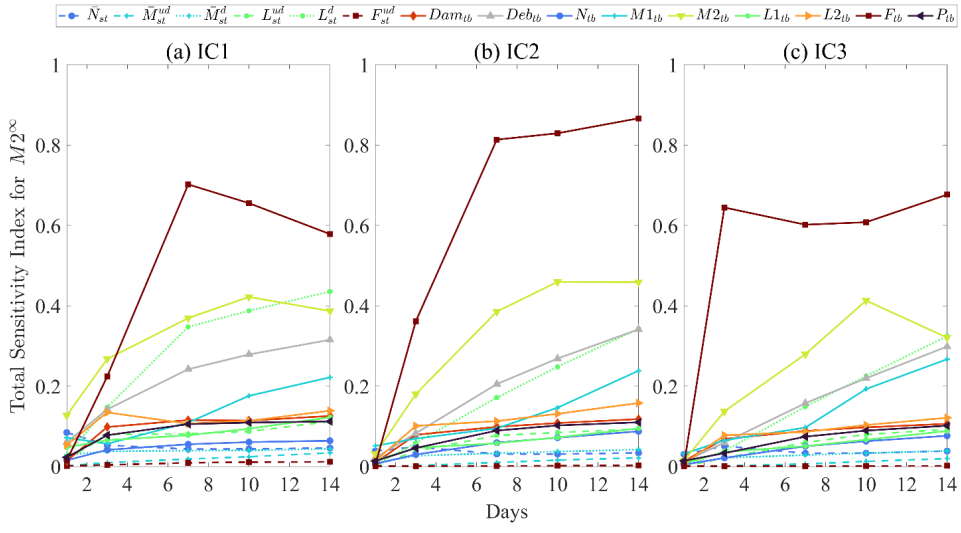
$\bar{N}_{st}$ $\bar{M}^{ud}_{st}$ $\bar{M}^{d}_{st}$ L^{ud}_{st} L^{d}_{st} F^{ud}_{st} Dam_{tb} Deb_{tb} N_{tb} $M1_{tb}$ $M2_{tb}$ $L1_{tb}$ $L2_{tb}$ F_{tb} P_{tb}
(a) IC1
(b) IC2
(c) IC3
Total Sensitivity Index for $M2^{\infty}$
Days

(B.57)

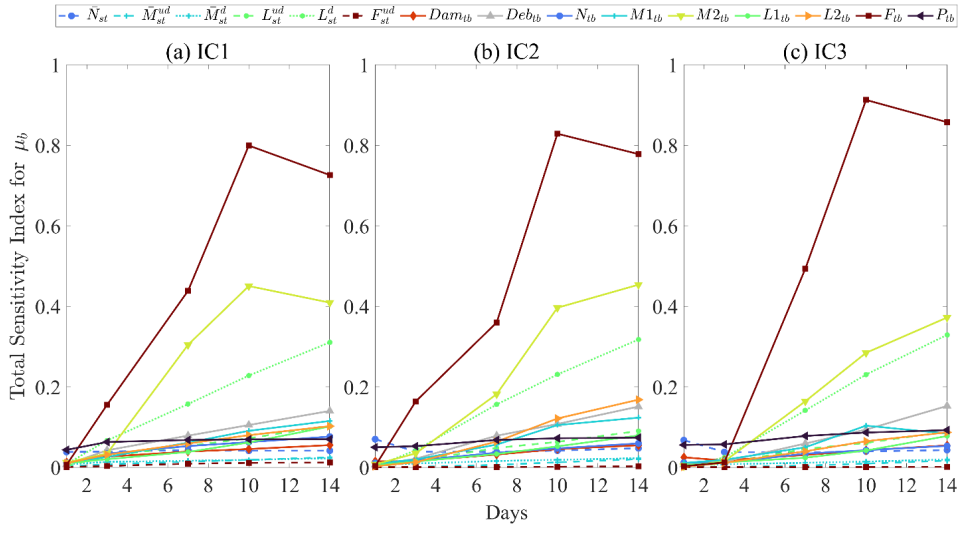
$\bar{N}_{st}$ $\bar{M}^{ud}_{st}$ $\bar{M}^{d}_{st}$ L^{ud}_{st} L^{d}_{st} F^{ud}_{st} Dam_{tb} Deb_{tb} N_{tb} $M1_{tb}$ $M2_{tb}$ $L1_{tb}$ $L2_{tb}$ F_{tb} P_{tb}
(a) IC1
(b) IC2
(c) IC3
Total Sensitivity Index for μ_b
Days

(B.58)

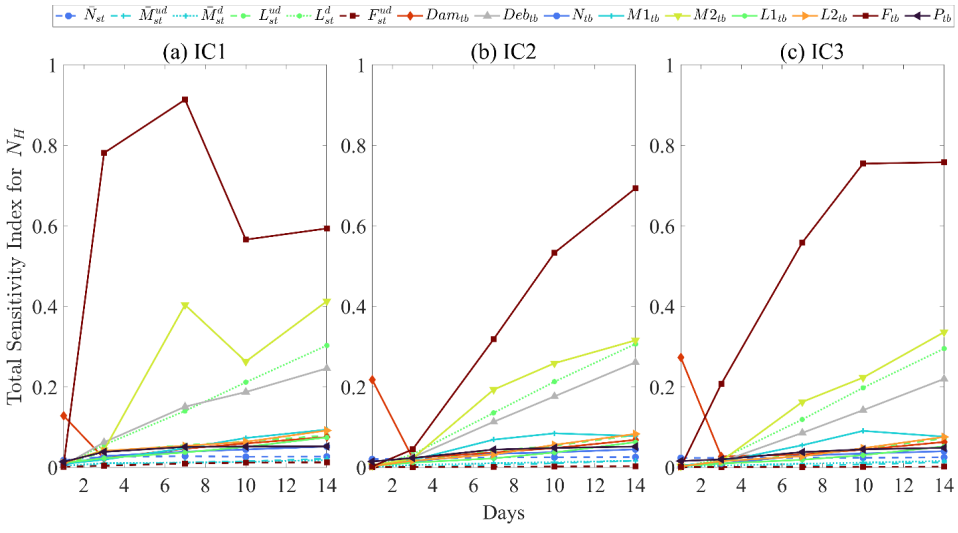
$\bar{N}_{st}$ $\bar{M}^{ud}_{st}$ $\bar{M}^{d}_{st}$ L^{ud}_{st} L^{d}_{st} F^{ud}_{st} Dam_{tb} Deb_{tb} N_{tb} $M1_{tb}$ $M2_{tb}$ $L1_{tb}$ $L2_{tb}$ F_{tb} P_{tb}
(a) IC1
(b) IC2
(c) IC3
Total Sensitivity Index for N_H
Days

(B.59)

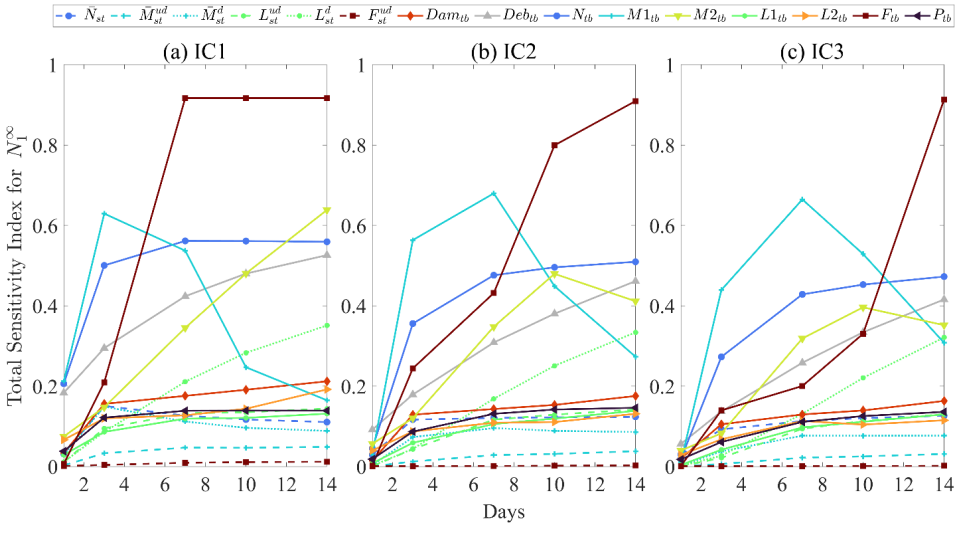
$\bar{N}_{st}$ $\bar{M}^{ud}_{st}$ $\bar{M}^{d}_{st}$ L^{ud}_{st} L^{d}_{st} F^{ud}_{st} Dam_{tb} Deb_{tb} N_{tb} $M1_{tb}$ $M2_{tb}$ $L1_{tb}$ $L2_{tb}$ F_{tb} P_{tb}
(a) IC1
(b) IC2
(c) IC3
Total Sensitivity Index for N_1^{∞}
Days

(B.60)

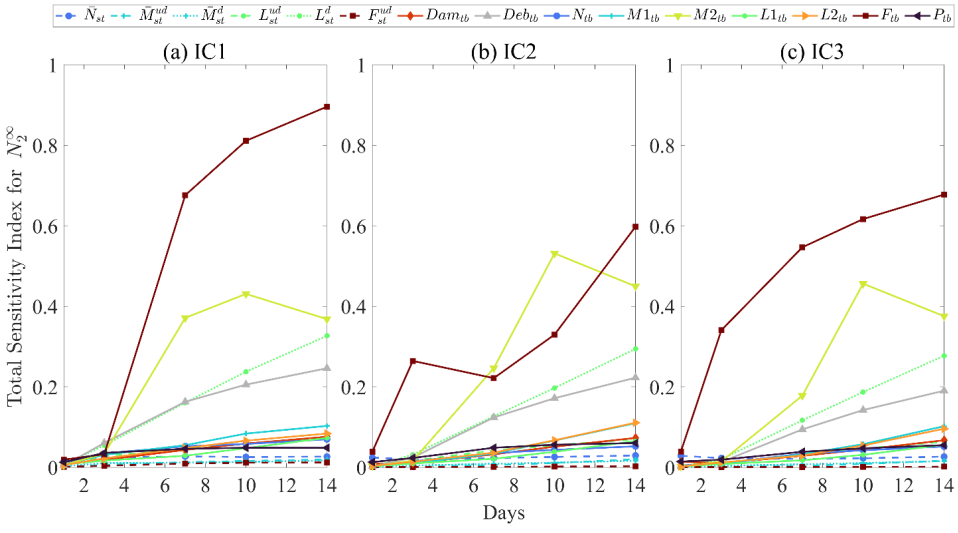
$\bar{N}_{st}$ $\bar{M}^{ud}_{st}$ $\bar{M}^{d}_{st}$ L^{ud}_{st} L^{d}_{st} F^{ud}_{st} Dam_{tb} Deb_{tb} N_{tb} $M1_{tb}$ $M2_{tb}$ $L1_{tb}$ $L2_{tb}$ F_{tb} P_{tb}
(a) IC1
(b) IC2
(c) IC3
Total Sensitivity Index for N_2^{∞}
Days

(B.61)

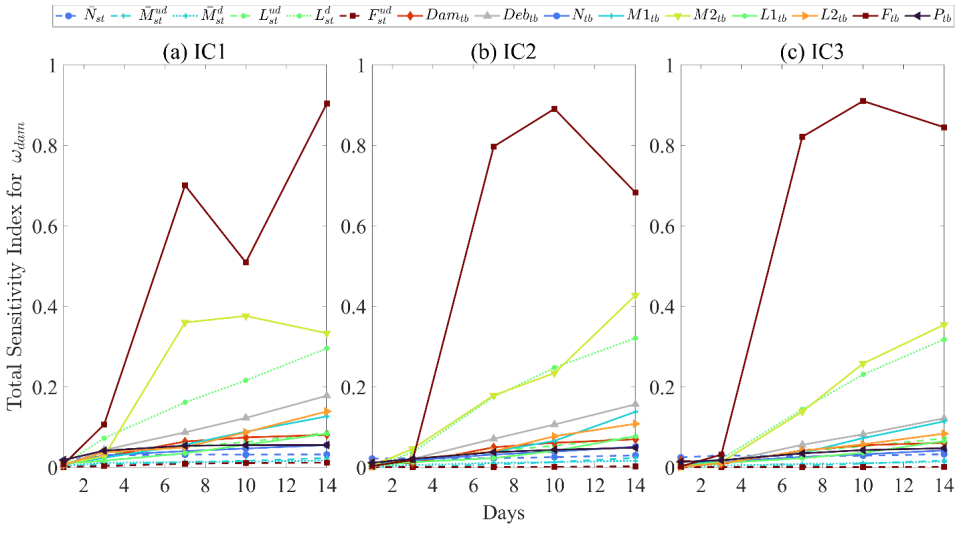
$\bar{N}_{st}$ $\bar{M}^{ud}_{st}$ $\bar{M}^{d}_{st}$ L^{ud}_{st} L^{d}_{st} F^{ud}_{st} Dam_{tb} Deb_{tb} N_{tb} $M1_{tb}$ $M2_{tb}$ $L1_{tb}$ $L2_{tb}$ F_{tb} P_{tb}
(a) IC1
(b) IC2
(c) IC3
Total Sensitivity Index for ω_{dam}
Days

(B.62)

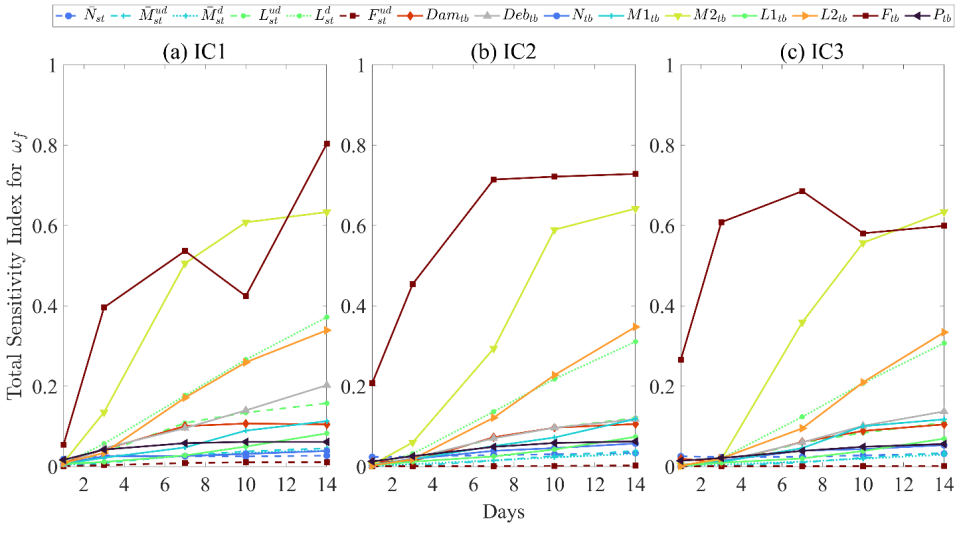
$\bar{N}_{st}$ $\bar{M}^{ud}_{st}$ $\bar{M}^{d}_{st}$ L^{ud}_{st} L^{d}_{st} F^{ud}_{st} Dam_{tb} Deb_{tb} N_{tb} $M1_{tb}$ $M2_{tb}$ $L1_{tb}$ $L2_{tb}$ F_{tb} P_{tb}
(a) IC1
(b) IC2
(c) IC3
Total Sensitivity Index for ω_f
Days

(B.63)

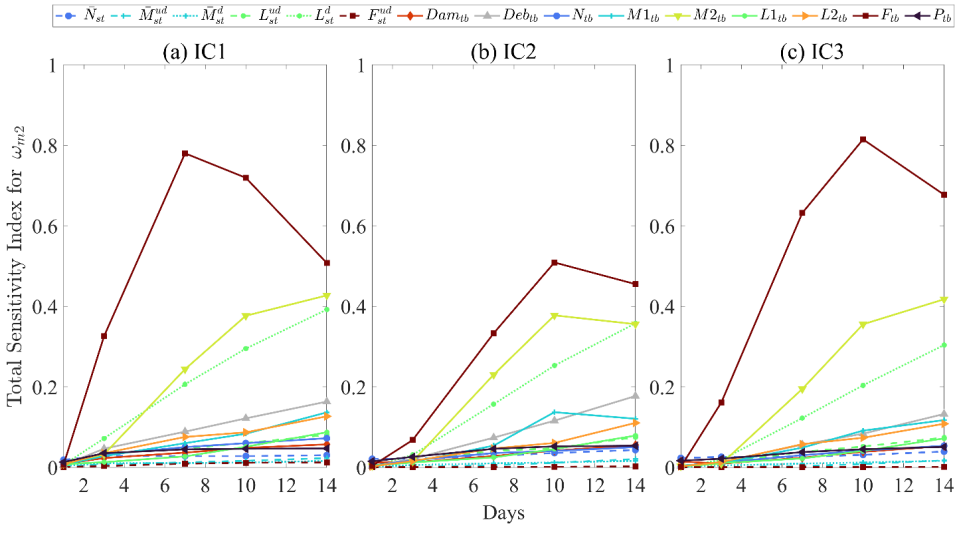
$\bar{N}_{st}$ $\bar{M}^{ud}_{st}$ $\bar{M}^{d}_{st}$ L^{ud}_{st} L^{d}_{st} F^{ud}_{st} Dam_{tb} Deb_{tb} N_{tb} $M1_{tb}$ $M2_{tb}$ $L1_{tb}$ $L2_{tb}$ F_{tb} P_{tb}
(a) IC1
(b) IC2
(c) IC3
Total Sensitivity Index for ω_{m2}
Days

(B.64)

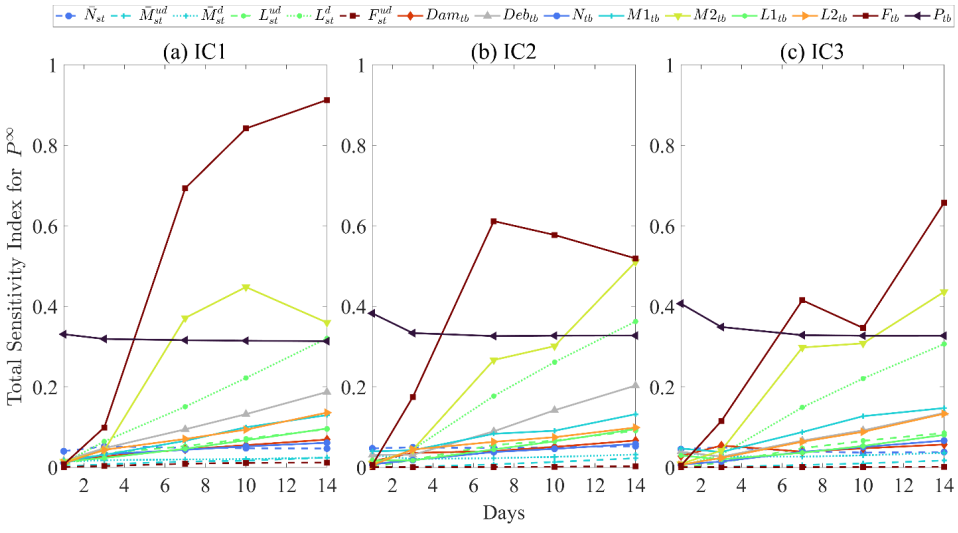
$\bar{N}_{st}$ $\bar{M}^{ud}_{st}$ $\bar{M}^{d}_{st}$ L^{ud}_{st} L^{d}_{st} F^{ud}_{st} Dam_{tb} Deb_{tb} N_{tb} $M1_{tb}$ $M2_{tb}$ $L1_{tb}$ $L2_{tb}$ F_{tb} P_{tb}
(a) IC1
(b) IC2
(c) IC3
Total Sensitivity Index for P^{∞}
Days

(B.65)

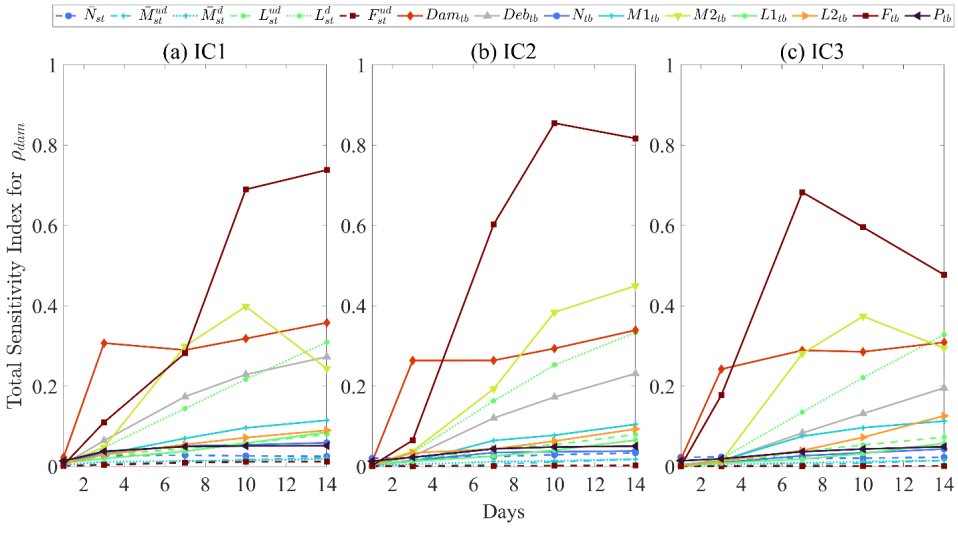
$\bar{N}_{st}$ $\bar{M}^{ud}_{st}$ $\bar{M}^{d}_{st}$ L^{ud}_{st} L^{d}_{st} F^{ud}_{st} Dam_{tb} Deb_{tb} N_{tb} $M1_{tb}$ $M2_{tb}$ $L1_{tb}$ $L2_{tb}$ F_{tb} P_{tb}
(a) IC1
(b) IC2
(c) IC3
Total Sensitivity Index for ρ_{dam}
Days

(B.66)

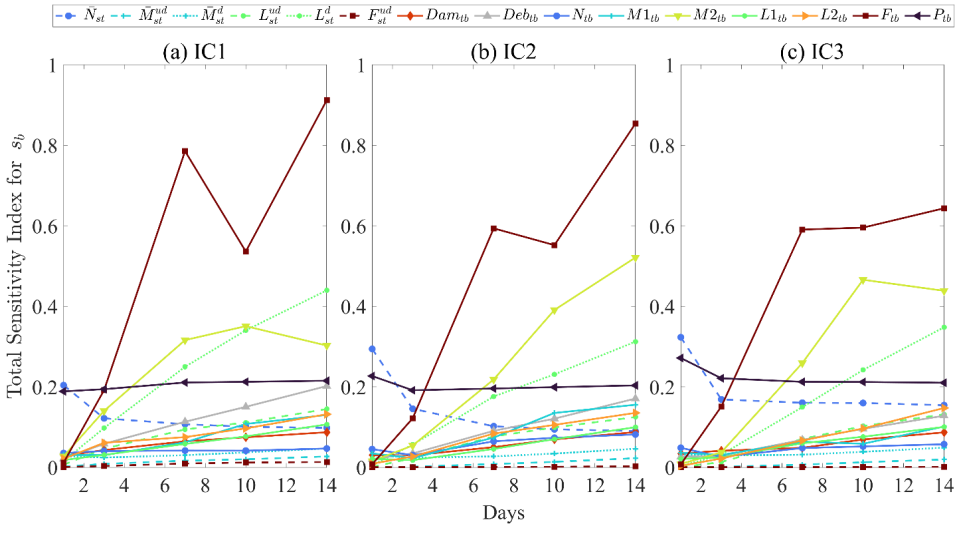
$\bar{N}_{st}$ $\bar{M}^{ud}_{st}$ $\bar{M}^{d}_{st}$ L^{ud}_{st} L^{d}_{st} F^{ud}_{st} Dam_{tb} Deb_{tb} N_{tb} $M1_{tb}$ $M2_{tb}$ $L1_{tb}$ $L2_{tb}$ F_{tb} P_{tb}
(a) IC1
(b) IC2
(c) IC3
Total Sensitivity Index for s_b
Days

(B.67)

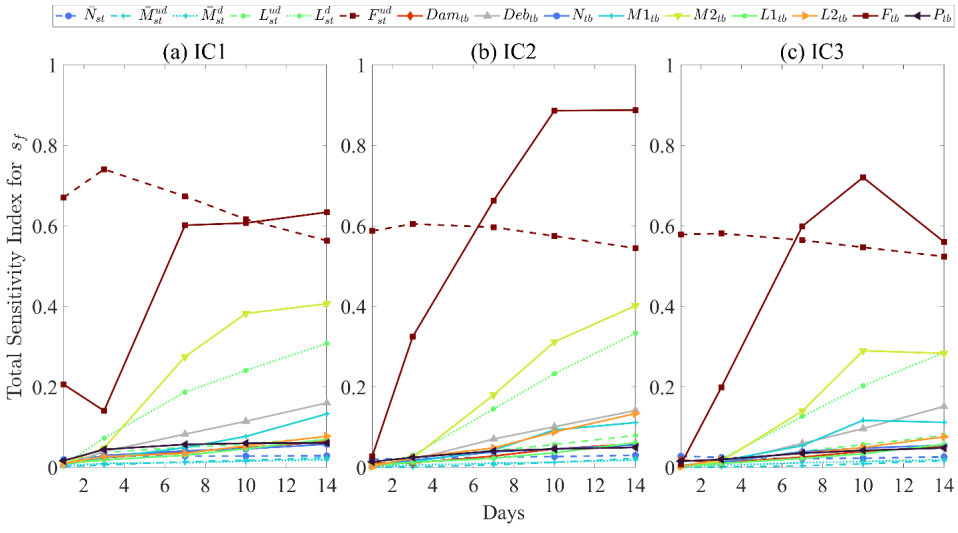
$\bar{N}_{st}$ $\bar{M}^{ud}_{st}$ $\bar{M}^{d}_{st}$ L^{ud}_{st} L^{d}_{st} F^{ud}_{st} Dam_{tb} Deb_{tb} N_{tb} $M1_{tb}$ $M2_{tb}$ $L1_{tb}$ $L2_{tb}$ F_{tb} P_{tb}
(a) IC1
(b) IC2
(c) IC3
Total Sensitivity Index for s_f
Days

(B.68)

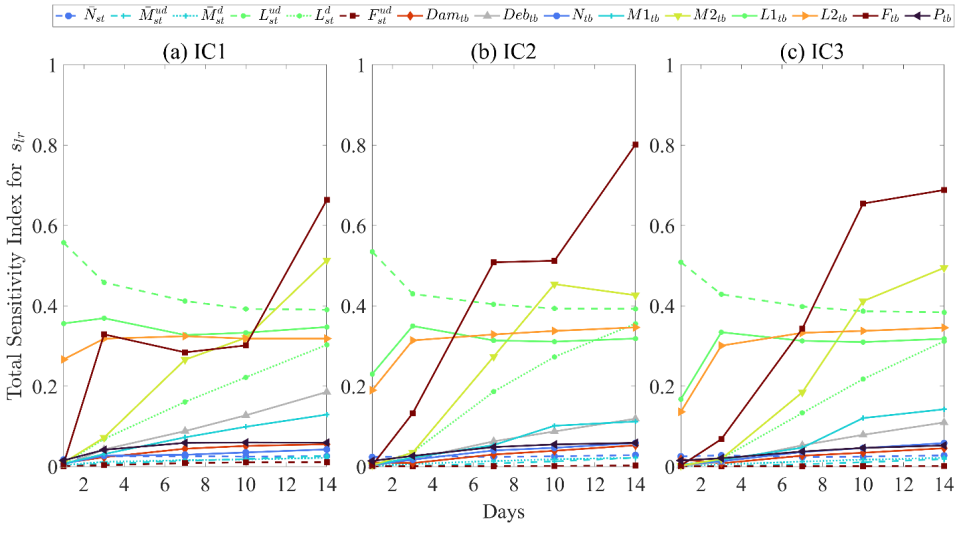
$\bar{N}_{st}$ $\bar{M}^{ud}_{st}$ $\bar{M}^{d}_{st}$ L^{ud}_{st} L^{d}_{st} F^{ud}_{st} Dam_{tb} Deb_{tb} N_{tb} $M1_{tb}$ $M2_{tb}$ $L1_{tb}$ $L2_{tb}$ F_{tb} P_{tb}
(a) IC1
(b) IC2
(c) IC3
Total Sensitivity Index for s_{tr}
Days

(B.69)

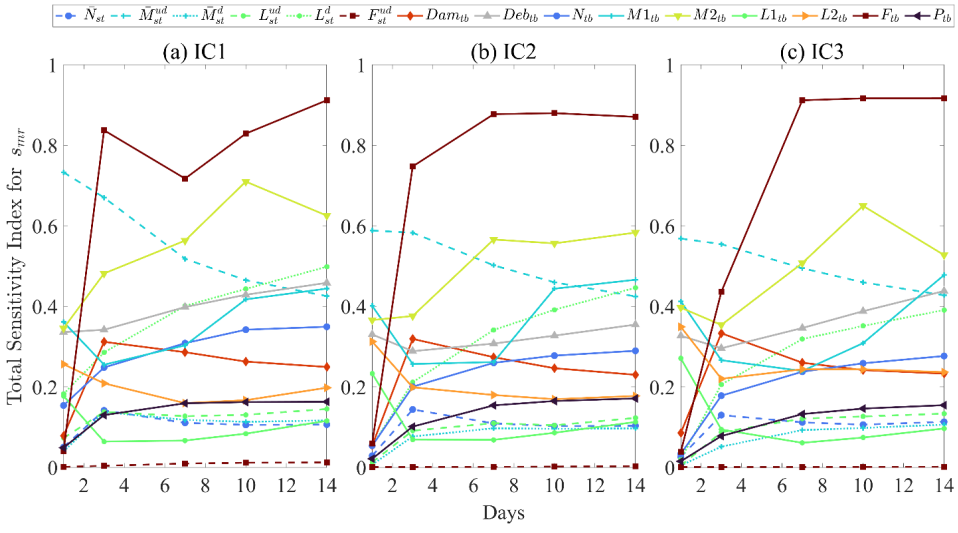
$\bar{N}_{st}$ $\bar{M}^{ud}_{st}$ $\bar{M}^{d}_{st}$ L^{ud}_{st} L^{d}_{st} F^{ud}_{st} Dam_{tb} Deb_{tb} N_{tb} $M1_{tb}$ $M2_{tb}$ $L1_{tb}$ $L2_{tb}$ F_{tb} P_{tb}
(a) IC1
(b) IC2
(c) IC3
Total Sensitivity Index for s_{mr}
Days

(B.70)

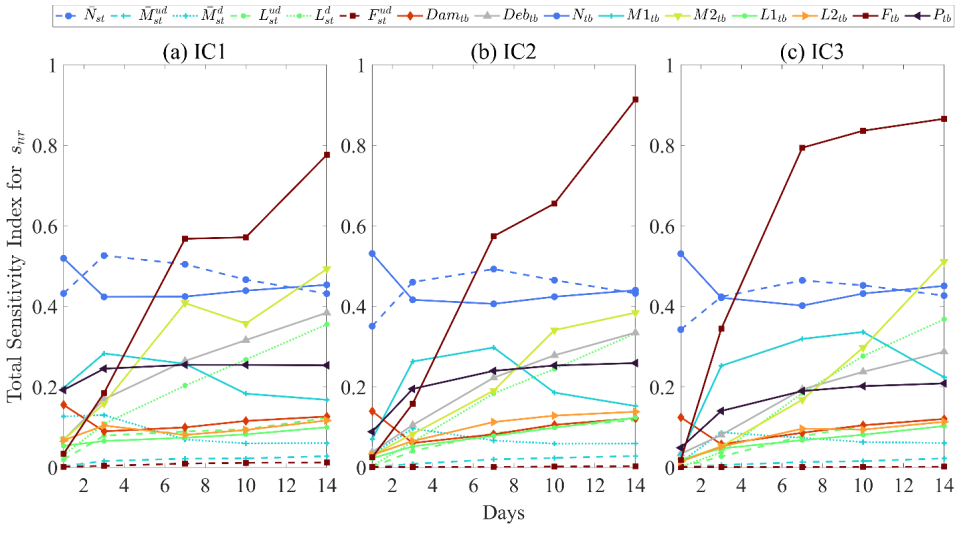
$\bar{N}_{st}$ $\bar{M}^{ud}_{st}$ $\bar{M}^{d}_{st}$ L^{ud}_{st} L^{d}_{st} F^{ud}_{st} Dam_{tb} Deb_{tb} N_{tb} $M1_{tb}$ $M2_{tb}$ $L1_{tb}$ $L2_{tb}$ F_{tb} P_{tb}
(a) IC1
(b) IC2
(c) IC3
Total Sensitivity Index for s_{nr}
Days

(B.71)

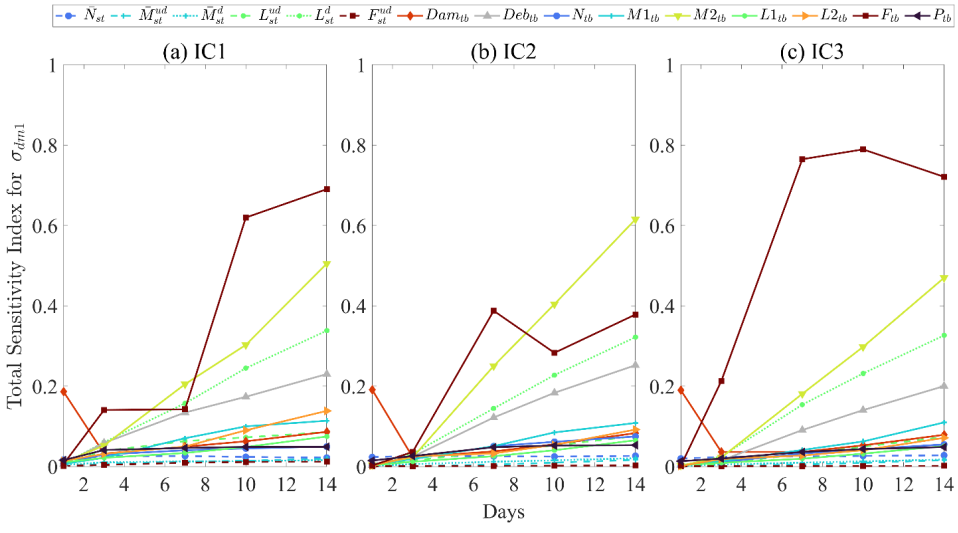
$\bar{N}_{st}$ $\bar{M}^{ud}_{st}$ $\bar{M}^{d}_{st}$ L^{ud}_{st} L^{d}_{st} F^{ud}_{st} Dam_{tb} Deb_{tb} N_{tb} $M1_{tb}$ $M2_{tb}$ $L1_{tb}$ $L2_{tb}$ F_{tb} P_{tb}
(a) IC1
(b) IC2
(c) IC3
Total Sensitivity Index for σ_{dm1}
Days

(B.72)

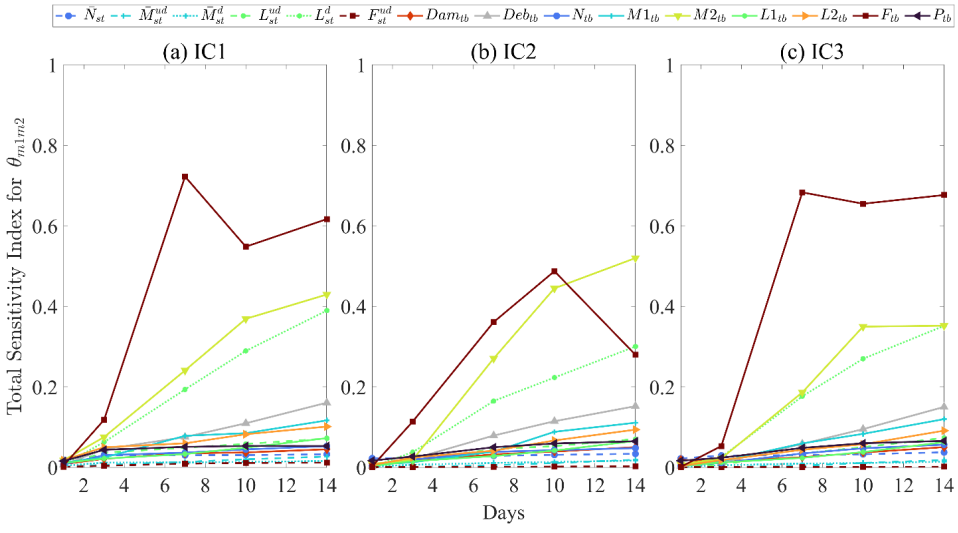
$\bar{N}_{st}$ $\bar{M}^{ud}_{st}$ $\bar{M}^{d}_{st}$ L^{ud}_{st} L^{d}_{st} F^{ud}_{st} Dam_{tb} Deb_{tb} N_{tb} $M1_{tb}$ $M2_{tb}$ $L1_{tb}$ $L2_{tb}$ F_{tb} P_{tb}
(a) IC1
(b) IC2
(c) IC3
Total Sensitivity Index for θ_{m1m2}
Days

(B.73)

Appendix C. Abbreviations and Acronyms

AC	Acceptability criteria
ARA	Applied Research Associates, Inc.
DTRA	Defense Threat Reduction Agency
eFAST	Extended Fourier amplitude sensitivity test
Gy	Gray, unit of ionizing radiation dose
HENRE	Health Effects from Nuclear and Radiological Environments
IC	Initial condition
LHS	Latin-hypercube sampling
LITBM	Locally irradiated thermal burn model
MeFAST	Multi-test extended Fourier amplitude sensitivity test
MSE	Mean sum square error
NUDET	Nuclear Detonation
PRCC	Partial rank correlation coefficient
SA	Sensitivity Analysis
STBM	Superficial thermal burn model
TDPM	Time-dependent physiological model
TN	Technical note
TR	Technical report